E.ON Energy Research Center
ACS | Institute for Automation of Complex Power Systems

RWTH AACHEN UNIVERSITY

Master Thesis

Analysis on Voltage Stability Indices

Christine E. Doig Cardet

Electrical Power Engineering

Aachen, _____ _____

Aachen, _____ _____

ACS | Institute for Automation of Complex Power Systems
ERC | E.ON Energy Research Center
RWTH Aachen University
Mathieustr. 6, 52074 Aachen, Germany

Tel.: +49 241 80 49700
Fax.: +49 241 80 49709
post_acs@eonerc.rwth-aachen.de
www.eonerc.rwth-aachen.de

Acknowledgment

I would like to express my thanks to the ACS Institute at the E.ON Research Center at RWTH Aachen and all of its members, for accepting me as a Master Thesis exchange student, letting me use their facilities and making me feel at home. Especially, I would like to thank Prof. Monti and Prof. Ponci for their valuable advice.

I am bound to thank my supervisor, Dipl.-Wirt.-Ing. Marco Cupelli, who has supported me in this thesis topic, made interesting suggestions and helped me in its development.

My special thanks go to Jungie Tang and Junqi Liu for providing me the two network systems in RTDS® as well as solving my doubts on the use of the software.

I also would like to express my thanks to all friends and colleagues in Aachen, especially Germán Díaz, who has looked after me during my stay, and Carmen, Klaus und Julia Neumann, who have always treated me as part of their family.

Last but not least, I would like to express my gratitude to my mother, father and sister, whose support has enabled me to complete this work.

Declaration of authorship

"I hereby declare that I have written this thesis without any help from others and without the use of documents and aids other than those stated; that I have mentioned all used sources and that I have cited them correctly according to established academic citation rules."

Aachen, (date)_____ _____

(signature)

Abstract

This thesis discusses the performance of different line voltage stability indices previously studied in literature including Lmn Index, Fast Voltage Stability Index (FVSI), Voltage Collapse Point Indicators (VCPI), and LQP Index, as well as the traditional Jacobian index based on the minimum eigenvalue of the Jacobian matrix. The indices were tested in a small 5-bus system and in a larger 39-bus system. The simulation tool used was RTDS® and the indices where computed using the control blocks components in order to monitor the values in real time. This method was chosen to have the indices values available for future control algorithm development. All the indices were found consistent with their theoretical background and the performance comparison was based on three characteristics: their accuracy, robustness to uncertainty and usable for control purposes. From the results and based on these comparison characteristics, VCPI (p) was found to have the best performance from the indices studied.

Table of Contents

Acknowledgment 1
Declaration of authorship 2
Abstract 3
1. Introduction 7
2. Voltage stability overview 9
2.1. Voltage stability definitions 10
2.2. Classification 10
2.3. Voltage stability analysis 12
2.3.1. Power-flow analysis 12
2.3.2. PV and QV curves 13
2.3.3. Analysis methods 16
2.3.3.1. Static, dynamic and quasi-steady-state analysis 16
2.3.3.2. Contingency analysis and loadability limit 17
3. Voltage stability indices 19
3.1. Jacobian matrix-based VSI 20
3.1.1. Test function 20
3.1.2. Second order index 21
3.1.3. Tangent vector 21
3.1.4. V/V0 22
3.1.5. Comparison between Jacobian matrix-based VSI 22
3.2. System variables-based VSI 22
3.2.1. Bus voltage computation indices 23
3.2.1.1. L index 23
3.2.1.2. Voltage Collapse Index (VCI) 24
3.2.1.3. Stability Index (SI) 24
3.2.2. Line stability indices 25
3.2.2.1. Lmn Index 26
3.2.2.2. Line Voltage Stability Index (LVSI) 27
3.2.2.3. LQP Index 27
3.2.2.4. Fast Voltage Stability Index (FVSI) 27

3.2.2.5. Voltage Collapse Point Indicators (VCPI) 28
3.3. Table summary 29
4. PMU-based voltage stability analysis 30
4.1. Synchrophasors and phasor measurement units 30
4.2. Methods based on local measurements 31
4.2.1. Thevenin equivalent using least-square method 32
4.2.2. Thevenin equivalent-Transmission corridors 33
4.2.3. Thevenin equivalent-Approximate approach 35
4.2.4. Voltage Instability Predictor (VIP) 36
4.2.5. Voltage Stability Load Bus Index (VSLBI) 37
4.2.6. S Difference Criterion (SDC) 37
4.3. Methods based on the observability of the whole region 38
4.3.1. Sensitivities 38
4.3.2. Sum of the absolute values Index 39
4.3.3. Voltage Collapse Proximity Indicator (VCPI) 39
4.3.4. Margin Voltage Stability Index (MVSI) 40
4.4. Table summary 42
5. Stability Indices and methods comparison 43
6. Implementation of Voltage Stability Indices and test networks 45
6.1. Introduction to RTDS 45
6.2. 5-bus test system 47
6.3. 39-bus test system 48
6.4. Index implementation 49
6.4.1. Jacobian index implementation 50
6.4.2. Line index implementation 50
6.5. Simulation Cases 53
7. Simulation results 54
7.1. 5-bus test network 54
7.1.1. Simulation Case 1: 5-Bus system with 5% load increase 54
7.1.1.1. Jacobian matrix index 56
7.1.1.2. Line indices 57
7.1.2. Simulation Case 2: 5 Bus system with 2,5% load increase 61
7.1.2.1. Jacobian matrix index 62
7.1.2.2. Line indices 63

7.1.3. Simulation Case 3: Very small load increase 66
7.1.3.1. Jacobian matrix index 67
7.1.3.2. Line indices 69
7.1.4. Simulation Case 4: Only reactive power increasing 70
7.1.4.1. Jacobian matrix index 71
7.1.4.2. Line indices 71
7.1.5. Case comparison 74
7.2. 39-bus test network 80
7.2.1. Simulation Case 1 80
7.2.1.1. Jacobian matrix index 81
7.2.1.2. Line indices 82
7.2.2. Simulation case 2 89
7.2.2.1. Jacobian matrix index 90
7.2.2.2. Line indices 91
8. Conclusions and Future Work 93
Bibliography 96
Appendix 101
A. 39-bus system parameters 101
B. Minimum eigenvalue of the Jacobian Matrix-MatLab code 103

1. Introduction

In recent years, several blackouts related to voltage stability problems have occurred in many countries. In particular, 2003 was an intense year regarding blackouts with a total of 6 major ones affecting the US, the UK, Denmark, Sweden and Italy. The U.S.-Canadian blackout of August 14th, 2003 affected approximately 50 million people in eight U.S. states and two Canadian provinces. In the same year, on September 23rd 2003, the Swedish/Danish system went down affecting 2.4 million customers and five days later, September 28th, another major blackout occurred in continental Europe which resulted in a complete loss of power throughout Italy.

In order to understand why these failures are happening, it should be taken into account that nowadays power systems have to operate closer to their limits. There is an ever-increasing power demand, which could in a near future expect a higher rise with the establishment of electrical vehicles. At the same time, transmission networks are not enlarged due to economic and environmental considerations and few lines are constructed. In addition, the growing usage of renewable energy tends to make the networks more stressed, since these sources have a higher dynamic and stochastic behaviour. Finally, another factor is the liberalisation of electricity supply industry (deregulation), which has resulted in a significant increase in inter-area or cross-border trades, which are not always well accounted for when planning system security.

As mentioned above, the actual scene is no longer the same as it used to be and power systems ought to adapt to this new situation. In [1], after analysing the sequence of events that preceded these recent catastrophic failures, the following conclusion was drawn. The root causes of these blackouts were among others a shortage of reliable real-time data, no time to take decisive and suitable remedial action against unfolding events and a lack of properly automated and coordinated controls to take immediate action to prevent cascading.

Because power systems are operating closer to their limits, voltage stability assessment and control, although not a new issue, is now receiving a special attention. As defined in [2], voltage stability is the ability of a power system to maintain steady acceptable voltages at all buses in the system under normal operating conditions and after being subjected to a disturbance. The study of voltage stability can be analysed under different approaches, but specially, the assessment of how close the system is to voltage collapse can be very useful for operators. This information on the proximity of voltage instability can be given through Voltage Stability Indices. These indices can be used online to enable the operators to take action or even to automate control actions to prevent voltage collapse from happening or offline for the designing and planning stages.

There are many studies on traditional Voltage Stability Indices (VSI) and some comparisons papers between them can be found in the literature, such as [9], [11]-[14] and [48]. Recently, with the development of the Phasor Measurement Units (PMU) technology, new methods are evolving to implement Wide Area Monitoring Systems (WAMSs). These new algorithms use voltages and currents provided by the PMU (synchronized to within a microsecond) to assess the stability of the power system, as in [29] and [30]-[40].

The main objective of this thesis is to describe, analyse and compare the performance of traditional Voltage Stability Indices. Simulations will be done using RTDS®, a Real-Time Digital Simulator installed at the Institute for Automation of Complex Power Systems at the E.ON Research Center at RWTH Aachen University, and two test networks: a 5-bus system and a 39-bus system. The computation of the indices will be done using RTDS® and MatLab.

The remaining of this thesis comprehends seven chapters.

Chapter 2 recalls a voltage stability overview. In this respect, basic definitions on voltage stability, a classification of instabilities and a description of different analysis methods are given.

Chapter 3 deals with traditional voltage stability indices, their classification, a presentation of some examples of each category and a comparison between them.

Chapter 4 details the methods for voltage stability assessment using PMU-based analysis.

Chapter 5 is devoted to summarize and compare both types of indices and methods (traditional versus PMU-based).

The topic addressed in Chapter 6 has to do with the description of the test network used for the simulations and how the different indices were implemented.

The purpose of Chapter 7 is to present the different test systems and cases used, show the simulation results and compare the different indices' behaviour.

Finally, general conclusions as well as future work directions are presented in Chapter 8.

2. Voltage stability overview

Before defining voltage stability, an overview on power system stability and its classification should be given in order to get a global perspective. The proposed definition in [4] describes power system stability as the ability of an electric power system, for a given initial operating condition, to regain a state of operating equilibrium after being subjected to a physical disturbance, with most system variables bounded so that practically the entire system remains intact.

A power system is a high-order multivariable nonlinear system that operates in a constantly changing environment with a dynamic response influenced by a wide array of devices. Because of this high dimensionality and complexity, there is a need to classify power system stability into appropriate categories to identify the factors that contribute to the instability. The classification of power system stability, shown in Fig.2.1, considers the system variable (rotor angle, frequency or voltage), the size of the disturbance (small or large) and the time span (short-term or long-term).

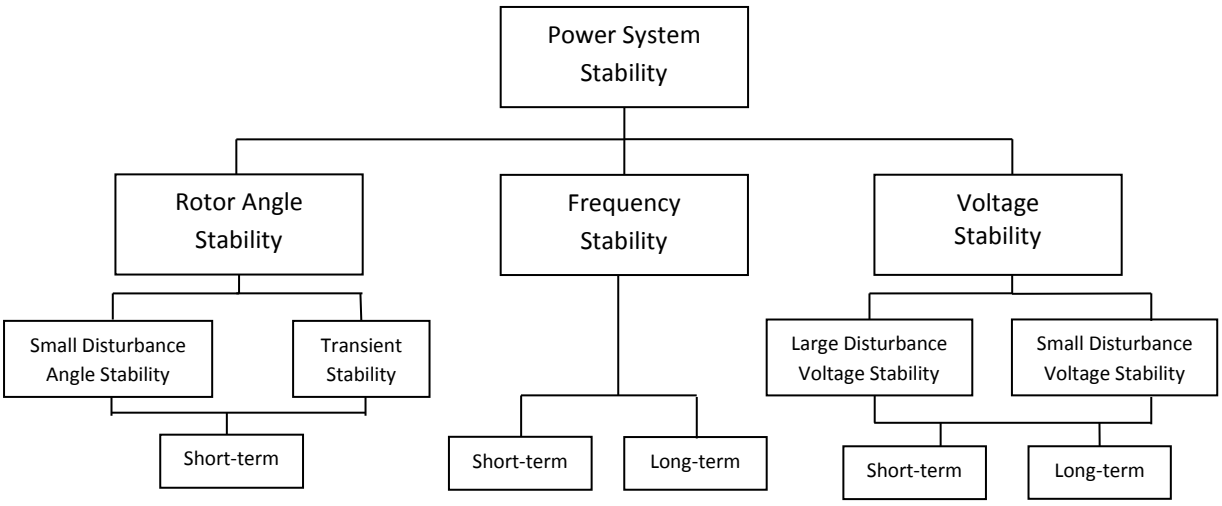

Fig. 2.1 Classification of power system stability [4]

This classification is done to identify the instability causes, apply an appropriate analysis and develop corrective measures. However, in many situations, in particular in highly stressed systems and cascading events, one form of instability may lead to another or a form of instability may not occur as a single type but a combination of several. However, the classification still remains a helpful tool to understand the underlying problem and operate accordingly.

The following sections will discuss voltage stability definitions and classification. For rotor angle stability and frequency stability definitions and considerations refer to [2] and [4].

2.1. Voltage stability definitions

One of the most common and accepted definitions of *voltage stability* states that voltage stability is the ability of a power system to maintain steady acceptable voltage at all buses in the system under normal operating conditions and after being subjected to a disturbance. A system enters a state of voltage instability when a disturbance, increase in load demand or change in system conditions, causes a progressive and uncontrollable drop in voltage [2]. Voltage stability depends on the ability to maintain or restore equilibrium between load demand and load supply from the power system.

According to [3], *voltage instability* stems from the attempt of load dynamics to restore power consumption beyond the capability of the combined transmission and generation system. Instability occurs in the form of a progressive fall or rise of voltages of some buses. A possible outcome of voltage instability is loss of load in an area, or tripping of transmission lines and other elements by their protective systems.

The main factor causing instability is the inability of the power system to meet the demand for the reactive power. The reactive power can be supplied by generators through transmission networks or compensated directly at load buses by compensators such as shunt capacitors. There are two side effects of reactive power transmission: transmission losses and voltage drops. In response to a disturbance, power consumed by the loads tends to be restored by the action of motor slip adjustment, distribution voltage regulators, tap-changing transformers and thermostats. Therefore, restored loads increase the stress on the high voltage network by increasing the reactive power consumption and causing further voltage reduction [4]. It is judged that a system is voltage unstable if, for at least one bus in the system, the bus voltage magnitude decreases as the reactive power injection in the same bus is increased [2].

The term *voltage collapse* refers to the process by which the sequence of events accompanying voltage instability leads to a blackout or abnormally low voltages in a significant part of the power system [4]. In complex practical power systems, many factors contribute to the process of system collapse because of voltage instability: strength of transmission system, power-transfer levels, load characteristics, generator reactive power capability limits and characteristics of reactive power compensating devices [2].

2.2. Classification

For analysis purposes, voltage stability can be classified, as seen in Fig.2.1, in two ways: according to the time frame of their evolution (long-term or short-term voltage stability) or to the disturbance (large disturbance or small disturbance voltage stability).

Short-term voltage stability involves a fast phenomenon with a timeframe in the order of fractions of a second to a few seconds. In some studies it is also referred as transient voltage stability, but in [4] it is recommended not to use this name to distinguish this type of stability with the transient rotor angle stability. Short-term stability problems are usually related to the

rapid response of voltage controllers such as generators' automatic voltage regulator (AVR) and power electronics converters like flexible AC transmission system (FACTS) or high voltage DC (HVDC) links. The analysis requires a solution of appropriate system differential equations [2].

On the other hand, *long-term voltage stability* involves slower acting equipment such as load recovery by the action of on-load tap changer or through load self-restoration and delayed corrective control actions such as shunt compensation switching or load shedding. The study period of interest may extend to several or many minutes. The modelling of long-term voltage stability requires consideration of transformer tap changers, characteristics of static loads, manual control actions of operators and automatic generation control.

Fig. 2.2 presents power system components and controls that play a role in voltage stability and their time frame. The figure was taken from [8] but adapting the notation of transient voltage stability to short-term voltage stability.

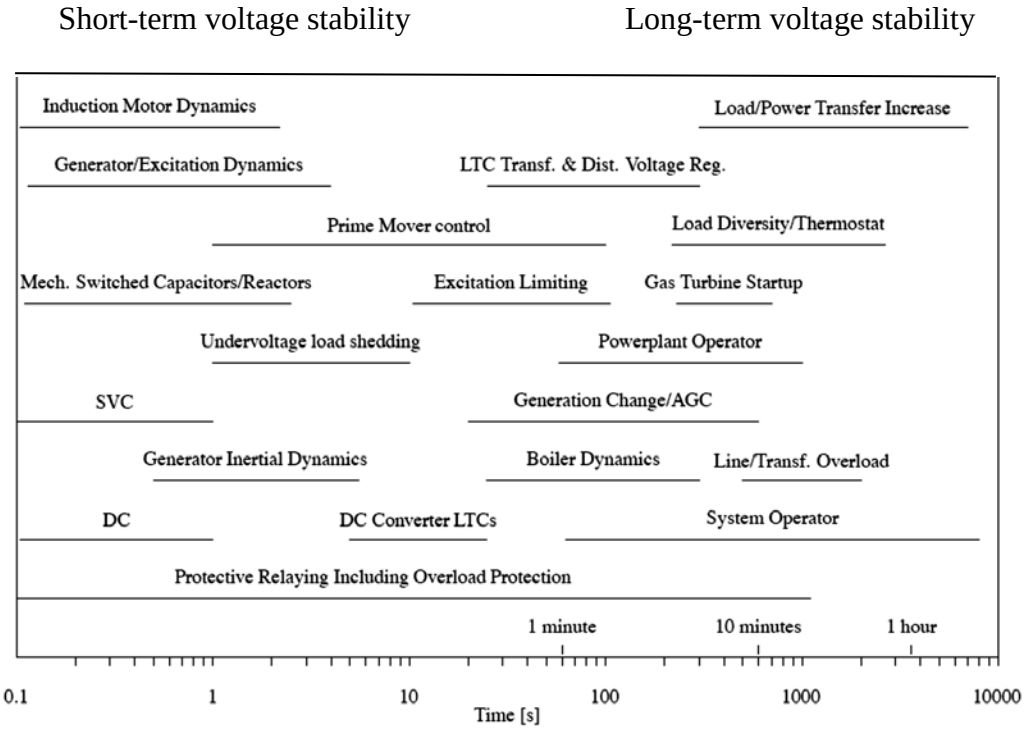

Fig. 2.2 Power system components and controls time frame [8]

For analysis purposes, it is also useful to classify voltage stability into small and large disturbances. *Large-disturbance voltage stability* refers to the system's ability to maintain steady voltages following large disturbances such as system faults, loss of generation, or circuit contingencies and the period of interest may extend from a few seconds to tens of minutes. Large-disturbance voltage stability can be studied using non-linear time domain simulations in the short-term time frame and load flow analysis in the long-term time frame. On the other hand, *Small-disturbance voltage stability* refers to the system's ability to maintain steady voltages when subjected to small perturbations such as incremental changes

in system load [4]. Usually, the analysis of small-disturbances is done in steady state with the power system linearized around an operating point.

2.3. Voltage stability analysis

2.3.1. Power-flow analysis

In large complex networks, power-flow analysis, also known as load-flow, is commonly used. In this section an introduction to power-flow analysis and its application to voltage stability will be given in order to understand the voltage stability indices exposed in the next chapter.

The power-flow (load-flow) analysis involves the calculation of power flows and voltages of a transmission network for specified terminal or bus conditions. The system is assumed to be balanced. Associated with each bus are four quantities: active power *P*, reactive power *Q*, voltage magnitude *V*, and voltage angle θ. The relationships between network bus voltages and currents can be represented by node equations [2]. The network equations in terms of node admittance matrix can be written as:

$$[\bar{I}] = [Y][\bar{V}] \tag{2.1}$$

If *n* is the total number of nodes, $\bar{I}$ is the vector (n x 1) of current phasors flowing into the network, *Y* (n x n) is the admittance matrix with Y_{ii} being the self-admittance of node *i* (sum of all the admittances of node *i*) and Y_{ij} being the mutual admittance between nodes *i* and *j* (negative of the sum of all admittances between nodes *i* and *j*), and $\bar{V}$ the vector of voltage phasors to ground at node *i*.

Equation (2.1) would be linear if injections $\bar{I}$ were known, but, in practice, are not known for most nodes. The current at any node *k* is related to *P*, *Q* and *V* as follows:

$$\bar{I}_k = \frac{P_k - jQ_k}{\bar{V}_k^*} \tag{2.2}$$

The relations between *P*, *Q*, *V* and *I* are defined by the characteristics of the devices connected to the nodes, which makes the problem nonlinear and have to solved using techniques such as Gauss-Seidel or Newton-Raphson method.

The Newton-Raphson method is an iterative technique for solving nonlinear equations. Using this method, the model can be linearized around a given point the following way:

$$\begin{bmatrix}\Delta P \\ \Delta Q\end{bmatrix} = \begin{bmatrix}\frac{\partial P}{\partial \theta} & \frac{\partial P}{\partial V} \\ \frac{\partial Q}{\partial \theta} & \frac{\partial Q}{\partial V}\end{bmatrix}\begin{bmatrix}\Delta\theta \\ \Delta V\end{bmatrix} \tag{2.3}$$

Where $\begin{bmatrix} \frac{\partial P}{\partial \theta} & \frac{\partial P}{\partial V} \\ \frac{\partial Q}{\partial \theta} & \frac{\partial Q}{\partial V} \end{bmatrix}$ is called the Jacobian matrix, ΔP is the incremental change in bus real power, ΔQ is the incremental change in bus reactive power injection, $\Delta\theta$ is the bus voltage angle and ΔV, the incremental change in bus voltage magnitude.

Equation (2.3) requires the solution of sparse linear matrix equations, which can be done using sparsity-oriented triangular factorization.

The Jacobian can provide useful information about voltage stability. System voltage stability is affected by both *P* and *Q*. However, at each operating point we may keep P constant and evaluate voltage stability by considering the incremental relationship between Q and V. Based on these considerations, ΔP in (2.3) is set to 0. Then,

$$\Delta Q = J_R \Delta V \tag{2.4}$$

Where,

$$J_R = \left[J_{QV} - J_{Q\theta} J_{P\theta}^{-1} J_{PV}\right] \tag{2.5}$$

And J_R is the reduced Jacobian matrix of the system.

Voltage stability characteristics can be determined by computing the eigenvalues and eigenvectors of this reduced Jacobian matrix defined by (2.5). Given an eigenvalue λ_i of the ith mode of the Q-V response, if it is greater than 0, then the modal voltage and modal reactive power are along the same direction which yields to a voltage stable system. If $\lambda_i < 0$, the modal voltage and modal reactive power are along opposite directions which indicates an unstable system. The magnitude of λ_i determinates the degree of stability. When $\lambda_i = 0$, voltage collapses because any change in the modal reactive power causes an infinite change in the modal voltage.

In conclusion, the Jacobian matrix allows defining the voltage collapse point as a system loadability limit in which the minimum magnitude of the eigenvalues of the power flow Jacobian matrix is zero.

2.3.2. PV and QV curves

Before detailing more complex and sophisticated analysis methods, a simple example is given using PV and QV curves, which are a traditional method for illustrating the voltage instability phenomenon.

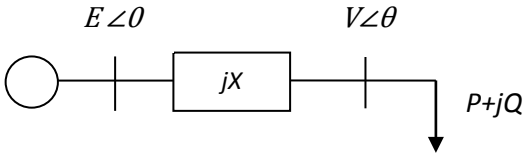

Fig. 2.3 Two-bus system

The model in Fig.2.3 considers a constant voltage source of magnitude *E* and a purely reactive transmission impedance *jX*. Using the load flow equations:

$$P = -\frac{EV}{X} sin\theta \tag{2.6}$$

$$Q = -\frac{V^2}{X} + \frac{EV}{X} cos\theta \tag{2.7}$$

Where *P* is the active power consumed by the load, *Q* is the reactive power consumed by the load, *V* the load bus voltage and θ the phase angle difference between the load and generator busses. Solving (2.6) and (2.7) with respect to *V*, the following equation is obtained:

$$V = \sqrt{\frac{E^2}{2} - QX \pm \sqrt{\frac{E^4}{4} - X^2P^2 - XE^2Q}} \tag{2.8}$$

The solutions to this load voltage are often presented in PV or QV curves, also known as nose curves or voltage profiles. In Fig. 2.4, different PV curves are shown. A constant power factor, i.e, $Q = P \cdot tan\Phi$ has been assumed for each curve.

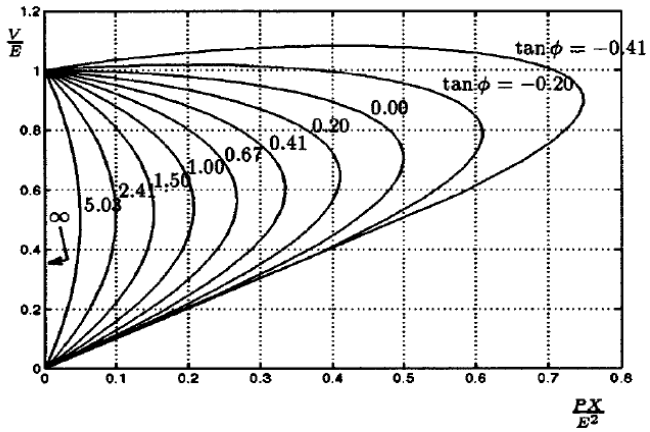

Fig. 2.4 PV curves [3]

Equation (2.8) yields two solutions of voltages to any set of load flow, represented by the upper and lower parts of the PV-curve. The upper voltage solution, which is corresponding to "+" sign in equation (2.8) is stable, while the lower voltage, corresponding to "-" sign, is unstable [3]. The tip of the "nose curve" is called the maximum loading point or critical point. Operation near the stability limit is impractical and sufficient power margin, that is, distance to the limit, has to be allowed [2], as represented in Fig.2.5.

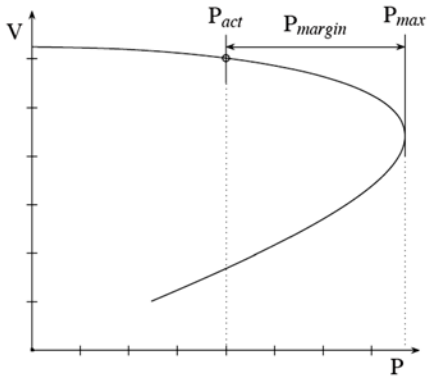

Fig. 2.5 Power margin [2]

Often, a more useful characteristic for certain aspects of voltage stability analysis is the Q-V curves. These can be used for assessing the requirements for reactive power compensation since they show the sensitivity and variation of bus voltages with respect to reactive power injections or absorptions.

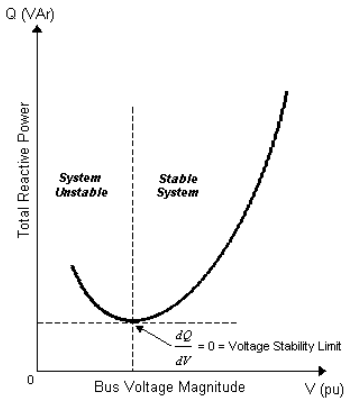

Fig. 2.6 Q-V curve [3]

Fig. 2.6 shows a Q-V curve. Similar to the P-V curves, Q-V curves have a voltage stability limit, which is the bottom of the curve, where dQ/dV is equal to zero. The right hand side is stable since an increase in Q is accompanied by an increase in V. The left hand side is unstable since an increase in Q represents a decrease in V, which is one of the instability factors described in section 2.1 that judges that a system is voltage unstable if, for at least one bus in the system, the bus voltage magnitude decreases as the reactive power injection in the same bus is increased.

In [2] it was seen that complex power systems have similar PV characteristics to those of simple radial systems such as the one in Fig. 2.3. That is the reason why, PV-curves play a major role in understanding and explaining voltage stability and are widely used for its study. From a PV curve, the variation of bus voltages with load, distance to instability and critical voltage at which instability occurs may be determined. However, it is not necessarily the most efficient way of studying voltage stability since it requires a lot of computations for large complex networks. In the following section other analysis methods will be presented.

2.3.3. Analysis methods

Voltage instability is a dynamic phenomenon which may involve the interaction of many devices. It may occur in different time frames and involve different parts of the system with nonlinear behaviours due to interaction of different elements in power systems. This complexity makes it hard to assess stability and many different approaches have been proposed in literature. Due to this complexity and difficulties, some assumptions and/or simplifications have to be made, which provides each method with its own characteristics. Therefore, each analysis presents advantages and weaknesses. A good understanding on the underlying assumptions is needed in order to choose to most appropriate method for the characteristics of each analysis.

The following sections give an overview of methods used to analyse voltage instability scenarios and assess system security. The first section is devoted to distinguish between static, dynamic and quasi-steady-state analysis, the second to the purpose of the analysis that can be study the reaction of the system to contingencies or determine how far it is from its loadability limit.

2.3.3.1. Static, dynamic and quasi-steady-state analysis

There are two main approaches of voltage stability analysis in nonlinear power systems: dynamic and static. Although they are classified as two different analyses, the two approaches should be used in a complementary manner depending on the study interest.

The *dynamic analysis* implies the use of a model characterized by non-linear differential and algebraic equations which include generators dynamics or tap changing transformers. The overall system equations may be expressed in the following general form [2]:

$$\dot{x} = f(x, V) \tag{2.9}$$

And a set of algebraic equations:

$$I(x, V) = Y_N V \tag{2.10}$$

With a set of known initial conditions (x_0, V_0), where x is the state vector of the system, V the bus voltage vector, I the current injection vector and Y_N the network node admittance matrix. It should also be stated that Y_N is a function of bus voltages and time, and I is a function of the system states and the bus voltage vector.

Equations (2.9) and (2.10) can be solved in time-domain using numerical integration methods such as Euler or Runge-Kutta. This approach requires a lot of computations as well as calculation time and does not provide information regarding the sensitivity or degree of instability [6]. However, it provides the most accurate response of the actual dynamics of voltage stability when appropriate modelling is included. In practice, dynamic simulation is used in applied in essential studies relating to coordination of protections and controls and in large-disturbance and short-term voltage stability analysis to capture the performance and

interactions of such devices as motors, under load transformer tap changers, and generator field-current limiters.

The *static analysis* involves only the solution of algebraic equations and therefore is computationally much more efficient than the dynamic analysis. Static analysis captures snapshots of system conditions at various time frames along the time-domain trajectory [2]. At each time frame, time derivatives of the state variables in Equation (2.9) are assumed to be zero. Although voltage stability is a dynamic phenomenon by nature, static analyses are used in many studies, due to its lower computation time and useful information for voltage stability assessment.

The *quasi-steady state* (QSS) analysis consists in simulating the long-term dynamics with the short-term dynamics replaced by their equilibrium equations. QSS long-term simulation offers an interesting compromise between the efficiency of static methods and the advantages of time-domain methods [5].

The quasi-steady state description of a power system is given by the following differential-algebraic equations,

$$\dot{x} = f(x, y, \lambda) \tag{2.11}$$

$$0 = g(x, y, \lambda) \tag{2.12}$$

where x represents the system state variables, y the algebraic variables and λ a parameter or set of parameters that slowly change in time. This allows the system to move from one equilibrium point to another. [14]

2.3.3.2. Contingency analysis and loadability limit

As presented in [5] a power system analysis has to deal with several aspects, which are classified in four categories: contingency analysis, loadability limit determination, determination of security limits and preventive and corrective control.

Contingency analysis [5] aims at analysing the system response to large disturbances that may lead to instability and collapse. The system is considered secure if it can withstand each set of credible incidents, referred to as contingencies. For long-term voltage stability analysis, the credible contingencies are outages of transmission and generation facilities; the sequence of events leading to such outages does not really matter. For short-term voltage stability, the system response to short-circuits is investigated in addition to outages.

While contingency analysis focus on a particular operating point, *loadability limit determination* deals with how far a system can move from this operating point and still remain in a stable state. Most of the voltage stability indices presented in the following chapters deal with this type of analysis.

After studying how the system reacts to different contingencies it is interesting to *determine security limits*. This analysis aims to account for the maximum stress that the system can accept, taking into account contingencies. Once the security limits are calculated it is useful to determine the best control actions to correct a weak situation. *Preventive controls* deal with actions to be taken in a precontingency situation in order to increase the security margin with respect to one (or several) “limiting” contingency (or contingencies). *Corrective controls*, on the other hand, deal with actions taken in a given postdisturbance configuration in order to restore system stability [5].

3. Voltage stability indices

In voltage stability analysis, it is useful to assess voltage stability of power systems by means of voltage stability indices (VSI), scalar magnitudes that can be monitored as system parameters change. Operators can use these indices to know how close the system is to voltage collapse in an intuitive manner and react accordingly.

After a literature research on voltage stability indices, a lack of an organized, detailed and complete classification of these indices was noticed. Although some comparison papers between indices has been found ([9]-[14]), the global picture of the classification, characteristics and differences was still missing. The purpose of this chapter is to give a unified and wide perspective of the actual state of VSI, including the most recent proposed indices.

The broader classification proposed in this thesis is based in [9] and [10], having adopted the notation of the first one, Jacobian matrix based VSI and system variables based VSI. Jacobian matrix based VSIs can calculate the voltage collapse point or maximum loadability limit and determine the voltage stability margin, for that, the computation time is high; hence, they are not suitable for online assessment. On the other hand, system variables based VSIs, which use the elements of the admittance matrix and some system variables such as bus voltages or power flow through lines, require less computation and, therefore, are adequate for online monitoring. The disadvantage of these indices is that they cannot accurately estimate the margin, so they can just present critical lines and buses.

This classification felt natural as they represented the two voltage stability aspects defined in [2]: proximity to voltage collapse (How close is the system to voltage instability?) and mechanism of voltage instability (What are the voltage-weak areas?).

Jacobian matrix-based VSI	System variables-based VSI
More amount of computing time	Less amount of computing time
Offline use	Online use
Determine voltage stability margin: Proximity to voltage collapse	Determine weak buses or lines: Mechanism of voltage instability

Fig. 3.1 Comparison on VSI

In the following sections the different indices on each category will be presented.

3.1. Jacobian matrix-based VSI

As seen in Section 2.3.1., the voltage collapse point is a system loadability limit in which the minimum magnitude of the eigenvalues of the power flow Jacobian matrix is zero. In [15], the minimum singular value of the Jacobian matrix was used as an indicator of voltage stability. This index, however, cannot accurately estimate the collapse point because it shows a very non-linear behaviour near that point. Based on the power flow Jacobian matrix, some other indices have been proposed trying to avoid this non-linearity problem.

In this section the main power-flow analysis-based VSI are presented: test function, second order index, tangent vector and V/V0. A detailed description on more VSI based on power flow analysis can be found in [14].

3.1.1. Test function

A test function based on the Jacobian matrix has been presented in [16]. When the system load increases the test function display a quadratic (or quartic) shape. This can be used to predict the voltage collapse point by fitting the test function using a quadratic (or quartic) model. It is shown that the test function is more reliable than eigen/singular value of Jacobian matrix [9].

The test function is defined by:

$$t_{lk} = |e_l^T J J_{lk}^{-1} e_l| \tag{3.1}$$

where, J represents the system Jacobian, e_l is the l^{th} unit vector, i.e., a vector with all entries zero except the l^{th} row, and J_{lk} is defined by:

$$J_{lk} = (I - e_l e_l^T)J + e_l e_k^T \tag{3.2}$$

where, I represents the identity matrix. Equation (3.2) can be interpreted as a modified Jacobian matrix with the l^{th} row removed and replaced by row e_k^T. J is singular at the voltage collapse point, but matrix J_{lk} is guaranteed not singular if the l^{th} and k^{th} are chosen so that they correspond to non-zero entries in the zero eigenvectors v and w associated with the zero eigenvalue of J [14]. Furthermore, if $l = k = c$, where c corresponds to the maximum entry in v, the test function becomes the critical test function:

$$t_{cc} = |e_c^T J J_{cc}^{-1} e_c| \tag{3.3}$$

The Jacobian matrices and test function family are functions of system variables and parameters. As the parameter λ changes and approaches the collapse point, the system variables change and as a result the critical test function t_{cc} displays a quadratic shape as a function of the load margin:

$$\Delta\lambda \approx a t_{cc}^2 \tag{3.4}$$

Where a is a scalar constant. This characteristic allows the use of t_{cc} for determining the system proximity to voltage collapse, but it makes it difficult to detect the critical bus c, since several buses should be monitored at the same time and that would increase the computational costs.

3.1.2. Second order index

In [17], a voltage stability index based on the maximum singular value of the inverse Jacobian matrix and its derivative has been presented. It is known as second order performance index or index *i*. This index tries to overcome the difficulties of first order indices such as the minimum singular value index, which are inadequate in presence of non-linearity or discontinuities.

The index is based on the maximum singular value of the inverse Jacobian matrix ($\sigma_{\max}$) and its derivative respect to the total system load (λ_{total}). The index is defined as:

$$i = \frac{1}{i_0} \frac{\sigma_{\max}}{d\sigma_{\max}/d\lambda_{total}} \tag{3.5}$$

where i_0 is the value of $\frac{\sigma_{\max}}{d\sigma_{\max}/d\lambda_{total}}$ in the initial operating point. At the initial operating point the index value is 1 and at the collapse point is 0. Because this index presents a linear trend, it can provide useful information regarding the distance to voltage collapse. It also overcomes the problem with non-linearity, since a quick increase in $\sigma_{\max}$ is compensated by the high value of the derivative $d\sigma_{\max}/d\lambda_{total}$ [9], [17].

3.1.3. Tangent vector

The voltage stability index proposed in [19] is based on the tangent vector, which gives information on how system variables are affected by changing the load λ. The vector elements are the sensitivity of state variables including the bus voltage magnitudes and angles with respect to the load increase. It is known that they tend to infinity as the voltage collapse point is approached and therefore, can be used as an index to assess how far away the system is to that point. The tangent vector index is defined as:

$$TVI_i = \left|\frac{dV_i}{d\lambda}\right|^{-1} \tag{3.6}$$

Where V_i is the voltage at bus i and λ, the load. As the system approaches voltage collapse $\frac{dV_i}{d\lambda} \to \infty$ and, therefore, $TVI_i \to 0$.

3.1.4. V/V0

A rather simple index to define and compute is presented in [20], the ratio V/V0. V is the bus voltage value known from load flow or state estimation studies. V0 are obtained solving load flow for the system at an identical state but with all loads set to zero. The ratio V/V0 at each node yields a voltage stability map of the system, allowing detection of weak spots. A problem with this index is that it presents a highly nonlinear profile with respect to changes on the system parameter, not allowing for accurate predictions of proximity to collapse [14].

3.1.5. Comparison between Jacobian matrix-based VSI

Some comparison between these indices can be found in [14]. The following table compares the presented indices according to their computational costs, the accuracy of collapse predictions and the adequacy to nonlinearities.

Index	Computational costs	Accuracy of collapse predictions	Adequacy to nonlinearities
Minimum eigenvalue	+++	+	+
Test function	++	+++	++
Index i - Second method	++++	++++	+++
Tangent vector	+	+++	++
V/V0	+	+	+

Fig. 3.2 Table comparison (+:poor, ++:regular, +++:good, ++++:exceptional)

3.2. System variables-based VSI

Besides the above indices that are based on power flow analysis and the Jacobian matrix, there are many other indices which use direct measurements, such as bus voltages and elements of the admittance matrix. These require less computational efforts and are suitable for a fast diagnosis of system condition and contingency ranking. These indices are based on the condition existing in maximum loadability point of a two-bus system. In this simple system, they tend to a known value as a loadability limit is approached, but may have some different and unpredictable values in the loadability limits when used in larger networks. Therefore, they cannot estimate the voltage stability margin, but can be used to determine critical lines or critical buses in a given load level [9].

These indices have been classified in two groups as in [12]: bus voltage computation indices (or nodal voltage stability indices) and line stability indices. Some comparison can be found in [12] and [13]. This chapter will combine both and present the most important indices in each group with references to their original developers.

3.2.1. Bus voltage computation indices

3.2.1.1. L index

The L index was first described in [22] and it is based on a hybrid representation of the transmission system with the following set of equations:

$$\begin{bmatrix} V_L \\ I_G \end{bmatrix} = H \begin{bmatrix} I_L \\ V_G \end{bmatrix} = \begin{bmatrix} Z_{LL} & F_{LG} \\ K_{GL} & Y_{GG} \end{bmatrix} \begin{bmatrix} I_L \\ V_G \end{bmatrix} \tag{3.7}$$

Where,

V_L, I_L are the voltage and current vectors at the load buses

V_G, I_G are the voltage and current vectors at the generator buses

$Z_{LL}, K_{GL,} F_{LG,} Y_{GG}$ are the sub-matrices of the hybrid matrix H.

The H matrix can be evaluated using a partial inversion of the Y bus matrix, where the voltages at the load buses are exchanged against their currents. This representation can then be used to define a voltage stability indicator at each load bus:

$$L_j = \left| 1 + \frac{\underline{V}_{0j}}{\underline{V}_j} \right| \tag{3.8}$$

Where,

$$\underline{V}_{0j} = -\sum_{i \in G} \underline{F}_{ji} \underline{V}_i \tag{3.9}$$

Thus, the index can also be expressed in power terms as following:

$$\mathrm{L_j} = \left| \frac{\underline{S}_{j+}}{\underline{Y}_{jj+}{}^{*} V_j^2} \right| \tag{3.10}$$

where $\underline{S}_{j+} = \underline{S}_j + \underline{S}_{jcorr}$, * indicates the complex conjugate of the vector,

$$\underline{S}_{jcorr} = \left(\sum_{\substack{i \in Loads \\ i \neq j}} \frac{\underline{Z}_{ji}{}^{*}}{\underline{Z}_{jj}{}^{*}} \frac{\underline{S}_i}{\underline{V}_i} \right) \underline{V}_j \tag{3.11}$$

and,

$$\underline{Y}_{jj+} = \frac{1}{\underline{Z}_{jj}} \tag{3.12}$$

The complex term S_{jcorr} represents the contributions of the other loads in the system to the index evaluated at node *j*.

When a load bus approaches a collapse point, the index value is 1. The nodes with the higher value are considered the weaker buses of the system.

3.2.1.2. Voltage Collapse Index (VCI)

This index has been taken from [23], but the notation of VSI has been changed to VCI (voltage collapse index) as in [13] in order to distinguish it from the general reference to other voltage stability indices. The index derives from the observation that when the load apparent power changes, load voltage and current change as well to satisfy the relationship:

$$S_i = V_i I_i \tag{3.13}$$

Using Taylor's theorem, the relationship between incremental changes in V_i and I_i due to incremental change in S_i can be written as:

$$\Delta S_i = \frac{\partial S_i}{\partial I_i}\Delta I_i + \frac{\partial S_i}{\partial V_i}\Delta V_i + higher\ order\ terms \tag{3.14}$$

Taking into account eq. 3.13, where the magnitude of load apparent power S_i is the product of load voltage magnitude and load current magnitude, and neglecting higher order terms, eq. 3.14 can be written as:

$$\Delta S_i = V_i \Delta I_i + I_i \Delta V_i \tag{3.15}$$

When the load of a bus approaches the critical value ΔS_i approaches zero. Therefore, to assure stability:

$$0 \leq V_i \Delta I_i + I_i \Delta V_i \tag{3.16}$$

If eq.3.16 is divided by $V_i \Delta I_i$:

$$0 \leq 1 + \frac{I_i \Delta V_i}{V_i \Delta I_i} \tag{3.17}$$

Then, a VSI at a bus *i* is defined by:

$$VCI_i = \left[1 + \frac{I_i \Delta V_i}{V_i \Delta I_i}\right]^{\alpha} \tag{3.18}$$

At no load, VCI equals unity and at the voltage collapse point its value is zero. This evaluation of this VSI is very simple and it only requires the magnitude of bus voltage and load current at two different operating points. It is raised to a power of α (>1) in order to give a more or less linear characteristic to the index. The value of α may depend on the system.

3.2.1.3. Stability Index (SI)

In [21], a voltage stability index for radial distribution networks is presented. Given a two-bus distribution system like the one in Fig. 3.3:

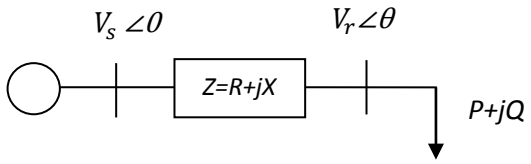

Fig. 3.3 Two-bus system

Then, the a VSI is defined as,

$$\mathrm{SI(r)} = 2\mathrm{V_s^2V_r^2} - \mathrm{V_r^4} - 2\mathrm{V_r^2(PR + QX)} - \mathrm{|Z|^2(P^2 + Q^2)} \tag{3.19}$$

After the load flow study, the voltages of all nodes and the branch currents are known, then P and Q can be calculated at the receiving end of each line and finally eq. 3.19 can be easily computed. It is considered that the node with the minimum value of the stability index is the most sensitive to voltage collapse.

This VSI has been developed from the mostly used quadratic equation to calculate the line sending end voltages in load flow analysis which can be written as:

$$\mathrm{V_r^4} + 2\mathrm{V_r^2(PR + QX)} - \mathrm{V_s^2V_r^2} + \mathrm{(P^2 + Q^2)|Z|^2} = 0 \tag{3.20}$$

From eq. 3.20, line receiving end active and reactive power can be written as:

$$P = (-\cos\theta V_r^2 \pm \sqrt{cos^2\theta V_r^4 - V_r^4 - \mathrm{|Z|^2Q^2} - 2\mathrm{V_r^2QX} + \mathrm{V_s^2V_r^2}})/\mathrm{|Z|} \tag{3.21}$$

$$Q = (-\sin\theta V_r^2 \pm \sqrt{sin^2\theta V_r^4 - V_r^4 - \mathrm{|Z|^2P^2} - 2\mathrm{V_r^2PR} + \mathrm{V_s^2V_r^2}})/\mathrm{|Z|} \tag{3.22}$$

The condition for the solution existence is therefore:

$$cos^2\theta V_r^4 - V_r^4 - \mathrm{|Z|^2Q^2} - 2\mathrm{V_r^2QX} + \mathrm{V_s^2V_r^2} \geq 0 \tag{3.23}$$

$$sin^2\theta V_r^4 - V_r^4 - \mathrm{|Z|^2P^2} - 2\mathrm{V_r^2PR} + \mathrm{V_s^2V_r^2} \geq 0 \tag{3.24}$$

The sum of both equations is then,

$$2\mathrm{V_s^2V_r^2} - \mathrm{V_r^4} - 2\mathrm{V_r^2(PR + QX)} - \mathrm{|Z|^2(P^2 + Q^2)} \geq 0 \tag{3.25}$$

which is the VSI previously described.

3.2.2. Line stability indices

Most of line stability indices are formulated based on the power transmission concept in a single line. A single line in an interconnected network is illustrated in Fig. 3.4

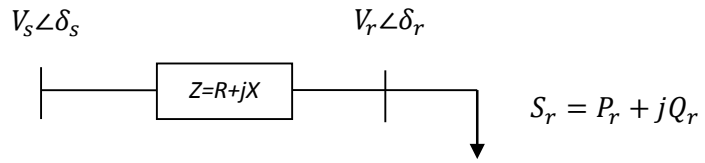

Fig. 3.4 Two bus system

Where,

V_s *and* V_r are the sending end and receiving end voltages, respectively.

δ_s *and* δ_r are the phase angle at the sending and receiving buses.

Z is the line impedance.

R is the line resistance.

X is the line reactance.

θ is the line impedance angle.

Q_r is the reactive power at the receiving end.

P_r is the active power at the receiving end.

3.2.2.1. Lmn Index

This index proposed in [24] is based on the concept of power flow through a single line and adopting the technique of reducing a power system network into a single line.

From the power flow equations,

$$S_r = \frac{|V_s||V_r|}{Z}\angle(\theta - \delta_s + \delta_r) - \frac{|V_r|^2}{Z}\angle\theta \tag{3.26}$$

If this equation is separated in real and reactive power, then,

$$P_r = \frac{V_s V_r}{Z}cos(\theta - \delta_s + \delta_r) - \frac{{V_r}^2}{Z}cos\theta \tag{3.27}$$

$$Q_r = \frac{V_s V_r}{Z}sin(\theta - \delta_s + \delta_r) - \frac{{V_r}^2}{Z}sin\theta \tag{3.28}$$

Defining $\delta = \delta_s - \delta_r$ and solving eq. for V_r, then,

$$V_r = \frac{V_s sin(\theta-\delta) \pm \{[V_s sin(\theta-\delta)]^2 - 4ZQ_r sin\theta\}^{0.5}}{2sin\theta} \tag{3.29}$$

If we substitute $Zsin\theta = X$ and consider the condition that the value of the square root has to be positive,

$$[V_s sin(\theta - \delta)]^2 - 4Q_r X \geq 0 \tag{3.30}$$

Or otherwise,

$$L_{mn} = \frac{4XQ_r}{[V_s \sin(\theta-\delta)]^2} \leq 1 \tag{3.31}$$

This VSI is used to find the stability index for each line connection between two bus bars in an interconnected network. As long as L_{mn} remains less than 1 the system is stable.

3.2.2.2. Line Voltage Stability Index (LVSI)

A similar index is proposed in [42], but from the viewpoint of the relationship between the lines reactive power and the bus voltage at the sending end. The index is defined as:

$$\text{LVSI} = \frac{4rP_r}{[V_s \cos(\theta - \delta)]^2} \leq 1$$

3.2.2.3. LQP Index

This index defined in [25] uses the same concept as in the previous index Lmn. Using the same notation, the proposed index is calculated as following:

$$LQP = 4\left(\frac{X}{V_i^2}\right)\left(\frac{X}{V_i^2}P_i^2 + Q_j\right) \tag{3.32}$$

3.2.2.4. Fast Voltage Stability Index (FVSI)

This index proposed by [26] stands for Fast Voltage Stability Index (FVSI) and it is also based on the concept of power flow through a single line. It is developed starting by taking the sending bus as the reference and using the general current equation:

$$I = \frac{V_s\angle 0 - V_r\angle \delta}{R + jX} \tag{3.33}$$

The roots for the receiving voltage can be written as:

$$V_r = \frac{\left(\frac{R}{X}\sin\delta + \cos\delta\right)V_s \pm \sqrt{\left[\left(\frac{R}{X}\sin\delta + \cos\delta\right)V_s\right]^2 - 4\left(X + \frac{R^2}{X}\right)Q_r}}{2} \tag{3.34}$$

To obtain real roots for V_r, the discriminant has to be set greater than or equal to zero, then:

$$\frac{4Z^2 Q_r X}{{V_s}^2 (R sin\delta + X cos\delta)^2} \leq 1 \tag{3.35}$$

Since the angle difference is normally very small, the following simplification is done:

$$\delta \approx 0 \ \rightarrow sin\delta = 0 \ \& \cos\delta = 1 \tag{3.36}$$

Then a stability index is calculated as:

$$FVSI_{sr} = \frac{4Z^2 Q_r}{V_S^2 X} \tag{3.37}$$

The line that exhibits FVSI closest to 1 is the weakest of the system.

3.2.2.5. Voltage Collapse Point Indicators (VCPI)

The Voltage Collapse Point Indicators (VCPI) proposed in [27] are based on the concept of maximum power transferred through a line.

$$VCPI(1) = \frac{P_r}{P_{r(\max)}} \tag{3.38}$$

$$VCPI(2) = \frac{Q_r}{Q_{r(\max)}} \tag{3.39}$$

The numerator is the real or reactive power transferred to the receiving end and it depends on system parameters, network topology, interconnections and load demand of the system. The denominator is the maximum power that can be transferred to the receiving end at a particular instant. It can be calculated the following way:

$$P_{r(\max)} = \frac{V_S^2}{Z} \frac{cos\Phi}{4cos^2(\frac{\theta-\Phi}{2})} \tag{3.40}$$

$$Q_{r(\max)} = \frac{V_S^2}{Z} \frac{sin\Phi}{4cos^2(\frac{\theta-\Phi}{2})} \tag{3.41}$$

where Φ is the load impedance $\Phi = \tan^{-1}(Q_r/P_r)$.

3.3. Table summary

In order to give the reader a clear overview on the voltage stability indices presented in this chapter a table summary has been included (Fig.3.5). This table presents the indices classified with the reference to their original publication, the formulas to compute them and their stability condition.

Type	Name		Publication	Index Calculation	Unstable condition	Stable condition
Jacobian -based VSI	Test function		[16]	$t_{cc} = \left\| e_c^T J J_{cc}^{-1} e_c \right\|$	Quadratic shape	Linear shape
	Second order index		[17]	$i = \frac{1}{i_0} \frac{\sigma_{\max}}{d\sigma_{\max} / d\lambda_{total}}$	i = 0	0 < i ≤ 1
	Tangent vector		[19]	$TVI_i = \left\| \frac{dV_i}{d\lambda} \right\|^{-1}$	$TVI_i \to 0$	$TVI_i \neq 0$
	V/V0		[20]	V/V0	V/V0 → 0	V/V0 → 1
System variable-based VSI	Bus	L index	[22]	$L_j = \left\| \frac{S_{j+}^*}{Y_{jj+} V_j^2} \right\|$	L=1	L<1
		VCI	[23]	$VCI_i = \left[1 + \frac{I_i \Delta V_i}{V_i \Delta I_i} \right]^{\alpha}$	VCI=0	0 < VCI ≤ 1
		SI	[21]	$SI(r) = 2V_s^2 V_r^2 - V_r^4 - 2V_r^2 (PR + QX) - \lvert Z \rvert^2 (P^2 + Q^2)$	SI<0	SI≥0
	Line	Lmn	[24]	$L_{mn} = \frac{4XQ_r}{[V_s \sin(\theta - \delta)]^2}$	$L_{mn} > 1$	$L_{mn} \leq 1$
		LQP	[25]	$LQP = 4\left(\frac{X}{V_i^2}\right)\left(\frac{X}{V_i^2} P_i^2 + Q_j\right)$	$LQP > 1$	$LQP \leq 1$
		FVSI	[26]	$FVSI_{sr} = \frac{4Z^2 Q_r}{V_s^2 X}$	$FVSI > 1$	$FVSI \leq 1$
		VCPI	[27]	$VCPI(1) = \frac{P_r}{P_{r(\max)}}$	$VCPI > 1$	$VCPI \leq 1$

Fig. 3.5 Table summary

4. PMU-based voltage stability analysis

The development of phasor measurement technology together with other advances in computational facilities, networking infrastructure and communications has opened new perspectives for wide-area monitoring and control [29]. This fact has enabled the development of new methods for assessing voltage stability. This chapter will firstly present phasor measurements units and its characteristics and secondly, will deal with the different methods that have evolved using this technology.

4.1. Synchrophasors and phasor measurement units

An AC waveform can be mathematically represented by the following equation:

$$x(t) = X_m cos(\omega t + \varphi) \tag{4.1}$$

where:

X_m is the magnitude of the sinusoidal waveform

ω is the angular frequency given by $\omega = 2\pi f$ and f being the frequency in Hz

φ is the angular starting point for the waveform.

The representation of power system sinusoidal signals is commonly done in phasor notation. The waveform is then represented as $\underline{X} = X_m \angle\varphi$. The phasor representation of a sinusoid is independent of its frequency and the phase angle φ of the phasor is determined by the starting time (t= 0) of the sinusoid.

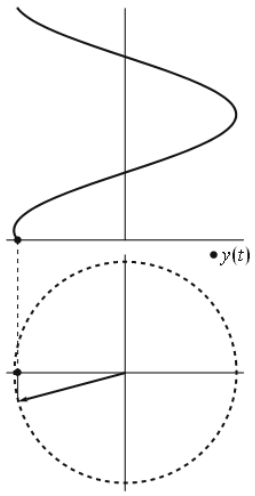

Fig. 4.1 Phasor representation of waveforms

The standard [28] defines the *synchronized phasors* (or synchrophasor) as a complex number representation of the fundamental frequency component of either a voltage or a current, with a time label defining the time instant for which the phasor measurement is performed. The synchrophasor representation *X* of a signal x(t) is the complex value given by:

$$X = X_r + jX_i = \left(\frac{X_m}{\sqrt{2}}\right)\left(e^{j\varphi}\right) = \left(\frac{X_m}{\sqrt{2}}\right)(cos\ \varphi\ +\ j\ sin\ \varphi) \tag{4.2}$$

where $\left(\frac{X_m}{\sqrt{2}}\right)$ is the RMS (Root Mean Square) value of the signal x(t) and φ is its instantaneous phase angle relative to a cosine function at nominal system frequency synchronized to universal time coordinated (UTC).

Note that the synchrophasor standard defines the phasor refered to the RMS value. Therefore, it should be taken into account that $\sqrt{2}$ should be multiplied to the synchrophasor value when computing the actual phasor magnitude.

Phasor Measurement Units (PMUs) units are devices that provide real time measurement of positive sequence voltages and currents at power system substations. Typically the measurement windows are one cycle of the fundamental frequency. Through the use of integral GPS (Global Positioning System) satellite receiver-clocks, PMUs sample synchronously at selected locations throughout the power system. Data from substations are collected at a suitable site, and by aligning the time stamps of the measurements a coherent picture of the state of the power system is created [46]. Therefore a wide implementation of PMU offers new opportunities in power system monitoring, protection, analysis and control.

The commercialization of PMU together with high-speed communications networks makes it possible to build wide area monitoring systems (WAMSs), which takes snapshots of the power system variables within one second and provides new perspectives for early detection and prevention of voltage instability. As stated in [29], PMU-based voltage instability monitoring can be classified in two broad categories: methods based on local measurements and methods based on the observability of the whole region. The first, need few or no information exchange between the monitoring locations, while the second one requires time-synchronized measurements. The following sections will provide information on both types and will expose different methods of each type.

4.2. Methods based on local measurements

PMU-methods based on local measurements, can be implemented in a distributed manner and require few or no information exchange between monitoring locations. These methods accommodate the time skew of SCADA data and no time synchronization is needed [29]. Most of these methods rely on the Thevenin impedance matching condition or its extensions and are based on the assumption that voltage instability is closely related to maximum loadability of a transmission network. Figure 4.1 shows a load bus and the rest of the system treated as a Thevenin equivalent.

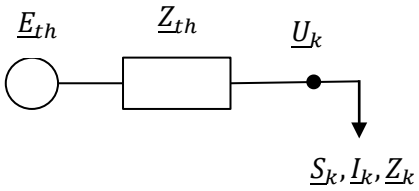

Fig. 4.1 Load bus Thevenin equivalent [43]

The receiving and sending currents for the power system as shown in Fig. 4.1 are

$$\frac{\underline{S}_k}{\underline{U}_k} = \underline{I}_k{}^* = \left(\frac{\underline{E}-\underline{U}_k}{\underline{Z}_{Th}}\right)^* \tag{4.3}$$

Equation (4.2) can be written as follows:

$$(\underline{E} - \underline{U}_k)^* \underline{U}_k - \underline{S}_k \underline{Z}_{Th}{}^* = 0 \tag{4.4}$$

For a given power $\underline{S}_k$, the phasor equation (4.3) permits at most two voltage solutions $\underline{U}_k$. Maximum power transfer occurs when these solutions become equal:

$$(\underline{E} - \underline{U}_k)^* = \underline{U}_k \tag{4.5}$$

Equation (4.4) leads to the following result:

$$|\underline{Z}_k| = |\underline{Z}_{Th}| \tag{4.6}$$

Therefore, when the magnitude of the load impedance becomes equal to the magnitude of the Thevenin's impedance, the system reaches the maximum deliverable power. The impedance $\underline{Z}_k$ is the ratio between the voltage $\bar{V}$ and current $\bar{I}$ phasors measured at the bus through PMU. When the loading is normal, $|\underline{Z}_k| \gg |\underline{Z}_{Th}|$ and are equal at the point of collapse. Therefore, calculating the distance between $\underline{Z}_k$ and $\underline{Z}_{Th}$ can be used as a voltage stability index to assess the closeness to voltage instability. This section will present both, on one hand, different methods to calculate the Thevenin equivalent and on the other hand, indices or criterions used once the equivalent is calculated to assess proximity to instability. The first three sections will deal with calculating the Thevenin equivalent, which can be done by least square method, though the use of both ends of a transmission corridor or using an approximation. The following sections will present voltage stability indices or margins that can be used once the Thevenin is computed.

4.2.1. Thevenin equivalent using least-square method

In [33], the measurements collected from one load bus are used to obtain the Thevenin equivalent of the system seen from the bus, as well as the impedance of the load. Therefore, it must use successive measurements and the parameters of the Thevenin are estimated using a least-square method once a couple of sets of measurements are available.

Considering the circuit in Figure 4.1

$$E_t = V + Z_t I \tag{4.7}$$

Where

$$E_t = E_{t,r} + jE_{t,i}, Z_t = R_t + jX_t \tag{4.8}$$

$$V = V_r + jV_i, I = I_r + jI_i \tag{4.9}$$

Assuming that the phasor measurements taken at time sample k are

$$V = V_{rk} + jV_{ik}, I = I_{rk} + jI_{ik} \tag{4.10}$$

Equations (4.3) can be written in matrix form as:

$$y_k = H_k x_k \tag{4.11}$$

where

$$x_k = \begin{bmatrix} E_{t,rk} \\ E_{t,ik} \\ R_{tk} \\ X_{tk} \end{bmatrix}; y_k = \begin{bmatrix} V_{rk} \\ V_{ik} \end{bmatrix}; H_k = \begin{bmatrix} 1 & 0 & -I_{rk} & I_{ik} \\ 0 & 1 & -I_{ik} & -I_{rk} \end{bmatrix} \tag{4.12}$$

With the sequences of voltage and current phasor measurements the Thevenin parameters can be estimated using the recursive least square (RLS) method:

$$x_k = x_{k-1} + G_k(y_k - H_k^T x_{k-1}) \tag{4.13}$$

$$G_k = P_{k-1}H_k(\lambda I + H_k^T P_{k-1} H_k)^{-1} \tag{4.14}$$

$$P_k = \frac{1}{\lambda}(I - G_k H_k^T)P_{k-1} \tag{4.15}$$

The relation between the calculated $\underline{Z}_k$ and $\underline{Z}_{Th}$ is then used as an index to assess how close the system is to collapse.

The weakness of this method is that it requires successive measures from the same load bus and making the assumption that the Thevenin equivalent remains constant in these successive measures.

4.2.2. Thevenin equivalent-Transmission corridors

This method, taken from [36], obtains the Thevenin equivalent using measurements taken at a single line but from both ends of the transmission corridor. This way the time delay of least-square estimation is avoided.

The method calculates the Thevenin equivalent in two steps as seen in Fig. 4.2.

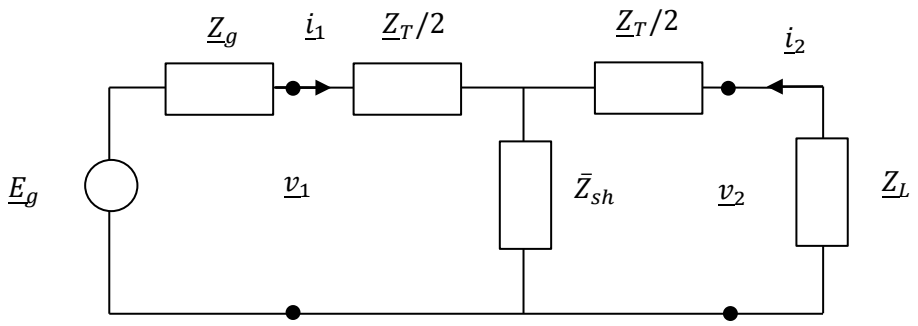

Fig. 4.2 First step calculation

First, the parameters of a T-equivalent of the transmission corridor can be determined through a direct calculation from the PMU measurements $\bar{v}_1, \bar{v}_2, \bar{\imath}_1, \bar{\imath}_2$:

$$\bar{Z}_T = 2\frac{\bar{v}_1 - \bar{v}_2}{\bar{\imath}_1 - \bar{\imath}_2} \tag{4.16}$$

$$\bar{Z}_{sh} = \frac{\bar{v}_1\bar{\imath}_2 - \bar{v}_2\bar{\imath}_1}{\bar{\imath}_2{}^2 - \bar{\imath}_1{}^2} \tag{4.17}$$

$$\bar{Z}_L = \frac{\bar{v}_2}{-\bar{\imath}_2} \tag{4.18}$$

$\bar{Z}_g$is assumed to be known since it typically comprises the step-up transformers and short transmission line to the beginning of the transmission corridor and $\bar{E}_g$is calculated as:

$$\bar{E}_g = \bar{v}_1 + \bar{Z}_g\bar{\imath}_1 \tag{4.19}$$

Then, the second step calculates the Thevenin equivalent shown in Fig. 4.3.

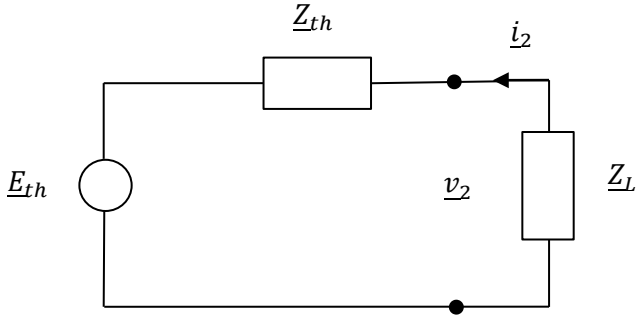

Fig. 4.3 : Second step calculation

The equations used to compute the voltage and impedance equivalent are the following:

$$\bar{Z}_{th} = \frac{\bar{Z}_T}{2} + \frac{1}{\frac{1}{\bar{Z}_{sh}} + \frac{1}{\frac{\bar{Z}_T}{2} + \bar{Z}_g}} \tag{4.20}$$

$$\bar{E}_{th} = v_2\frac{\bar{Z}_{th} + \bar{Z}_L}{\bar{Z}_L} \tag{4.21}$$

Based on this Thevenin equivalent, stability analysis can then be performed. In terms of load impedance in percentage, stability margin can be expressed as:

$$MARGIN_Z = 100(1 - k_{crit}) \tag{4.22}$$

$$k_{crit} = \left|\frac{\bar{Z}_{th}}{\bar{Z}_L}\right| \tag{4.23}$$

4.2.3. Thevenin equivalent-Approximate approach

The buses in an interconnected power system can generally be classified into three categories: generator bus, load bus and tie bus (without generators and loads connecting to it). A generator bus will become a load bus if its power capacity limit is reached. Since the injection currents to the tie buses are zero, the injection currents into the three types of buses can be generally expressed as [45],

$$\begin{bmatrix} -i_L \\ 0 \\ i_G \end{bmatrix} = \begin{bmatrix} Y_{LL} & Y_{LT} & Y_{LG} \\ Y_{TL} & Y_{TT} & Y_{TG} \\ Y_{GL} & Y_{GT} & Y_{GG} \end{bmatrix} \begin{bmatrix} v_L \\ v_T \\ v_G \end{bmatrix} \tag{4.24}$$

where the Y matrix is known as the system admittance matrix, V and I stand for the voltage and current vectors, and the subscript L, T and G represent load bus, tie bus and generator bus, respectively.

According to (4.23), the load bus voltages can be expressed as

$$V_L = E_{open} - Z_{LL} I_L \tag{4.25}$$

where

$$Z_{LL} = (Y_{LL} - Y_{LT} Y_{TT}^{-1} Y_{TL})^{-1} \tag{4.26}$$

$$E_{open} = Z_{LL}(Y_{LT} Y_{TT}^{-1} Y_{TG} - Y_{LG}) V_G \tag{4.27}$$

Then, (4.24) can be rewritten as

$$V_{Li} = E_{open,i} - Z_{LLii} \mathrm{I}_{Li} - \sum_{i=1, i \neq j}^{N} Z_{LLji} \mathrm{I}_{Lj} \tag{4.28}$$

where Z_{LLii} denotes the ith diagonal element of Z_{LL}, Z_{LLji} is the i–j element of Z_{LL}, $E_{open,i}$ is the open-circuit voltage of load i, n is the number of load buses, and V_{Li} and I_{Li} are the voltage and current of load i, respectively.

In (4.27), V_{Li} consists of three terms: the open-circuit voltage, the voltage related to the self-impedance Z_{LLii} and the coupling voltage related to the mutual-impedance Z_{LLji}, which represents the impact of other loads on load i [45].

In [45] an approximate approach is presented to combine the coupling term with the open-circuit voltage to form the equivalent voltage, which is shown Fig. 4.4.

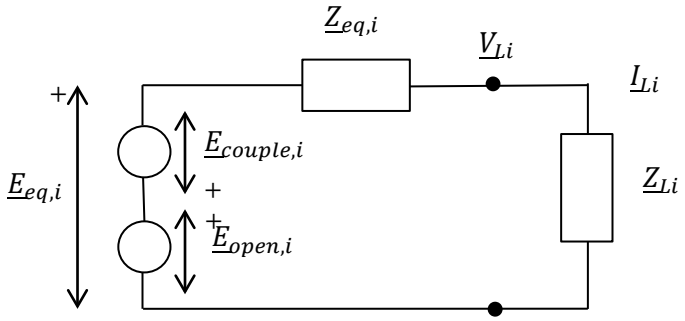

Fig. 4.4 Equivalent circuit combining the coupling voltage with the open voltage [45]

The equivalent is written as:

$$E_{eq,i} = E_{open,i} - E_{couple,i} \tag{4.29}$$

where

$$E_{couple,i} = \sum_{i=1,i\neq j}^{N} Z_{LLji} \mathrm{I}_{Lj} \tag{4.30}$$

Then, the following equivalent equation is obtained

$$V_{Li} = E_{eq,i} - Z_{eq} \mathrm{I}_{Li} \tag{4.31}$$

where

$$Z_{eq} = Z_{LLii} \tag{4.32}$$

With this approach, Z_{eq} is calculated though the network parameters and it is constant if the network topology, transformer and line parameters and generator's bus types do not change. Then, $E_{eq,i}$ is computed using equation (4.30). The advantage of this method is that it only requires one-time measurement using the voltage and current gathered from the PMU at the studied load bus.

4.2.4. Voltage Instability Predictor (VIP)

In [34], the same concept as in least-square method is used but proximity in expressed in terms of power margin. The VIP method also tracks the distance between $\underline{Z}_k$ and $\underline{Z}_{Th}$. Since the proximity to instability in terms of distance between two voltage curves or impedance curves is not intuitive, a more useful measure is proposed. The VIP measures the proximity to collapse in terms of power margin.

The power margin is expressed as:

$$\Delta S = \frac{(V_k - Z_{Th} I_k)^2}{4 Z_{Th}} \tag{4.33}$$

A problem with the VIP method is the same as in the RLS method since the Thevenin equivalent seen from any given bus is not observable. There are more unknowns than there

are equations, which mean that there is an infinite set of Thevenin equivalents that could all produce the same results as the one that is observed. This is solved by taking measurements at two or more different times, and treating the Thevenin equivalent as a constant.

4.2.5. Voltage Stability Load Bus Index (VSLBI)

In [37], the Thevenin equivalent is calculated using the RLS method explained in section 4.2.1 and then a voltage stability load bus index (VSLBI) is defined as:

$$VSLBI_k = \frac{|V_i(k)|}{|\Delta V_i(k)|} \tag{4.34}$$

Where $V_i(k)$ is the amplitude of the load bus voltage i at time step k and $\Delta V_i(k) = Z_{Th,k} I_k$ is the voltage drop across the Thevenin equivalent impedance Z_{Th}. If the value approaches 1, the system may be close to instability. This index can be calculated in each load bus and then a system voltage stability index can be defined as the smallest of all VSLBI:

$$VSI = \min_{i \in \alpha_{PQ}} VSLBI_{i,k} \tag{4.35}$$

4.2.6. S Difference Criterion (SDC)

The S difference criterion (SDC) method proposed in [38] and [39] uses consecutive measurements of the apparent power S in a line's relay points. It is based in the fact that in the vicinity of voltage instability an increase in the apparent power flow at the sending end of the line no longer yields an increase in the received power. Therefore, at the voltage instability point, $\Delta \bar{S} = 0$.

The apparent power supplied at the receiving end can be written as:

$$\bar{S}_{j,k} = \bar{U}_{j,k} \bar{I}_{ji,k}^{\ *} \tag{4.36}$$

An increase in the apparent power loading in the time interval between t_k and $t_{k+1} = t_k + \Delta t$ is:

$$\bar{S}_{j,k+1} = \bar{S}_{j,k} + \Delta \bar{S}_{j,k+1} = \left(\bar{U}_{j,k} + \Delta \bar{U}_{j,k+1}\right)\left(\bar{I}_{ji,k} + \Delta \bar{I}_{ji,k+1}\right)^* =$$

$$\bar{S}_{j,k} + \Delta \bar{U}_{j,k+1} \bar{I}_{ji,k}^{\ *} + \bar{U}_{j,k} \Delta \bar{I}_{ji,k+1}^{\ *} + \Delta \bar{U}_{j,k+1} \Delta \bar{I}_{ji,k+1}^{\ *} \tag{4.37}$$

The term $+\Delta \bar{U}_{j,k+1} \Delta \bar{I}_{ji,k+1}^{\ *}$ can be neglected, since it represents a very small value.

Then,

$$\Delta \bar{S}_{j,k+1} = \Delta \bar{U}_{j,k+1} \bar{I}_{ji,k}^{\ *} + \bar{U}_{j,k} \Delta \bar{I}_{ji,k+1}^{\ *} \tag{4.38}$$

Since it is known that $\Delta \bar{S}_{j,k+1} = 0$ at the point of collapse, an index can be defined dividing Equation (4.23) by $\bar{U}_{j,k} \Delta \bar{I}_{ji,k+1}^{\ *}$:

$$SCD = 1 + \frac{\Delta\bar{U}_{j,k+1}\bar{I}_{ji,k}^{*}}{\bar{U}_{j,k}\Delta\bar{I}_{ji,k+1}^{*}} = 1 + ae^{j\varphi} \quad (4.39)$$

4.3. Methods based on the observability of the whole region

On the other hand, PMU-methods based on the observability of the whole region require time-synchronized measurements and offer the potential advantages of wide-area monitoring [29].

4.3.1. Sensitivities

A PMU-method based on the observability of the whole region is presented in [29]-[31]. The work focuses on detecting the onset of voltage instability triggered by a large disturbance. The method fits a set of algebraic equations to the sampled states, computed from PMUs measurements and performs an efficient sensitivity computation, which tracks the eigenvalue movement around a maximum load power point.

As seen in Section 2.3.1, voltage stability can be determined by computing the eigenvalues and eigenvectors of the reduced Jacobian matrix. Given an eigenvalue λ_i of the ith mode of the Q-V response, if it is greater than 0, then the modal voltage and modal reactive power are along the same direction which yields to a voltage stable system. If $\lambda_i < 0$, the modal voltage and modal reactive power are along opposite directions which indicates an unstable system. Therefore, the change of sign of the eigenvalue can indicate the pass from a stable to an unstable point. This fact is used in [28] to assess voltage stability.

It is stated in [29]-[31], that in order to detect this change in sign, there is no need to explicitly compute the eigenvalues. Instead, sensitivities involving the inverse Jacobian can be used.

Given the static model of a power system:

$$0 = g(x, y) \quad (4.40)$$

where x represents the state vector of the system and y, the algebraic variables such as the active and reactive power consumed by the loads.

The sensitivities of the total reactive power generation to individual load reactive powers can be obtained using the following formula:

$$S_{Q_g q} = -g_q^T (g_x^T)^{-1} \nabla_x Q_g \quad (4.41)$$

Where, $\nabla_x Q_g$denotes the gradient of Q_g with respect to x, g_q is the Jacobian of g with respect to q and the load reactive powers are grouped into $q = [Q_1 \dots Q_N]^T$.

Computing $S_{Q_g q}$ requires solving one linear system with g_x^Tas a matrix of coefficients and $\nabla_x Q_g$ as independent term.

4.3.2. Sum of the absolute values Index

The new method developed in [40] relies on measurements taken at current time and it is based on the fact that the amplitude of the complex voltage drop on the Thevenin's impedance is equal to the amplitude of the voltage at the node at the point of maximum loadability, the nose of the PV curve. The assumption made is the generator nearest to a load can give information comparable with the Thevenin's voltage.

The method defines the *distance to a generator* as the sum of the absolute values of the complex voltage drop for each line along the shortest path from a node to the generator. Nearest generator is the one this defined distance is minimum. Only generators that are in PV mode, controlling the active power and voltage at its output, should be considered for this calculation.

The voltage stability index is defined as:

$$VSI_k = \frac{V_k}{\Delta V_k} \tag{4.42}$$

Where V_k is the voltage at node k and ΔV_k is the distance to the nearest generator as described in the paper. This distance approximates the voltage drop across the Thevenin's impedance.

The minimum value of VSI represents the weakest bus of the system. If no assumption were made, it would be one at the maximum loadability point, therefore, a margin should be given, and the real maximum loadability point value will be greater than one.

Weakness of the method is also presented in the paper. Firstly, by using a global index, the location of the problem is not visible and secondly, a bad bus index that does not evolve taken as the global index could hide bad evolutions elsewhere.

4.3.3. Voltage Collapse Proximity Indicator (VCPI)

The technique described in [32] uses the voltage magnitude and voltage angle information at buses provided by PMUs, but also the network admittance matrix to predict proximity to voltage collapse.

The proposed index at bus k is calculated as:

$$VCPI_k = \left| 1 - \frac{\sum_{\substack{m=1 \\ m \neq k}}^{N} V'_m}{V_k} \right| \tag{4.43}$$

Where:

$$V'_m = \frac{Y_{km}}{\sum_{\substack{j=1 \\ j \neq k}}^{N} Y_{kj}} V_m \tag{4.44}$$

V_k is the voltage phasor at bus k

Y_{km} is the admittance between buses k and m

The index varies from 0 to 1, being 1 if the voltage at the bus has collapsed.

4.3.4. Margin Voltage Stability Index (MVSI)

Another method based also on time-synchronized phasor measurements and network parameters is proposed in [10].

The index is based on the maximum transferable power through a transmission line and is expressed as:

$$MVSI = \min\left(\frac{P_{margin}}{P_{max}}, \frac{Q_{margin}}{Q_{max}}, \frac{S_{margin}}{S_{max}}\right) \tag{4.45}$$

where

$$P_{margin} = P_{max} - P \tag{4.46}$$

$$Q_{margin} = Q_{max} - Q \tag{4.47}$$

$$S_{margin} = S_{max} - S \tag{4.48}$$

and

$$P_{max} = \sqrt{\frac{V_s^4}{4X^2} - Q\frac{V_s^2}{X}} \tag{4.49}$$

$$Q_{max} = \frac{V_s^4}{4X} - \frac{P^2 X}{V_s^2} \tag{4.50}$$

$$S_{max} = \frac{(1-sin\theta)V_s^2}{2(cos\theta)^2 X} \tag{4.51}$$

In larger interconnected power systems the equivalent source voltage and equivalent impedance has to be calculated in each bus in order to calculate eq. (), () and (). The system admittance matrix can be calculated as:

$$\begin{bmatrix} i_L \\ i_T \\ i_G \end{bmatrix} = \begin{bmatrix} Y_{LL} & Y_{LT} & Y_{LG} \\ Y_{TL} & Y_{TT} & Y_{TG} \\ Y_{GL} & Y_{GT} & Y_{GG} \end{bmatrix} \begin{bmatrix} v_L \\ v_T \\ v_G \end{bmatrix} \tag{4.52}$$

$$v_L = Z_{LL} i_L + Z_{LT} i_T + H_{LG} v_G \tag{4.53}$$

Where,

$$Z_{LL} = (Y_{LL} - Y_{LT} Y_{TT}^{-1} Y_{TL})^{-1} \tag{4.54}$$

$$Z_{LT} = -Z_{LL} Y_{LT} {Y_{TT}}^{-1} \tag{4.55}$$

$$H_{LG} = Z_{LL}(Y_{LT} Y_{TT}^{-1} Y_{TG} - Y_{LG}) \tag{4.56}$$

Then for a given bus j, the equivalent voltage source and line impedance can be calculated with the following equations:

$$v_{eq_j} = \sum_{k=1}^{M} H_{LGjk} v_{Gk} + \sum_{i=1, i\neq j}^{N} Z_{LLji} \left(\frac{-S_{Li}}{v_{Li}}\right)^{*} \tag{4.57}$$

$$Z_{eqj} = Z_{LLjj} \tag{4.58}$$

The load bus with the lowest MVSI has the smallest load margin and, therefore, is the closest to voltage collapse.

4.4. Table summary

Similar to the previous Fig. 3.5 in chapter 3.3, the table, Fig. 4.5, aims to summarize and offer a general overview of the presented PMU-methods. It uses the adopted classification, local measurements and observability of the whole network. It should be noted that in the local measurements type has been classified in methods to calculate the Thevenin equivalent and actual indices that are used once the Thevenin has been calculated. The original papers that presented these indices used one of the mentioned methods to estimate the Thevenin equivalent.

Type		Name	Ref.	Calculation
Local measurements	Thevenin Calculation	RLS	[33]	$x_k = x_{k-1} + G_k(y_k - H_k^T x_{k-1})$ $G_k = P_{k-1}H_k(\lambda I + H_k^T P_{k-1} H_k)^{-1}$ $P_k = \frac{1}{\lambda}(I - G_k H_k^T)P_{k-1}$
		Transmission corridors	[36]	$\bar{Z}_{th} = \frac{\bar{Z}_T}{2} + \frac{1}{\frac{1}{\bar{Z}_{sh}} + \frac{1}{\frac{\bar{Z}_T}{2} + \bar{Z}_g}}$ $\bar{E}_{th} = v_2 \frac{\bar{Z}_{th} + \bar{Z}_L}{\bar{Z}_L}$
		Approximation	[45]	$E_{eq,i} = E_{open,i} - E_{couple,i}$ $E_{couple,i} = \sum_{i=1, i\neq j}^{N} Z_{LLji} \mathrm{I}_{Lj}$
	Indices	VIP	[34]	$\Delta S = \frac{(V_k - Z_{Th} I_k)^2}{4 Z_{Th}}$
		VSLBI	[37]	$VSLBI_k = \frac{\lvert V_i(k) \rvert}{\lvert \Delta V_i(k) \rvert}$
		SDC	[38]-[39]	$SCD = 1 + \frac{\Delta \bar{U}_{j,k+1} \bar{I}_{ji,k}^*}{\bar{U}_{j,k} \Delta \bar{I}_{ji,k+1}^*}$
Observability of the whole network		Sensitivities	[29]-[31]	$S_{Q_g q} = -g_q^T (g_x^T)^{-1} \nabla_x Q_g$
		Sum of absolute values	[40]	$VSI_k = \frac{V_k}{\Delta V_k}$
		VCPI	[32]	$VCPI_k = \left\lvert 1 - \frac{\sum_{m=1}^{N} V_m'}{V_k} \right\rvert$
		MVSI	[10]	$VSI = \min(\frac{P_{margin}}{P_{max}}, \frac{Q_{margin}}{Q_{max}}, \frac{S_{margin}}{S_{max}})$

Fig. 4.5 PMU-methods table summary

5. Stability Indices and methods comparison

In the previous chapters, different indices and methods to assess voltage stability were presented. Since there has been a large amount of information given, this chapter aims to provide a summary of the indices and methods and present their main characteristics and difference. The three main types of indices were classified in Jacobian matrix-based, System parameters-based and PMU methods. From the system parameters, two subtypes were presented, line and bus indices; and the PMU methods are classified in two subtypes, local measurements and observability.

Jacobian matrix based VSIs can calculate the voltage collapse point or maximum loadability limit and determine the voltage stability margin, for that, the computation time is high; hence, they are not suitable for online assessment. They also present a high nonlinear profile near the voltage collapse point and they do not offer information on weak area or buses of the system, just a general view of the whole system. Therefore, they do not provide enough information to know where in the system there is a problem, and are difficult to use for control purposes.

On the other hand, system variables based VSIs, which use the elements of the admittance matrix and some system variables such as bus voltages or power flow through lines, require less computation and, therefore, are adequate for online monitoring. The disadvantage of these indices is that they cannot accurately estimate the margin, so they can just present critical lines and buses. By ranking the critical lines and buses, decisions on where to place shunt FACTS controllers, as done in [48], can be made. Some studies on how uncertainty affects line indices are pursued in [49], but conclude that more tests should be done in order to draw a general conclusion.

As stated in [29], PMU-based voltage instability monitoring can be classified in two broad categories: methods based on local measurements and methods based on the observability of the whole region. PMU-methods based on local measurements, can be implemented in a distributed manner and require few or no information exchange between monitoring locations. These methods accommodate the time skew of SCADA data and no time synchronization is needed [29]. Most of these methods rely on the Thevenin impedance matching condition or its extensions and are based on the assumption that voltage instability is closely related to maximum loadability of a transmission network. Three methods to compute the Thevenin equivalent are presented: RLS, Transmission corridor method and Approximation method. Once the Thevenin has been computed, there are several indices that can provide information on voltage stability; VSLBI and SLD, among others.

On the other hand, PMU-methods based on the observability of the whole region require time-synchronized measurements and offer the potential advantages of wide-area monitoring [29]. Therefore, the measurements require to be processed in a centralized manner.

Type	Index	Characteristics
Jacobian matrix-based	Test function	Compute the whole network. Centralized measurements. High computational costs. Non-linearity near voltage collapse. Difficult to use for control purposes.
	Second order	
	Tangent vector	
	V/V0	
System variables. Bus indices.	L index	Easy to compute. Small computational costs. Better results in transmission-radial networks than in interconnected networks.
	VCI	
	SI	
System variables. Line indices.	Lmn	Easy to compute. Small computational costs. Good for control purposes: Identifies the weakest line in the network. FACTS placement. Distributed measurements.
	LVSI	
	LQP	
	FVSI	
	VCPI	
PMU-Local measurements	VIP	Distributed measurements and processing. Usable for control purposes.
	VSLBI	
	SDC	
PMU-Observability	Sensitivities	Centralized measurements and processing.
	Sum of absolute value	
	VCPI	
	Margin VSI	

Fig. 5.1 Index classification and comparison

6. Implementation of Voltage Stability Indices and test networks

The software used to simulate the networks is RSCAD, which is the Graphical User Interface of RTDS, a Real-Time Digital Simulator designed to study electromagnetic transient phenomena. Two test networks have been used to implement some of indices presented in previous chapters, a small 5-bus test network and a large 39-bus test network.

This chapter will, firstly, introduce the RTDS and its characteristics; then, a detailed description of both test-networks will be presented, and finally, how the different indices have been implemented will be exposed and what cases have been studied.

6.1. Introduction to RTDS

RTDS stands for Real−Time Digital Simulator and it is designed to study electromagnetic transient phenomena in real−time. RTDS is an effective tool for modelling and simulating power and control systems, and is especially useful for large systems. RTDS is comprised of both specially designed hardware and software.

RTDS hardware (Fig. 6.1) is based on Digital Signal Processor (DSP) and Reduced Instruction Set Computer (RISC), and utilizes advanced parallel processing techniques in order to achieve the computation speeds required to maintain continuous real−time operation [41]. Digital simulators compute the state of the power system model only at discrete instants in time. The time between these discrete instants is referred to as the simulation time−step (Δt). By definition, in order to operate in real−time a 50 μsec time−step would require that all computations for the system solution be complete in less than 50 μsec of actual time.

Fig. 6.1 RTDS hardware at E.ON ACS Institute

In order to realize and maintain the required computation rates for real−time operation, many high speed processors operating in parallel are utilized by the RTDS. Two types of processor cards may be installed in each RTDS rack: 3PC and RPC. The Triple Processor Card (3PC) contains three Analogue Devices ADSP 21062 digital signal processors. The ADSP 21062 DSP clock speed is 40 MHz. The RISC Processor Card (RPC) contains two PowerPC 750CXe RISC processors operating at a clock speed of 600 MHz. The RTDS Simulator can be configured as 3PC only or as a combination of 3PC and RPC [41].

RTDS software includes a Graphical User Interface (GUI), referred to as RSCAD, through which includes a model library of power and control system components. The overall network solution technique employed in RTDS is based on nodal analysis and the algorithms used are those introduced in the paper “Digital Computer Solution of Electromagnetic Transients in Single and Multiphase Networks” by H.W. Dommel, which is used in virtually all digital simulation programs designed for the study of electromagnetic transients [41].

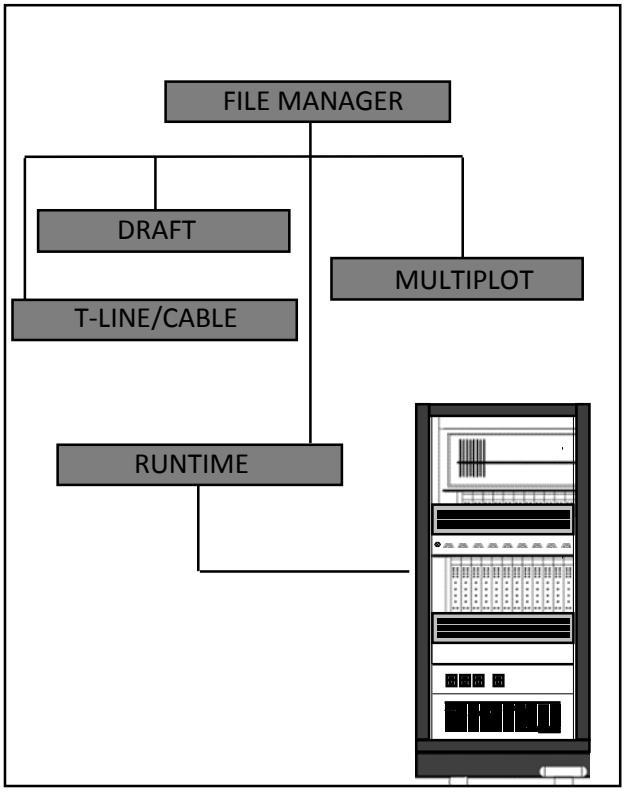

Fig. 6.2 RSCAD Software modules

RSCAD is composed of several modules as shown in Fig.6.2. The File Manager represents the entry point to the RSCAD interface software and it is used for project and case management and facilitates information exchange between RTDS users. The Draft module is used for circuit assembly and parameter entry. The Draft screen is divided into two sections: the library section and the circuit assembly section. The T−Line is used to define the properties of overhead transmission lines and underground cables respectively. The RunTime is used to control the simulation case(s) being performed on the RTDS hardware. Simulation control, including start / stop commands, sequence initiation, set point adjustment, fault application, breaker operation, etc. are performed through the RunTime Operator’s Console.

Additionally, on line metering and data acquisition and disturbance recording functions are available in RunTime. Finally, MultiPlot is used for post processing and analysis of results captured and stored during a simulation study [41].

6.2. 5-bus test system

A first 5-bus test system network taken from [43] was provided by ACS. The network consists of two synchronous generators, two step-up transformers and three constant power loads as depicted in Figure 6.3. Three PMU units are assumed to be installed at all the load buses and measure the voltage and current phasors.

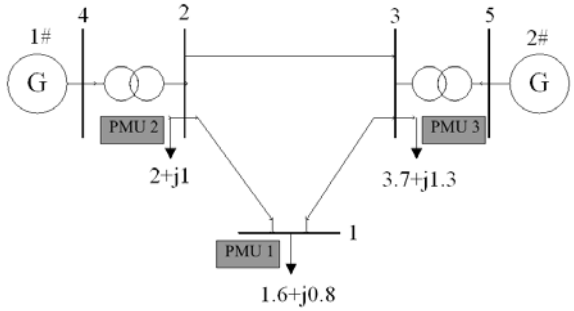

Fig. 6.3 5-bus test network [43]

The reference voltage and the reference power are chosen by 230 kV and 100 MVA, respectively. Two synchronous machines are chosen as the generator model for the power sources at bus 4 and bus 5 with the IEEE Type AC1 excitation system and gas governor control models. The ratios of the step-up transformers are chosen by 13.8/230 kV and its wire style is Y-Δ [43]. The transmission lines are modelled as ideal RLC with the values shown in Fig. 6.4. The system modelled in RSCAD is shown in Fig. 6.5.

Line	From	To	Resistance (Ω)	Reactance (H)
1	2	1	21,16	0,421
2	3	1	52,9	0,589
3	2	3	42,32	0,505
4	4	2	-	0,0252
5	5	3	-	0,505

Fig.6.4 Network data for 5-bus test system

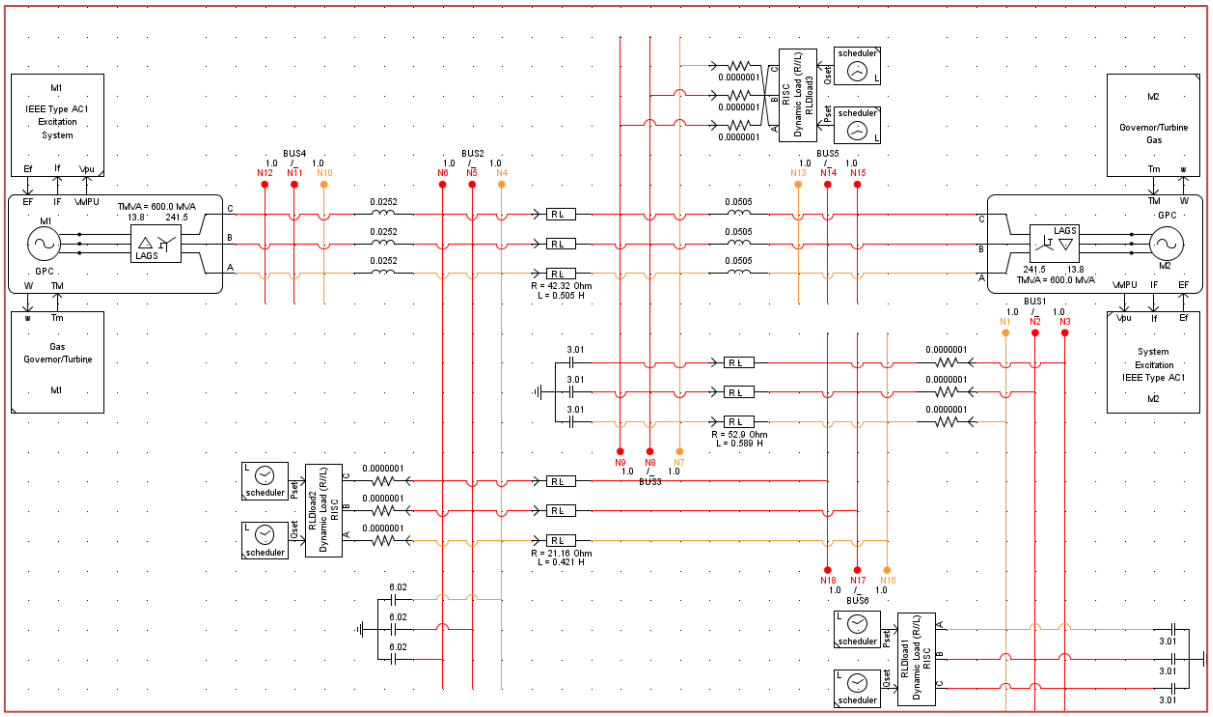

Fig. 6.5 RSCAD Draft of 5-bus test system

6.3. 39-bus test system

The 39-bus system used to implement the different indices is the IEEE 10-Generator 39 Bus System, also known as New-England Power System. The parameters are taken from [47] and the network in RSCAD was provided by ACS. The full system parameters can be found in Appendix A. Fig.6.6 shows the global network diagram and Fig.6.7, some snapshots of the view of the system modelled in RSCAD.

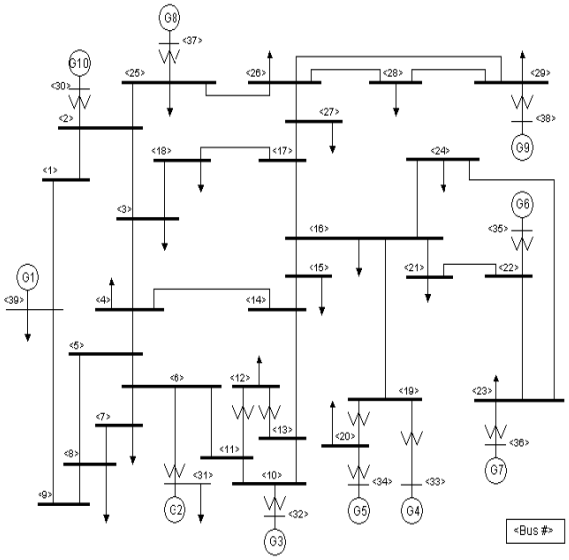

Fig. 6.6 39-bus test network [47]

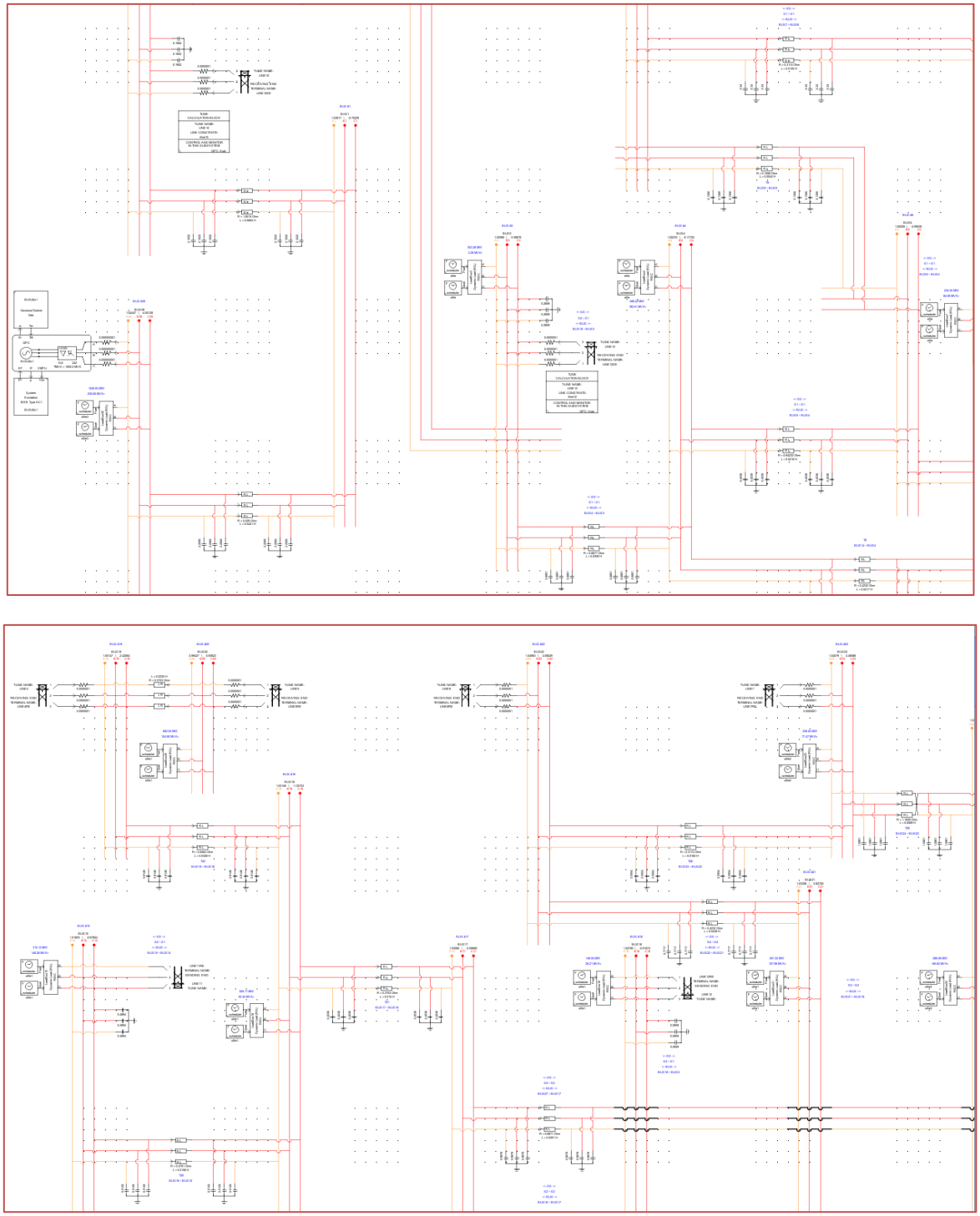

Fig. 6.5 RSCAD Draft of parts of the 39-bus test system

6.4. Index implementation

The implementation of the different voltage stability indices has been done using two different approaches depending on the type of index. For the line stability indices, the implementation was done directly on RTDS using the control components blocks. This

approach allows viewing the indices in RunTime and makes them available to use in control strategy design that could feed the indices results back to the generators.

The second method used to calculate the indices was gathering the data from RTDS RunTime and exporting them into MatLab, where they are computed. This was done for the Jacobian index implementation, since the control blocks were insufficient to calculate it due to their more sophisticated computation. The main code was provided by T. Junjie from ACS and I just adapted it to this Thesis needs.

The following table (Fig.6.5.1) summarizes the computed indices and informs on the method used to compute them.

Index type	Index	Implementation
Jacobian index	Minimum eigenvalue of the Jacobian matrix	RTDS simulation values + MatLab code
Line indices	Lmn	RTDS using the control blocks
	FVSI (with and without approximation)	
	VCPI (p) and VCPI(l)	
	LVSI	
	LQP	

Fig. 6.5.1 Indices and implementation used in each case

6.4.1. Jacobian index implementation

Using the PMU component (Fig.6.6), the magnitude and angle at each node was obtained. The data was saved and loaded in MatLab, where the calculation of the Jacobian matrix is done and the minimum eigenvalue computed. The MatLab code can be found in Appendix B.

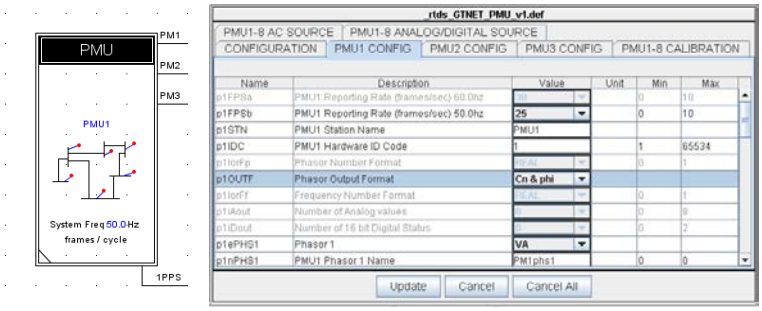

Fig. 6.6 PMU component in Draft

6.4.2. Line index implementation

The line index implementation in RTDS has been done using the control blocks of the library. This implementation allows viewing the indices in RunTime and makes them available to use in control strategy design that could feed the indices results back to the generators.

The following table (Fig.6.7) shows the block diagram of each implemented index using the control components of the RSCAD library.

Index	RSCAD implementation
$L_{mn} = \frac{4XQ_r}{[V_s \sin(\theta - \delta)]^2}$	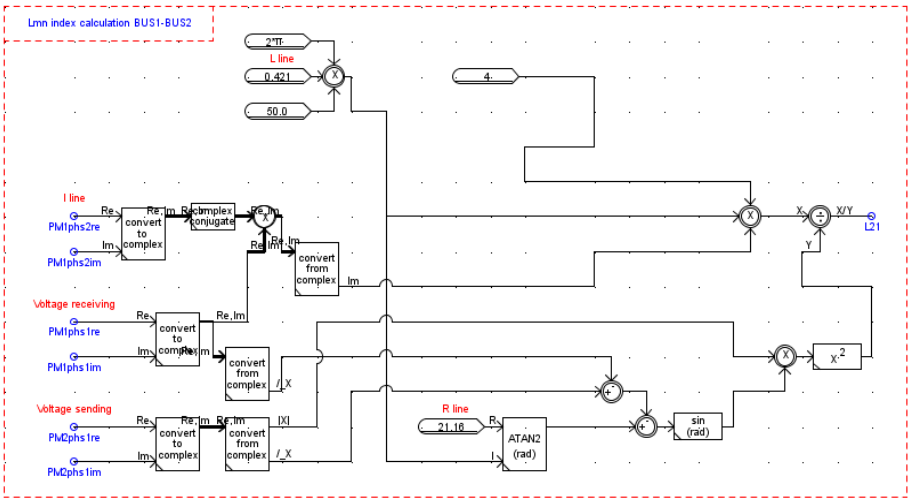
$FVSI_{sr} = \frac{4Z^2Q_r}{V_s^2X}$	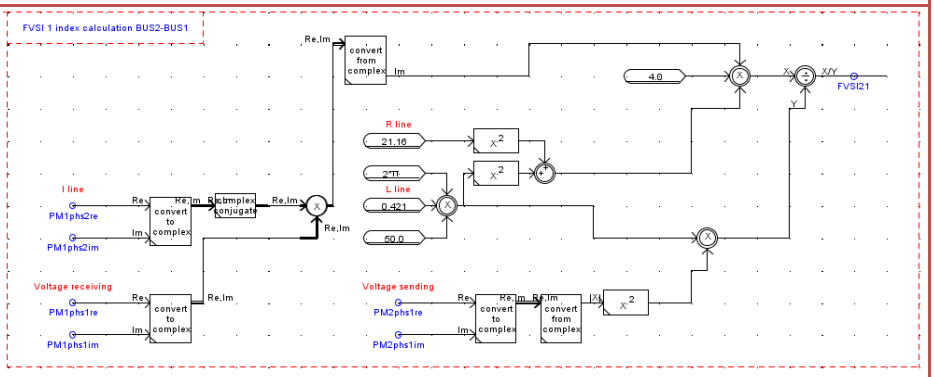
$FVSI_{sr} = \frac{4Z^2XQ_r}{V_s^2(R\sin\delta + X\cos\delta)^2}$	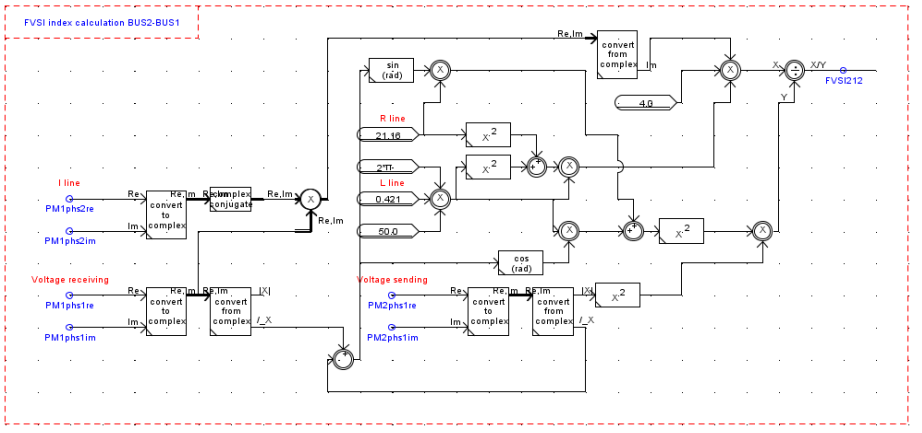

$$VCPI(1) = \frac{P_r}{P_{r(\max)}}$$

$$P_{r(\max)} = \frac{V_s^2}{Z}\frac{cos\Phi}{4cos^2(\frac{\theta-\Phi}{2})}$$

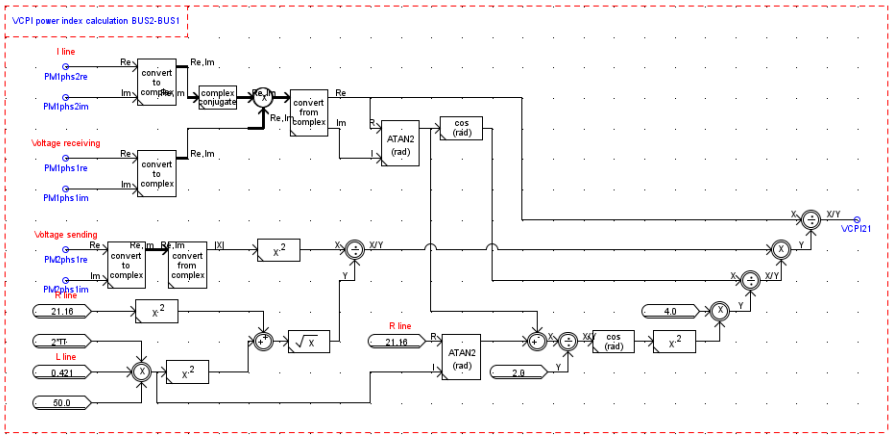

$$VCPI(2) = \frac{P_l}{P_{l(\max)}}$$

$$P_{l(\max)} = \frac{V_s^2}{Z}\frac{cos\theta}{4cos^2(\frac{\theta-\Phi}{2})}$$

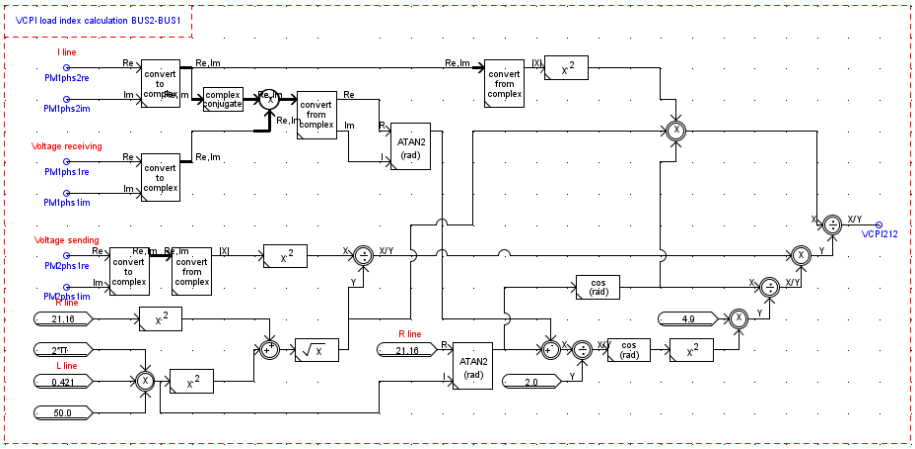

$$\mathbf{LVSI} = \frac{4rP_r}{[V_s\cos(\theta-\delta)]^2}$$

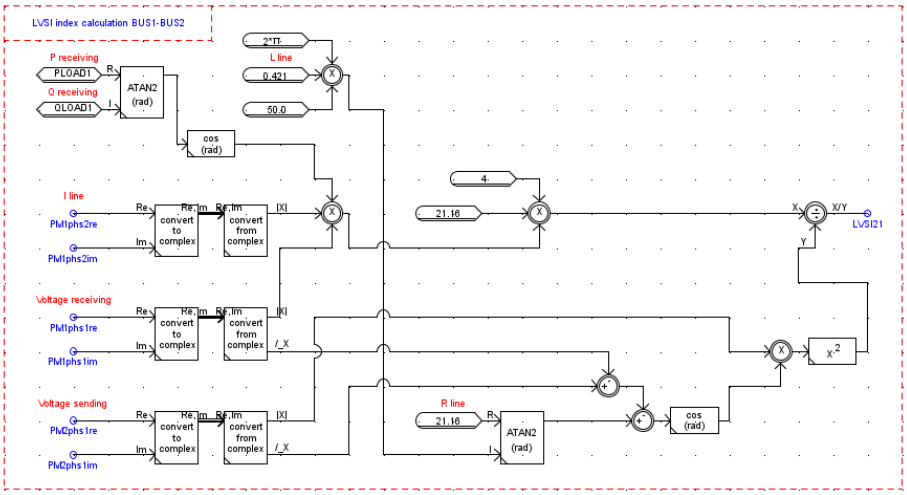

$$LQP = 4\left(\frac{X}{V_i^2}\right)\left(\frac{X}{V_i^2}P_i^2 + Q_j\right)$$

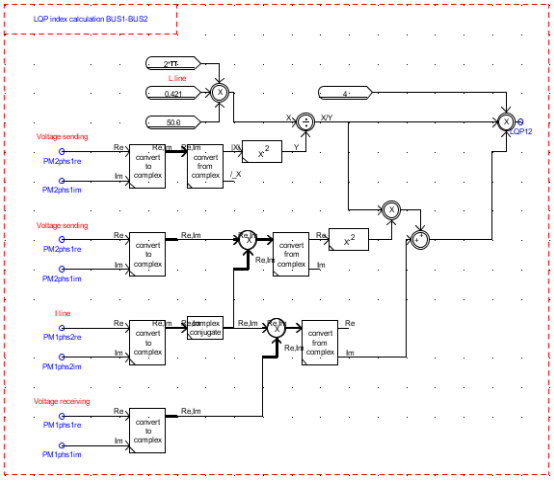

Fig. 6.7 Implementation of line indices in RSCAD

6.5. Simulation Cases

In the previous sections the two bus systems have been presented, as well as the implementation of the indices. In this section, the simulation cases used and the indices computed in each of them are summarized in Fig.6.8 in order to give a first entire view of the simulation before presenting the results in the following chapter.

Test network	Cases	Indices
5-bus	Case 1: Large load increase (5%)	Jacobian, Lmn, LQP, FVSI, VCPI, VCPI(2)
	Case 2: Small load increase (2,5%)	Jacobian, Lmn, LQP, FVSI, VCPI, VCPI(2)
	Case 3: Very small load increase (0,1%)	Jacobian, Lmn, LQP, VCPI, VCPI(2)
	Case 4: Only Q load increase (5%)	Jacobian, Lmn, LQP, VCPI, VCPI(2)
39-bus	Case 1: Large load increase (10%)	Jacobian, Lmn, VCPI
	Case 2: Small load increase (1%)	Jacobian, Lmn, VCPI

Fig. 6.8 Simulation cases and indices summary

As shown in Fig.6.8, and previously stated, two test networks have been used, a 5-bus and a 39-bus. The 5-bus network has been studied using four cases, depending on their load increase at each step change: large (5%), small(2,5%) and very small(0,1%), as well as a case where only the reactive power was increased by 5%. On the other side, the 39-bus system used two cases: a large load increase (10%) and a small load increase (1%). The load increase is constant and is computed as the stated percentage of the load base case.

7. Simulation results

7.1. 5-bus test network

For the 5-bus test network, four cases have been studied. Starting from a steady state base case, the 5-bus test system in Fig. 6.3, the active and/or reactive power consumption of the loads at bus 1, bus 2 and bus 3 are increased. At a certain operating point the two generators cannot sustain the voltage with sufficient reactive power anymore due to the increasing loads, and then the voltage collapses. In case 1, the active and reactive power load are increased stepwise by 5 % every 5 s and by 2.5% in case 2, as shown in Fig.7.1. Case 3 represents a very small load increase, 0,1% of the load base every 0,109 seconds and in case 4 the active power remains constant and the reactive power is increased by 5% of the load base every 10 seconds, as shown in Fig.7.2.

Bus	Load in base case		Large load increase (5%)		Small load increase (2,50%)	
	P (MW)	Q(MVar)	ΔP(MW)	ΔQ(MVar)	ΔP(MW)	ΔQ(MVar)
1	160	80	8	4	4	2
2	200	100	10	5	5	2,5
3	370	130	19	7	9,5	3,5
Total	730	310				

Fig.7.1 Load in base case and load increase information for case 1 and 2

Bus	Load in base case		Very small load increase (0,1%)		Only Q load increase (5%)	
	P (MW)	Q(MVar)	ΔP(MW)	ΔQ(MVar)	ΔP(MW)	ΔQ(MVar)
1	160	80	0,16	0,08	0	4
2	200	100	0,2	0,1	0	5
3	370	130	0,37	0,13	0	7
Total	730	310				

Fig.7.2 Load in base case and load increase information for case 3 and 4

7.1.1. Simulation Case 1: 5-Bus system with 5% load increase

As previously mentioned, the first case in the 5-Bus system increases the load at each load node by a constant rate of 5% of the load base case every 5 seconds. The simulation runs for 50 seconds. The voltage collapse point is observed at the 4^{th} load increase, 20 seconds after the simulation begins. Fig. 7.2 illustrates the active and reactive power at the load buses; Fig. 7.3 shows the node voltages and Fig.7.4, the branch currents.

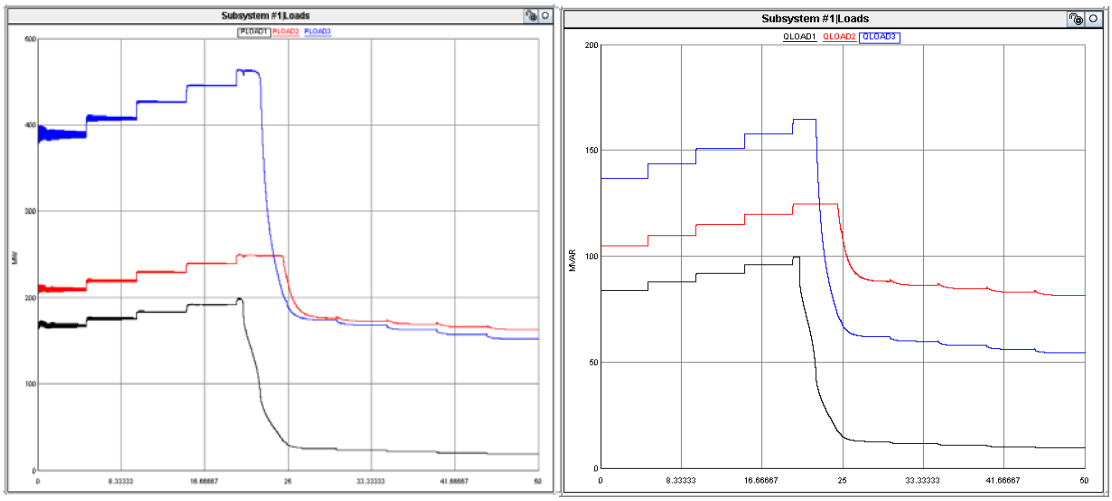

Fig. 7.3 Active and reactive power consumed by the loads (PloadN: Active power consumed by the load bus N; QloadN: Reactive power consumed by load bus N)

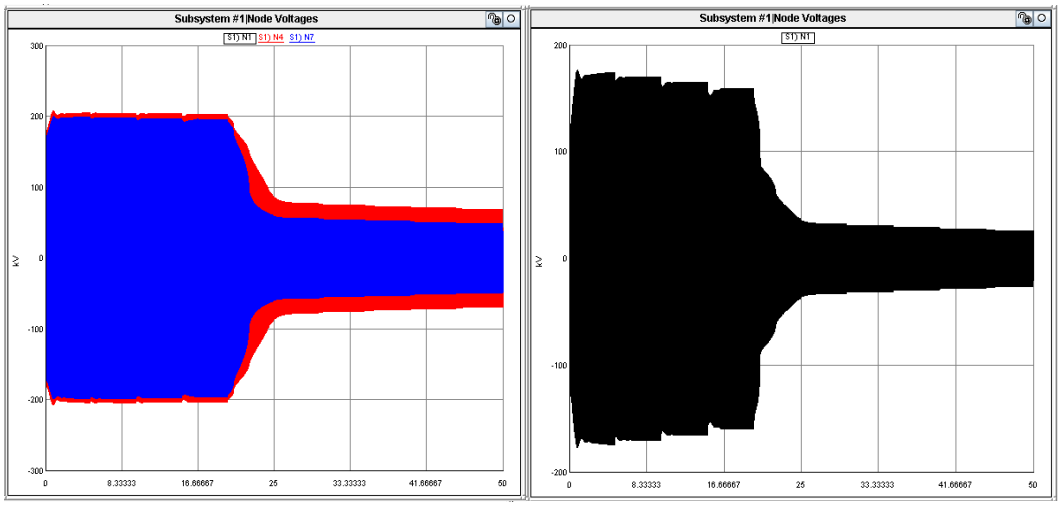

Fig. 7.4 Node voltages (N1: Voltage at Node 1, N4: Voltage at Node 2, N7: Voltage at Node 3)

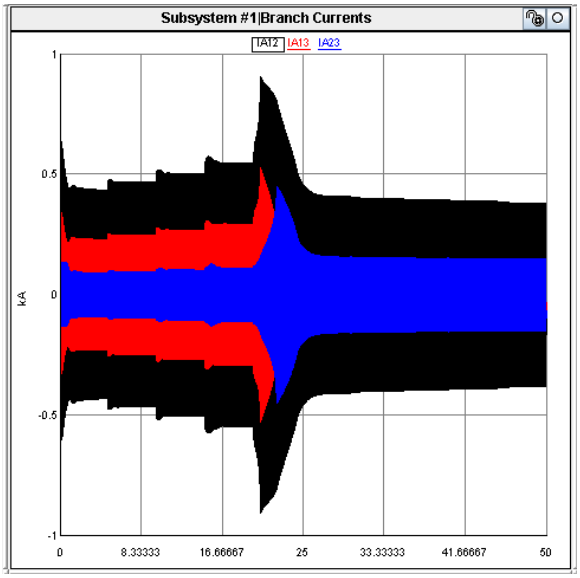

Fig. 7.5 Branch currents (IANM: Branch current in phase A between nodes N and M)

7.1.1.1. Jacobian matrix index

After gathering the voltage measurements, magnitude and phase from the PMU component in RTDS, the data is loaded into MATLAB to calculate the eigenvalues of the Jacobian matrix and the minimum value is plotted at each load step (Fig 7.6).

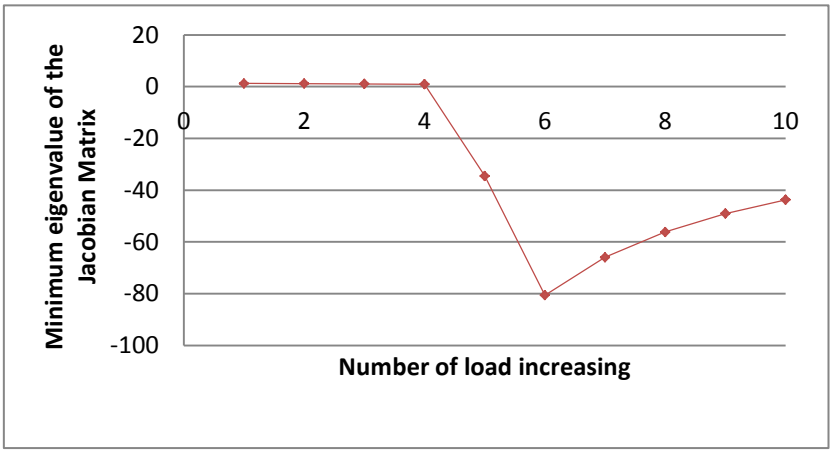

Fig. 7.6 Minimum eigenvalue of the Jacobian Matrix at each load step

Fig 7.6 shows how the minimum eigenvalues are positive while the system is stable and how the eigenvalues become negative when the system turns unstable. As mentioned in chapter 3.1., this index presents nonlinearity near the voltage collapse point, which can also be noticed in the simulation results. As commented earlier, this index is a global index and therefore, it does not provide any information on the location of the weak bus or line of the system and just gives information on the global system, making it difficult to apply any control strategy to avoid voltage collapse from happening.

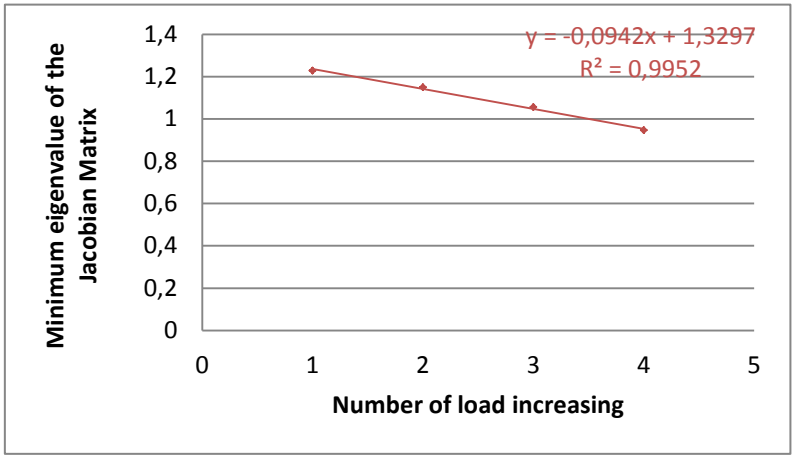

Fig. 7.7 Minimum eigenvalue of the Jacobian Matrix in the stable region.

Fig. 7.7 plots the results on the stable region. In this region, the index is linear, which can be used to know how far the system is to voltage collapse. Although the theoretical approach states that zero is the limit of the stable region, in this particular case, the index changes from 0,95 to -34,5 in the voltage collapse load step change. For this reason, the use of this index in real-time operations, it should be taken into account the results of offline simulations to fix the practical limit index to calculate the margin.

7.1.1.2. Line indices

Using the implementation in RSCAD of the line stability indices as described in chapter 6.4.1, the different line indices can be monitored in Runtime as any other control signal and therefore, their plots can be directly observed. The following figures Fig.7.8-Fig7.10 show the Index-Time plots for this case.

These indices were developed for steady state analysis. In dynamic analysis, they present a transient period presenting oscillations before the steady state value is reached and a nonlinearity near the voltage collapse point. All of these indices should cross 1 at the voltage collapse point. This is true for most of them: Lmn, FVSI without approximation and both VCPI. LQP is passes 1 at the voltage collapse point, but remains under 1 in its steady state value. On the other hand, these results show that the approximation used to compute the FVSI is not acceptable in this case, since the difference on the values used with and without approximation are too big.

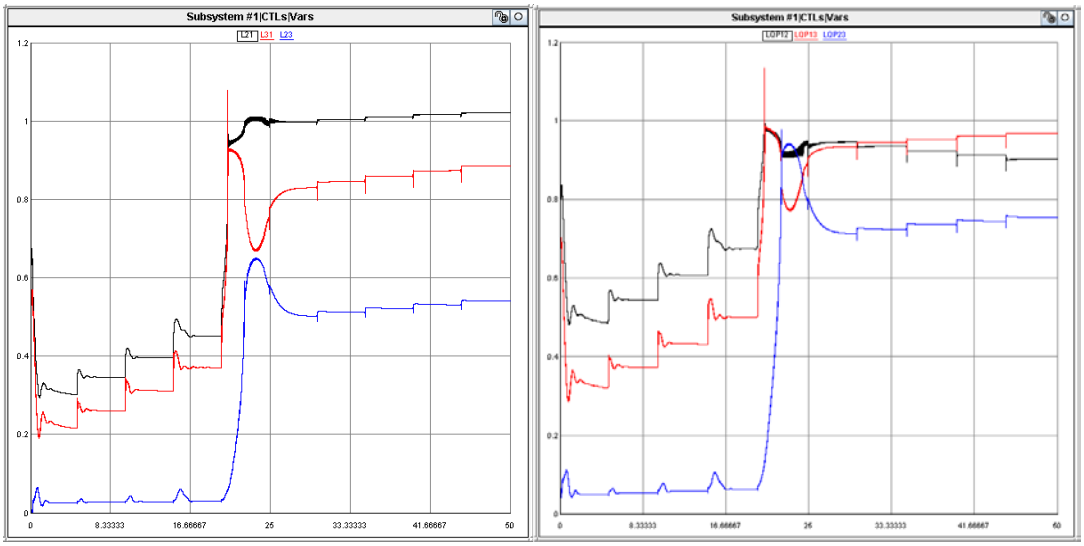

Fig. 7.8 Lmn and LQP results

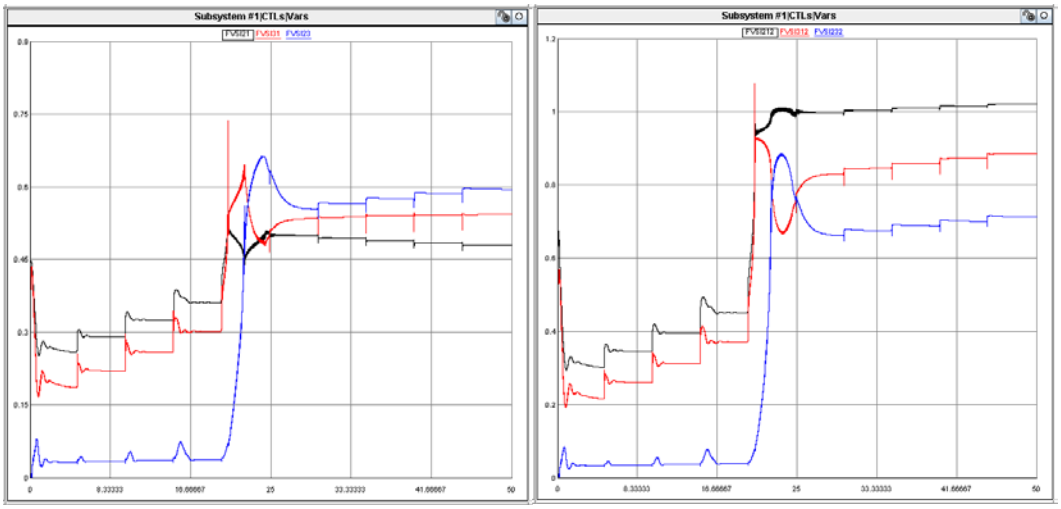

Fig. 7.9 FVSI results (left-with approximation, right-without)

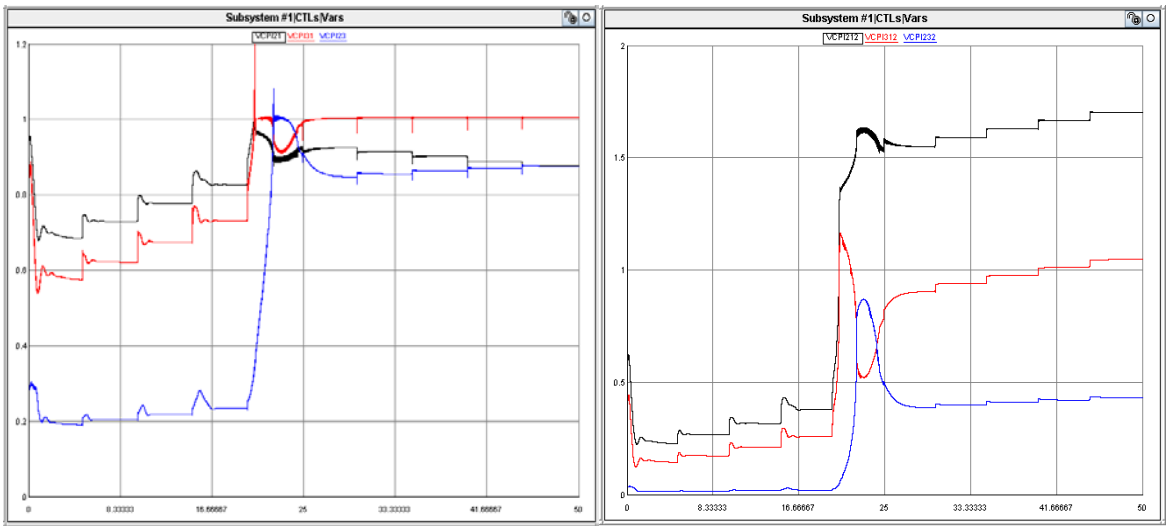

Fig. 7.10 VCPI results (left-power, right-loss)

As described earlier, these indices are useful to determine the weakest line of the system. These results show that all indices agree in the ranking of the weakest lines in the system as gathered in Fig. 7.11: Line 2-1 is the weakest line of the system, followed by line 3-1 and finally 2-3.

Line	Lmn	LQP	FVSI	VCPI(p)	VCPI(l)
2-1	1	1	1	1	1
3-1	2	2	2	2	2
2-3	3	3	3	3	3

Fig. 7.11 Ranking of weakest lines of the system

After gathering the data from the Runtime, the steady state values where saved and plotted, as shown in the following figures Fig.12-Fig.14.

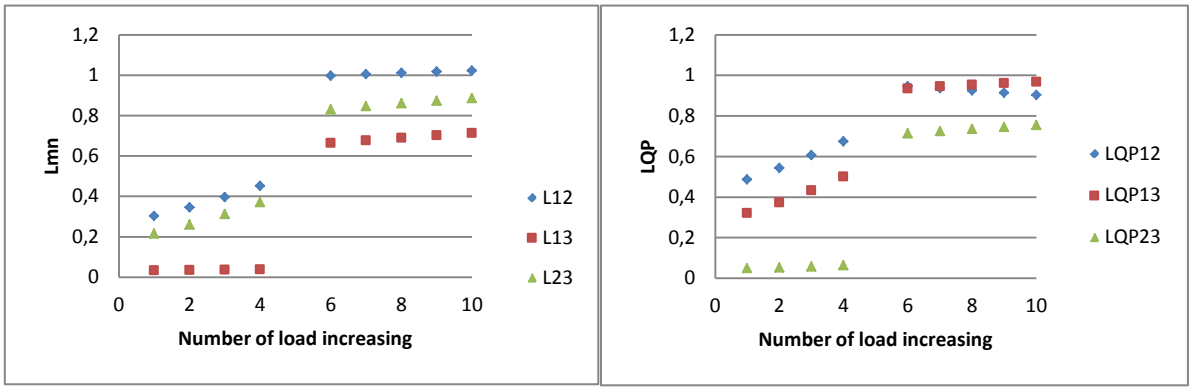

Fig. 7.12 Steady state values Lmn and LQP indices

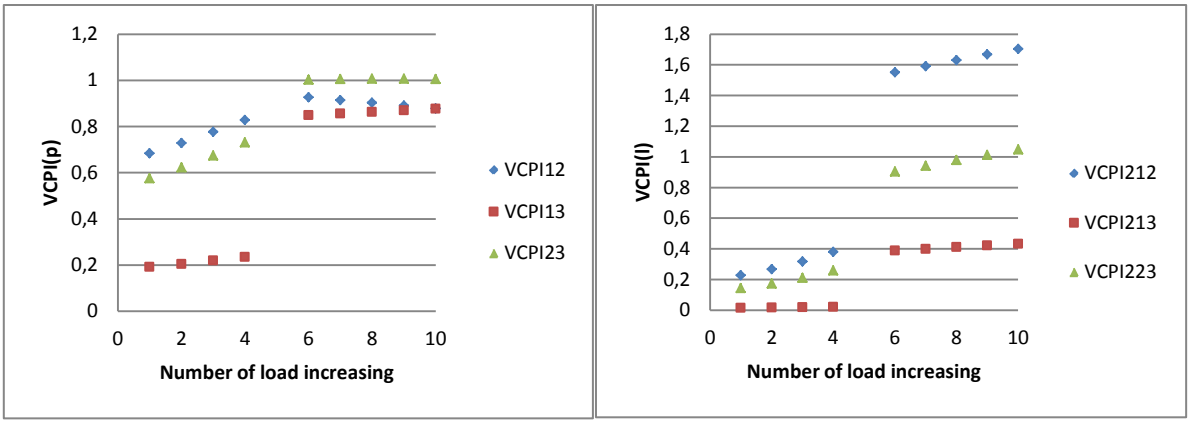

Fig. 7.13 Steady state values VCPI indices

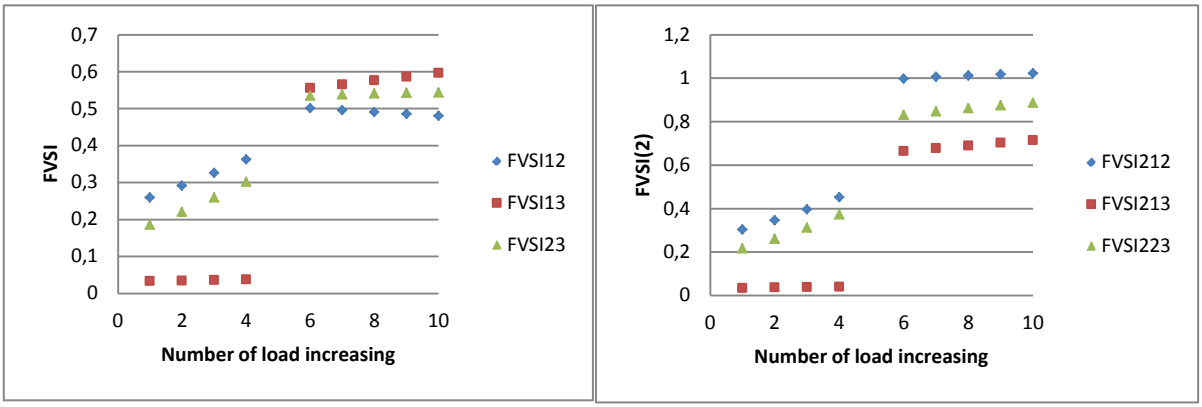

Fig. 7.14 Steady state values FVSI indices

A global index, defined by the maximum line index of the system can be also computed as shown in Fig.15. The value at number of load increasing 5 is not plotted since the steady state value is not reached.

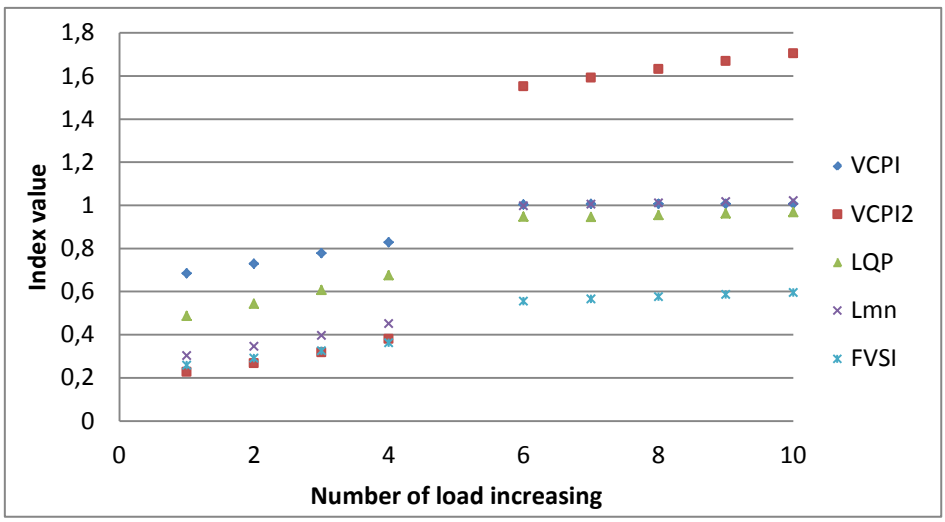

Fig. 7.15 Steady state values for global system indices

In order to compare the performance of these indices, several quantitative measures have been summarized in the following table Fig.17: Last value before voltage collapse occurs, first value after voltage collapse, increase of value at the voltage collapse point and linearity in the

stable region. The quantitative value for assessing the linearity is R^2 obtained by a standard linear regression in Excel, which is shown in Fig.7.16.

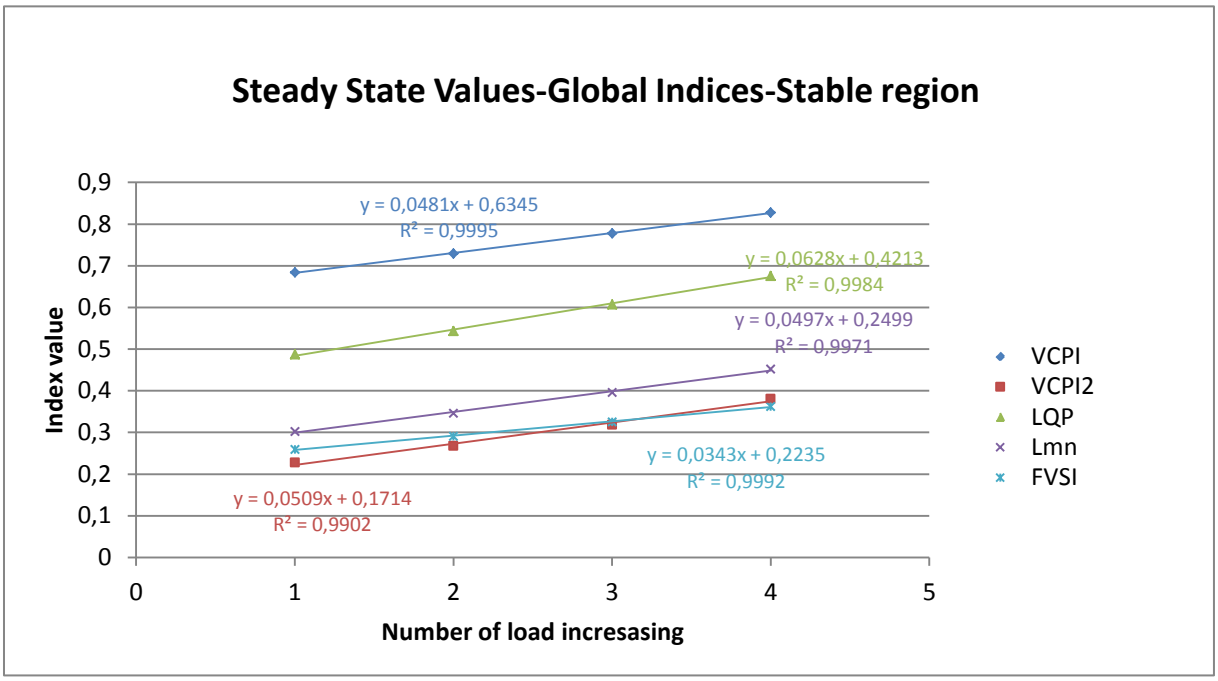

Fig. 7.16 Steady state values for global system indices in stable region and linear line tendency calculation

Index	Last value before voltage collapse	First value after voltage collapse	Increase of value at the voltage collapse point	Linearity in the stable region
VCPI(p)	0,828047	1,00393	0,175883	0,9995
VCPI(2)(l)	0,380708	1,55145	1,170742	0,9902
LQP	0,675284	0,946578	0,271294	0,9984
Lmn	0,451693	0,997581	0,545888	0,9971
FVSI	0,361822	0,555516	0,193694	0,9992

Colour	Last value before voltage collapse	First value after voltage collapse	Increase of value at the voltage collapse point	Linearity in the stable region
green	0,7-1	>1	≤0,2	≥0,999
orange	0,5-0,69	0,9-1	0,2-0,6	0,99-0,998
red	0-0,49	<0,9	≥0,6	<0,99

Fig. 7.17 Quantitative values indices comparison and colour interval classification

The quantitative values in the table above have been classified in three categories: good (green), neutral (orange) and bad (red). The values classification for each colour has been defined as shown in Fig.7.17, and will remain this way for the rest of the cases. The reasons for these values classification is explained next. For the last value before voltage collapse a good value is one near 1 because it alerts that the system is close to collapse. For the first value after voltage collapse, a value above 1 clearly indicates that the system has crossed its voltage stability limit. The increase value, should not be very high, in order to maintain as

much as possible the linear trend of the index although crossing a nonlinearity point. Finally, the linearity at the stable region could help calculate the voltage stability margin.

Analysing the quantitative values in Fig.7.17, the index that provides the most useful information is VCPI(p), which has a good value for all of the categories, the second best indices will be LQP and Lmn, followed by VCPI(2)(l) and FVSI.

7.1.2. Simulation Case 2: 5 Bus system with 2,5% load increase

As previously mentioned, the second case in the 5-Bus system increases the load at each load node by a constant rate of 2,5% of the load base case every 5 seconds. The simulation runs for 60 seconds. The voltage collapse point is observed at the 9th load increase, 50 seconds after the simulation begins. Fig. 7.18 illustrates the active and reactive power at the load buses; Fig.7.19 shows the node voltages and Fig.7.20, the branch currents.

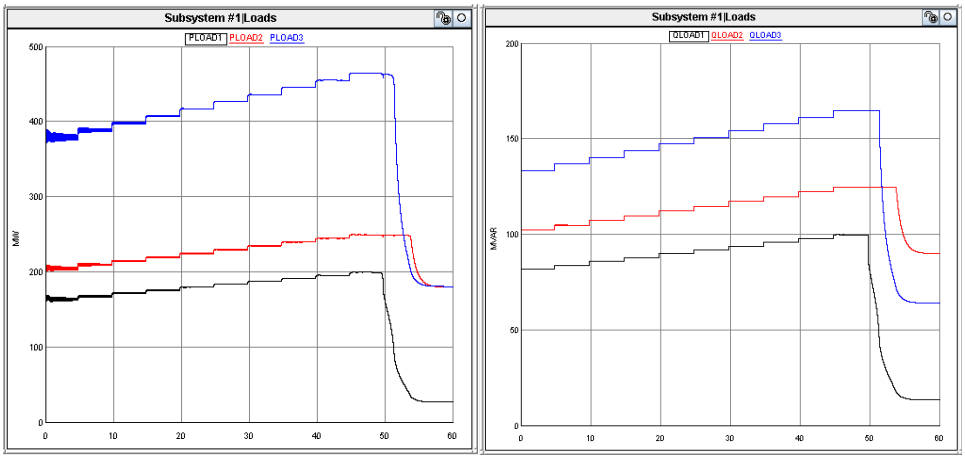

Fig. 7.18 Active and reactive power consumed by the loads (PloadN: Active power consumed by the load bus N; QloadN: Reactive power consumed by load bus N)

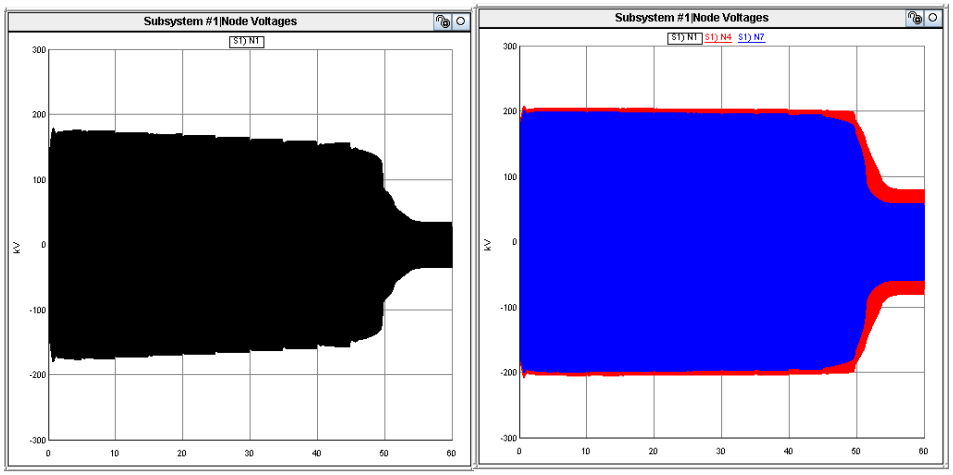

Fig. 7.19 Node voltages (N1: Voltage at Node 1, N4: Voltage at Node 2, N7: Voltage at Node 3)

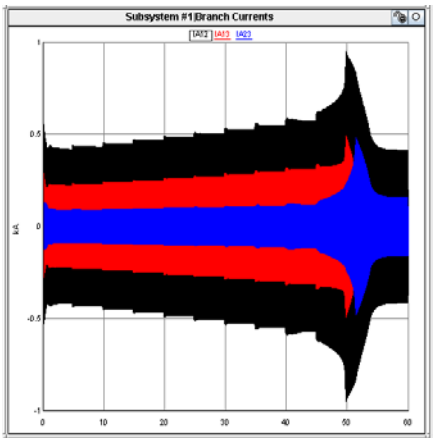

Fig. 7.20 Branch currents (IANM: Branch current in phase A between nodes N and M)

7.1.2.1. Jacobian matrix index

As done in case 1, the eigenvalues of the Jacobian matrix are computed and the minimum value is plotted at each load step in Fig 7.21. The figure also shows how the minimum eigenvalues are positive while the system is stable and how the eigenvalues become negative when the system turns unstable. In this case, the index also presents a high drop when crossing the voltage stability limit (Fig.7.21) and has a linear trend in the stable region (Fig.7.22).

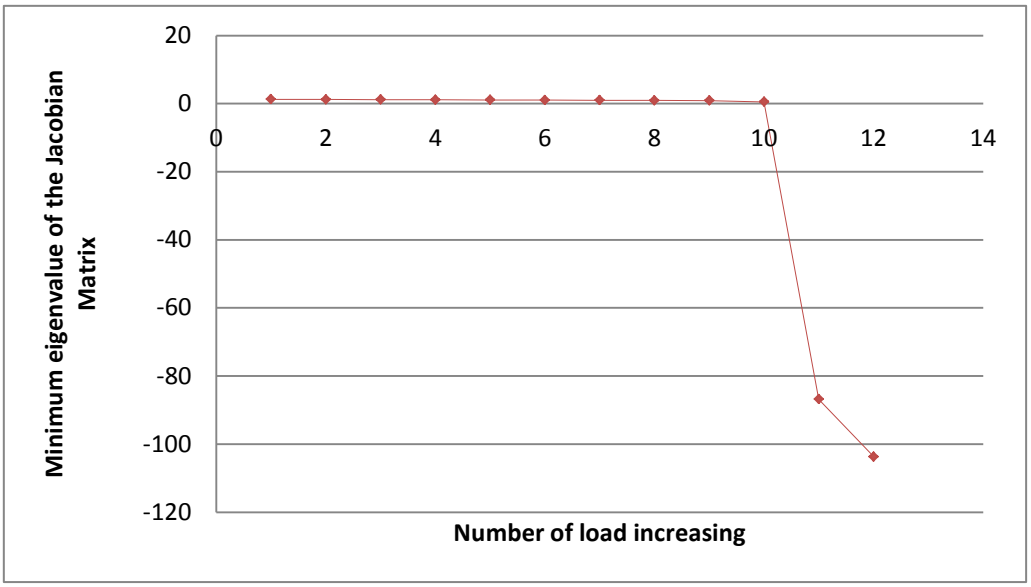

Fig. 7.21 Minimum eigenvalue of the Jacobian Matrix at each load step

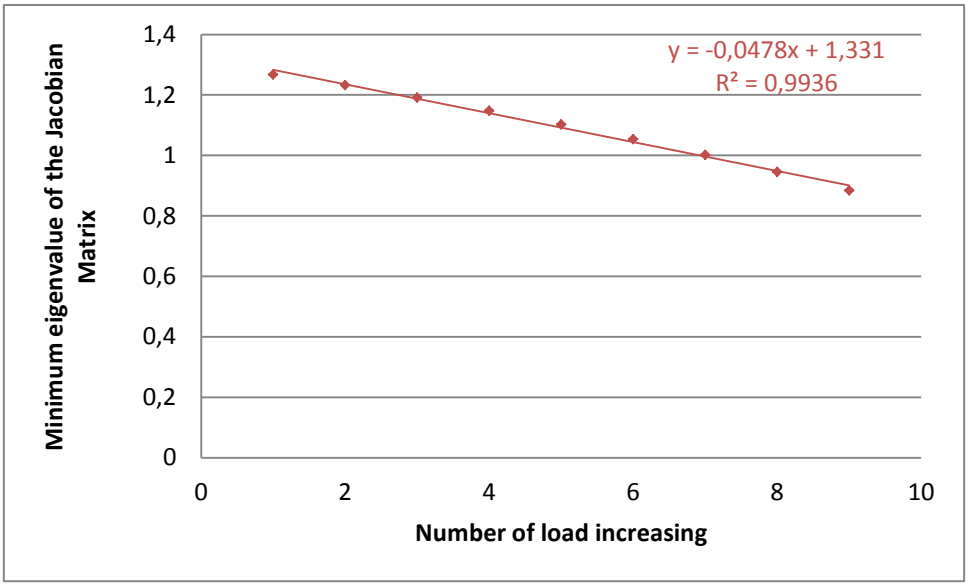

Fig.7.22 Minimum eigenvalue of the Jacobian Matrix in the stable region

7.1.2.2. Line indices

As in the previous case, the implementation of the line stability indices was done using the control blocks as described in chapter 6.4.1 and the line indices were monitored in Runtime, obtaining their plots. The following figures Fig.7.23-Fig7.25 show the Index-Time plots for this case.

As already noticed in the previous case, the indices present a transient period before they become stable, since the increment is smaller than in the previous case, the pic value at each load increase is also smaller. At the voltage collapse point it also presents a unregularly form and it does not reach the steady state value in that interval. It is also observed that the FVSI approximation index has a mean relative error of 16% in the values in the stable region and after the voltage collapse it is even greater, with a relative error of 45%.

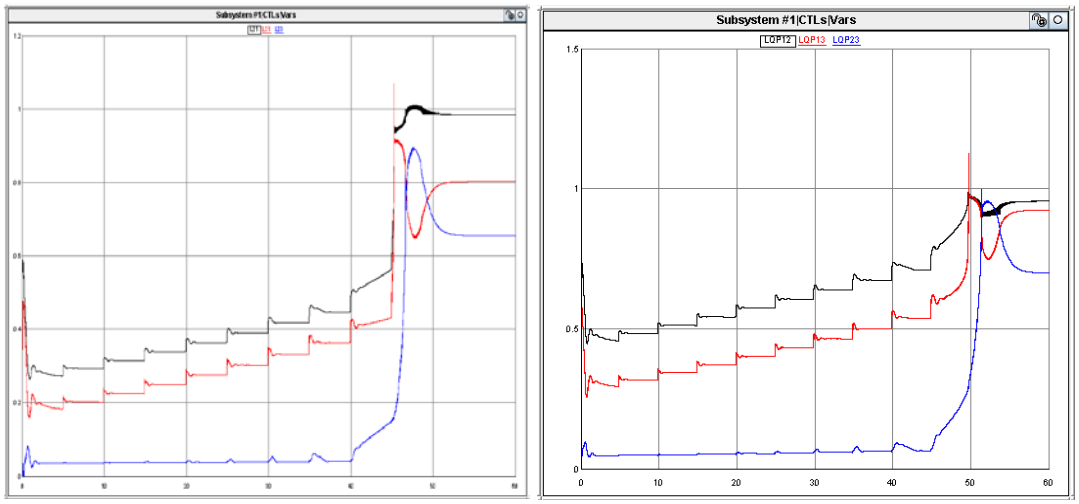

Fig. 7.23 Lmn and LQP results

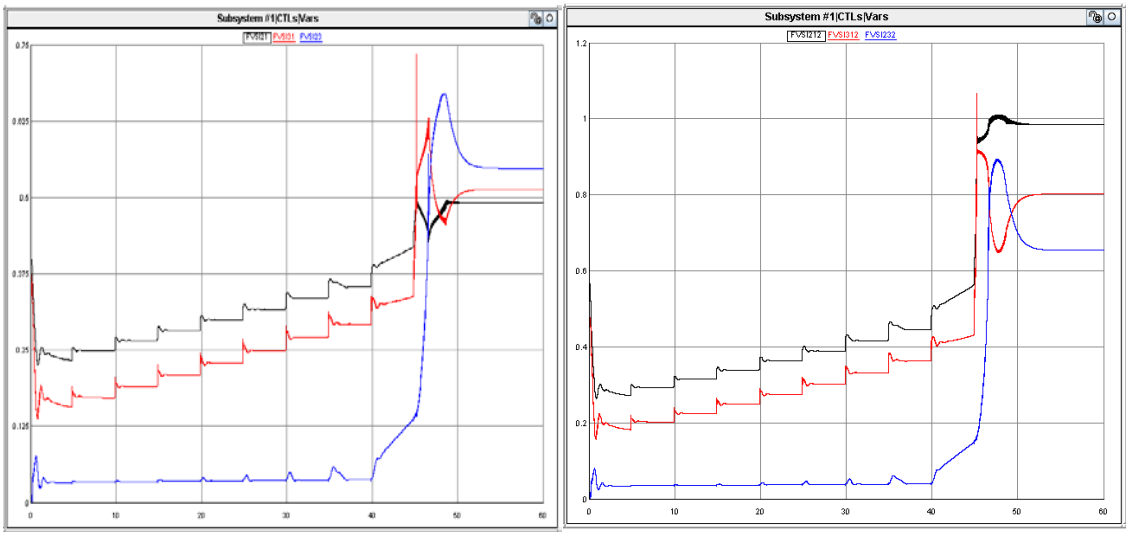

Fig. 7.24 FVSI results (left-with approximation, right-without)

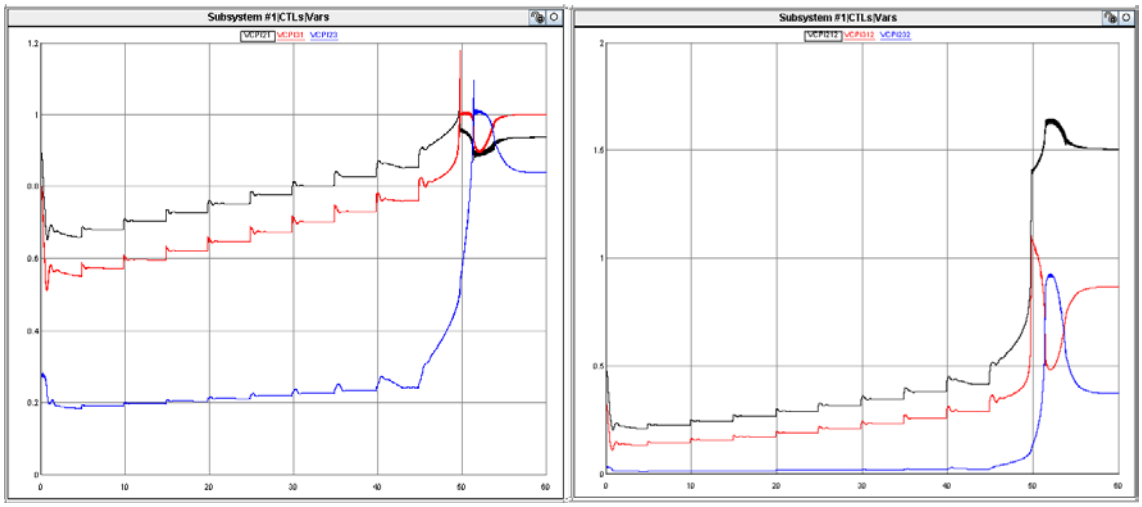

Fig. 7.25 VCPI results (left-power, right-loss)

These results show that all indices agree in the ranking of the weakest lines in the system: 2-1 is the weakest line of the system, followed by line 3-1 and finally 2-3. Fig.7.26-Fig.28 show the steady state values of each index and line.

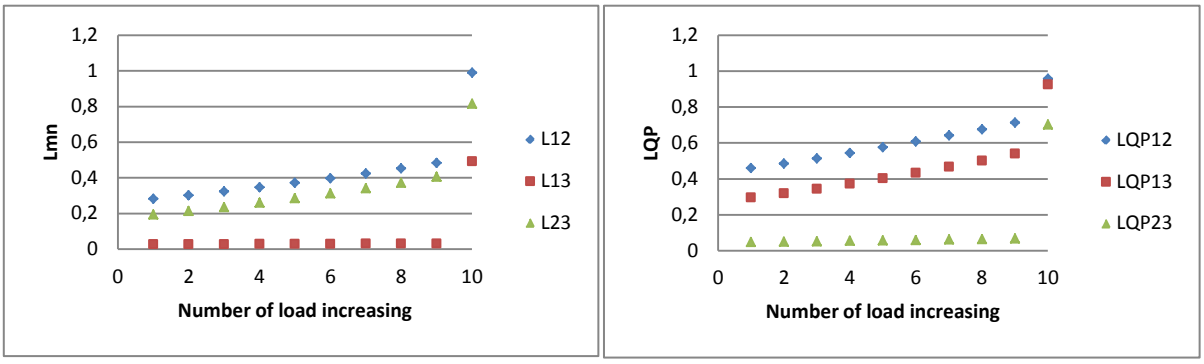

Fig. 7.26 Steady state values Lmn and LQP indices

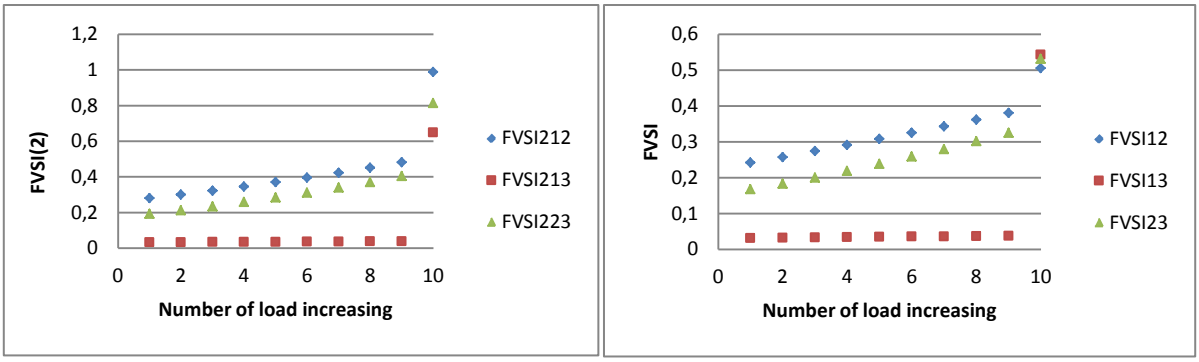

Fig. 7.27 Steady state values FVSI indices

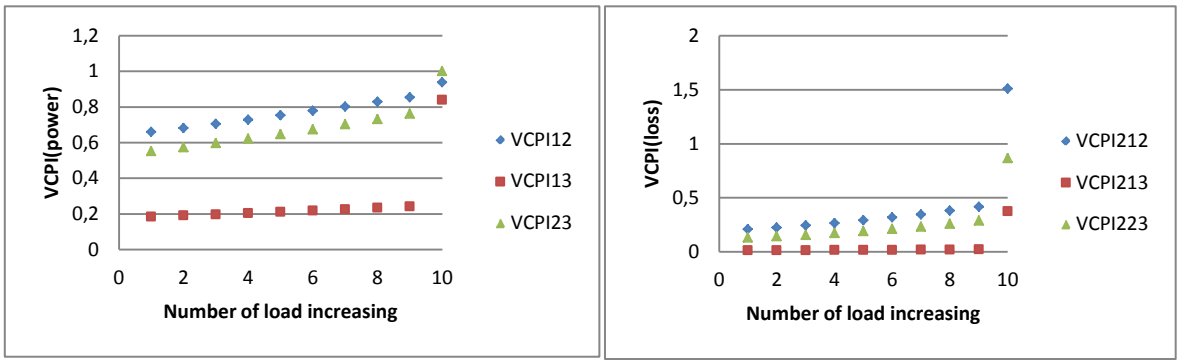

Fig. 7.28 Steady state values VCPI indices

A global index, defined by the maximum line index of the system can be also computed as shown in Fig.7.29. Note that the value at number of load increasing 10 is not plotted since the steady state value is not reached.

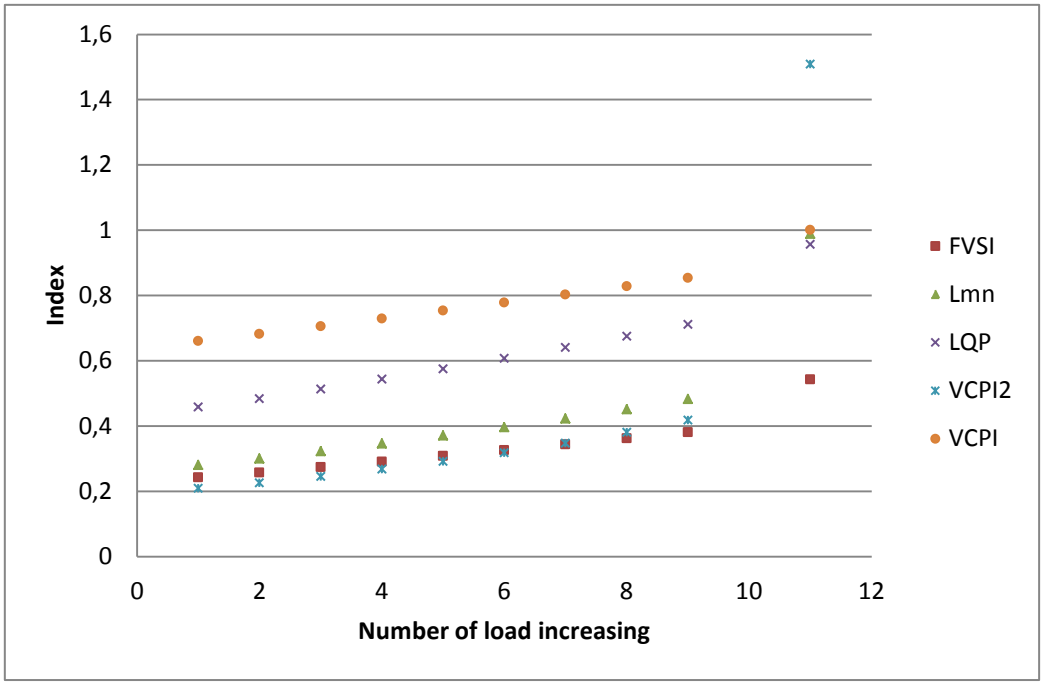

Fig. 7.29 Steady state values for global system indices

In order to compare the performance of these indices, the same quantitative measures as in case 1 have been summarized in the following table Fig.31: Last value before voltage collapse

occurs, first value after voltage collapse, increase of value at the voltage collapse point and linearity in the stable region (R^2), which is shown in Fig.30.

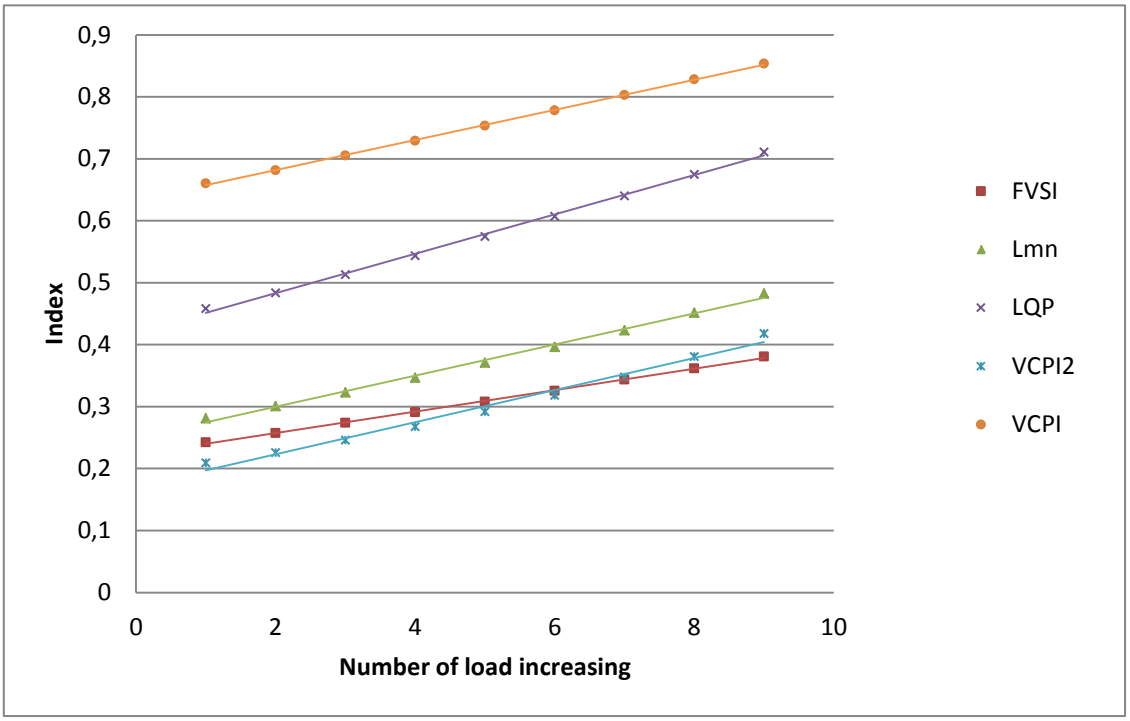

Fig. 7.30 Steady state values for global system indices in stable region and linear line tendency calculation

Index	Last value before voltage collapse	First value after voltage collapse	Increase of value at the voltage collapse point	Linearity in the stable region
VCPI(p)	0,853651	1,00108	0,147429	0,9995
VCPI(2)(l)	0,418139	1,50854	1,090401	0,9855
LQP	0,711157	0,956645	0,245488	0,9980
Lmn	0,482533	0,988773	0,50624	0,9962
FVSI	0,380585	0,543011	0,162426	0,9992

Fig. 7.31 Quantitative values indices comparison

The results obtained are similar to the ones in case 1. Analysing the quantitative values in Fig.7.31, the index that provides the most useful information is also VCPI(p), which has a good value for all of the categories, the second best indices will be LQP and Lmn, followed by VCPI(2)(l) and FVSI.

7.1.3. Simulation Case 3: Very small load increase

As previously mentioned, the third case in the 5-Bus system increases the load at each load node by a constant rate of 0,1% of the load base case every 0,109 seconds. The simulation runs for 50 seconds. The voltage collapse point is approximately 25 seconds after the simulation begins. Fig. 7.32 illustrates the active and reactive power at the load buses and Fig.7.33 shows the node voltages.

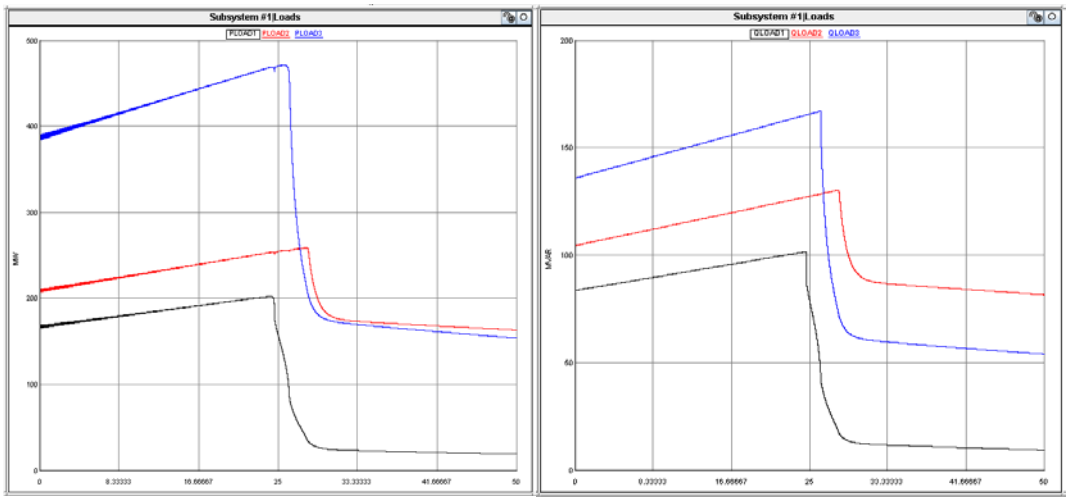

Fig. 7.32 Active and reactive power consumed by the loads (PloadN: Active power consumed by the load bus N; QloadN: Reactive power consumed by load bus N)

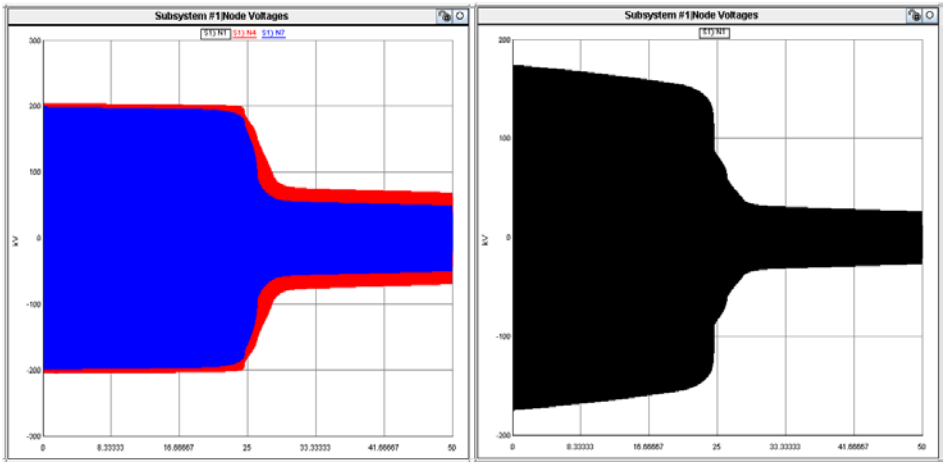

Fig. 7.33 Node voltages (N1: Voltage at Node 1, N4: Voltage at Node 2, N7: Voltage at Node 3)

7.1.3.1. Jacobian matrix index

As done in case 1 and 2, the eigenvalues of the Jacobian matrix are computed and the minimum value is plotted at each load step in Fig 7.34. The main characteristics of the minimum eigenvalues of the Jacobian matrix are repeated in this case: positive values in the stable region, negative values in the unstable region, linearity in the stable region and high drop near the voltage collapse point. Because the step load change is much smaller and the Jacobian is computed at each of this load step changes, the form of the function can be better observed than in the past cases. The values in the stable region are plotted separately again in Fig.7.35 to view the line form better.

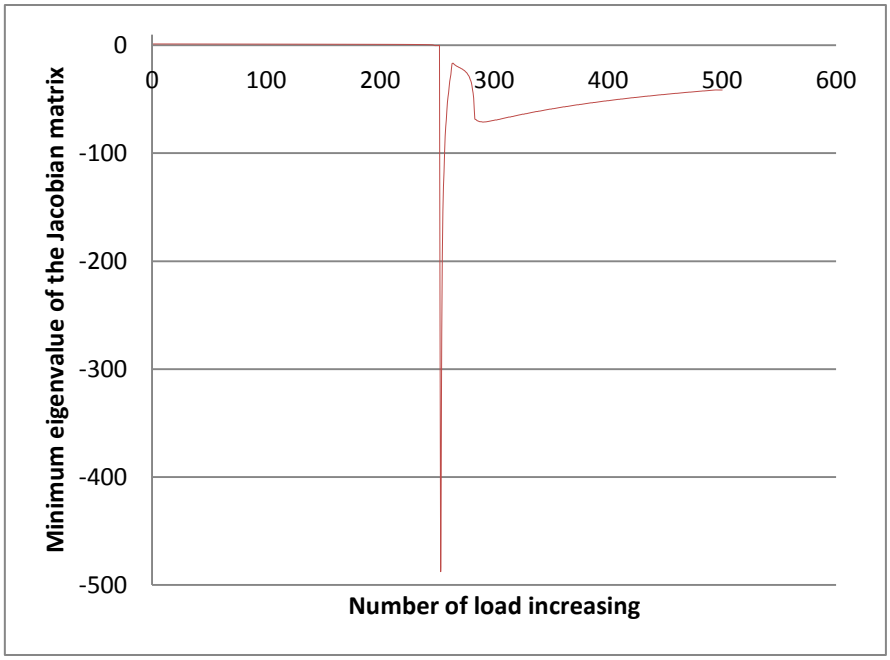

Fig. 7.34 Minimum eigenvalue of the Jacobian Matrix at each load step

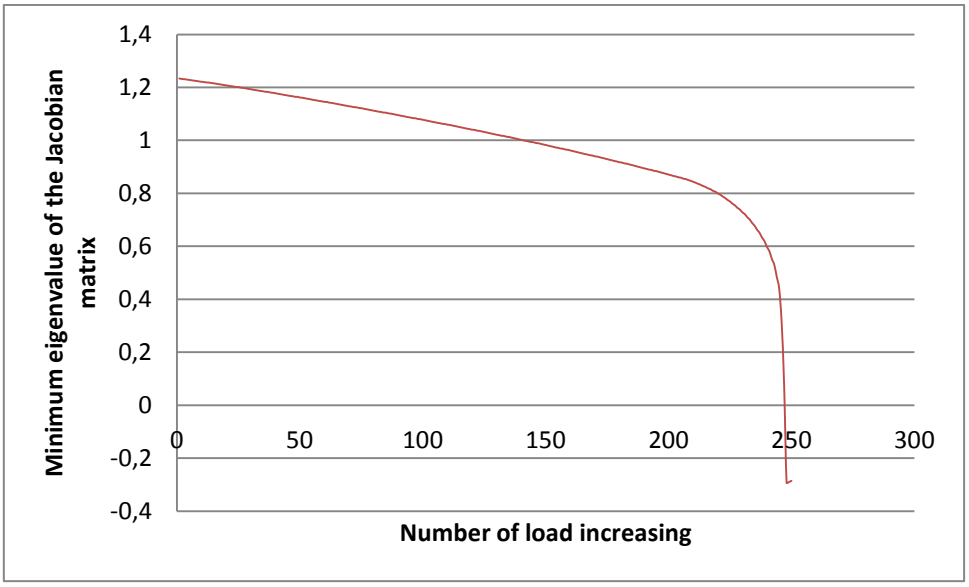

Fig. 7.35 Minimum eigenvalue of the Jacobian Matrix at each load step in the stable region

7.1.3.2. Line indices

Again, the line indices are plotted in the RunTime. As in the Jacobian matrix index, the form of functions can be clearer observed (Fig.7.36-Fig.7.37), since there are more steps and therefore, more points computed. The steady state values where not computed since the plots in Runtime already offer this information.

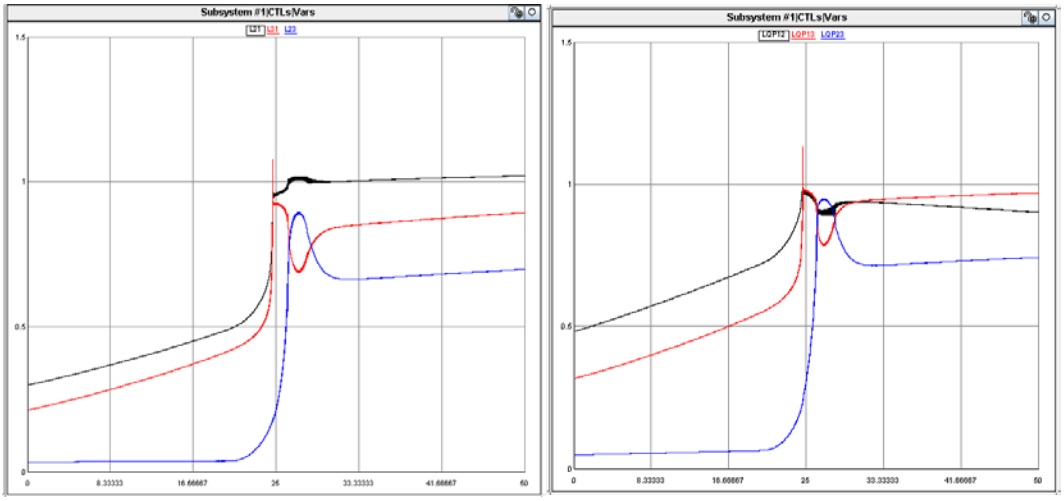

Fig. 7.36 Lmn and LQP results

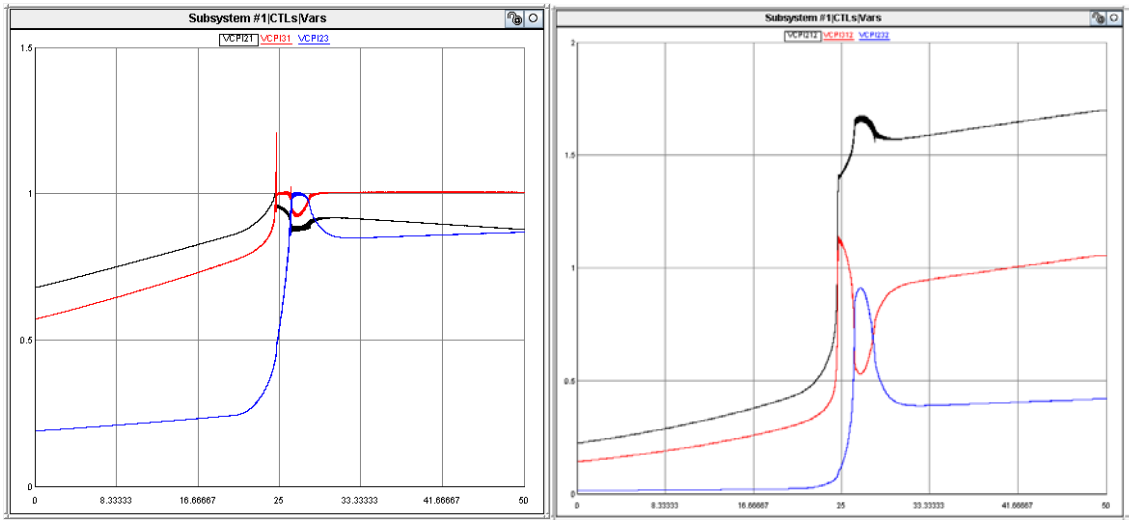

Fig. 7.37 VCPI results (left-power, right-loss)

7.1.4. Simulation Case 4: Only reactive power increasing

As previously mentioned, the fourth case in the 5-Bus system increases the reactive power at each load node by a constant rate of 5% of the load base case every 10 seconds. The simulation runs for 150 seconds. The voltage collapse point is observed 120 seconds after the simulation begins. Fig. 7.38 illustrates the active and reactive power at the load buses and Fig.7.39 shows the node voltages.

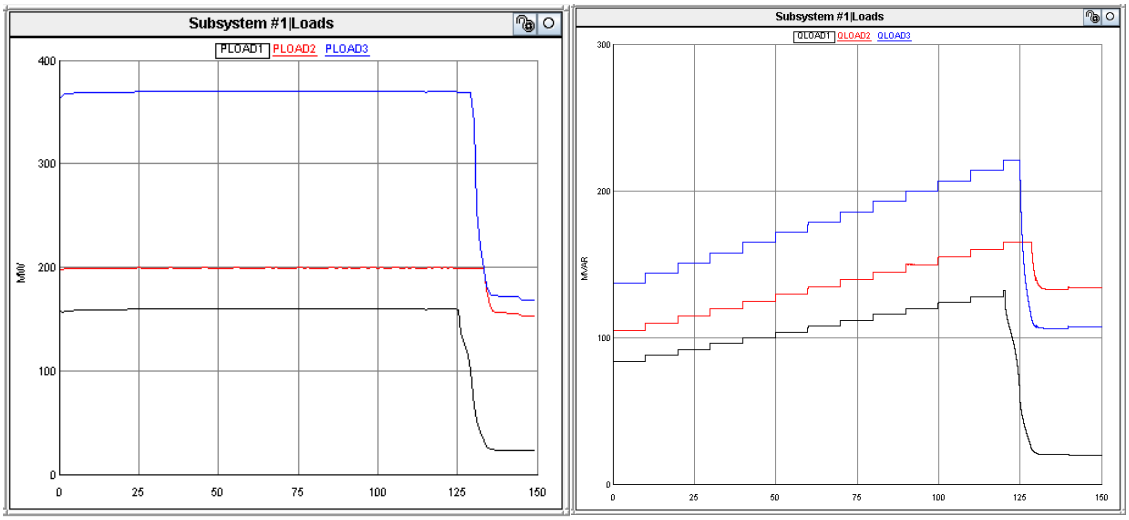

Fig. 7.38 Active and reactive power consumed by the loads (PloadN: Active power consumed by the load bus N; QloadN: Reactive power consumed by load bus N)

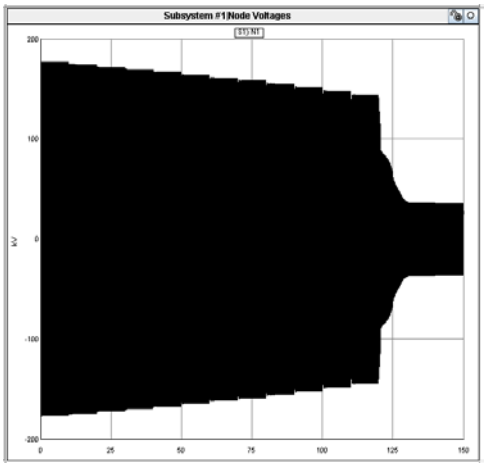

Fig. 7.39 Node voltage (N1: Voltage at Node 1)

7.1.4.1. Jacobian matrix index

As in all of the previous cases, the first figure plots the minimum eigenvalue of the Jacobian matrix at each load step and second one, the minimum eigenvalue in the stable region.

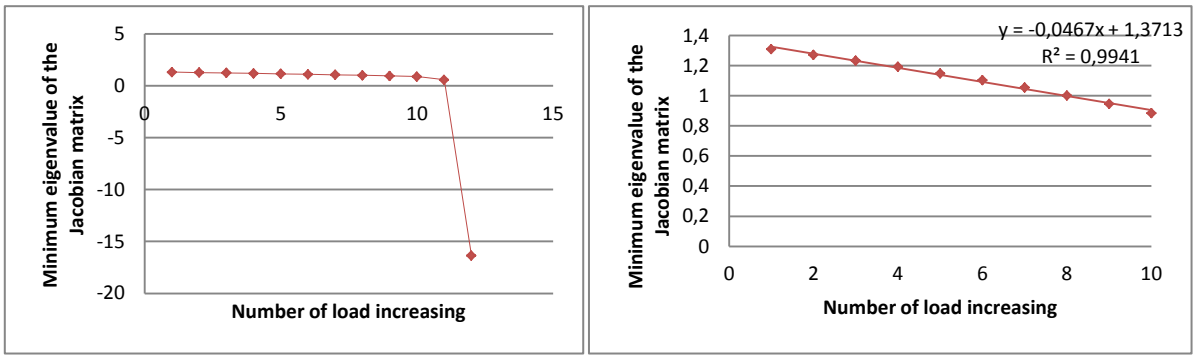

Fig. 7.40 Minimum eigenvalue of the Jacobian Matrix at each load step (left)

and in the stable region only(right)

7.1.4.2. Line indices

Again, the line indices are plotted in the RunTime (Fig.7.41-Fig.7.42), and the values at each loading point are saved and plotted separately (Fig.7.43-7.44).

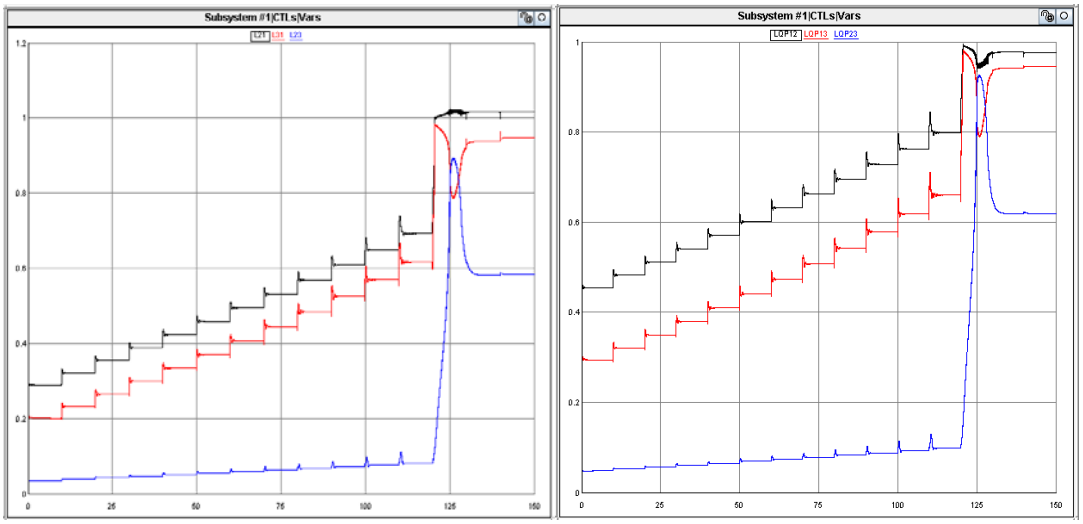

Fig. 7.41 Lmn and LQP results

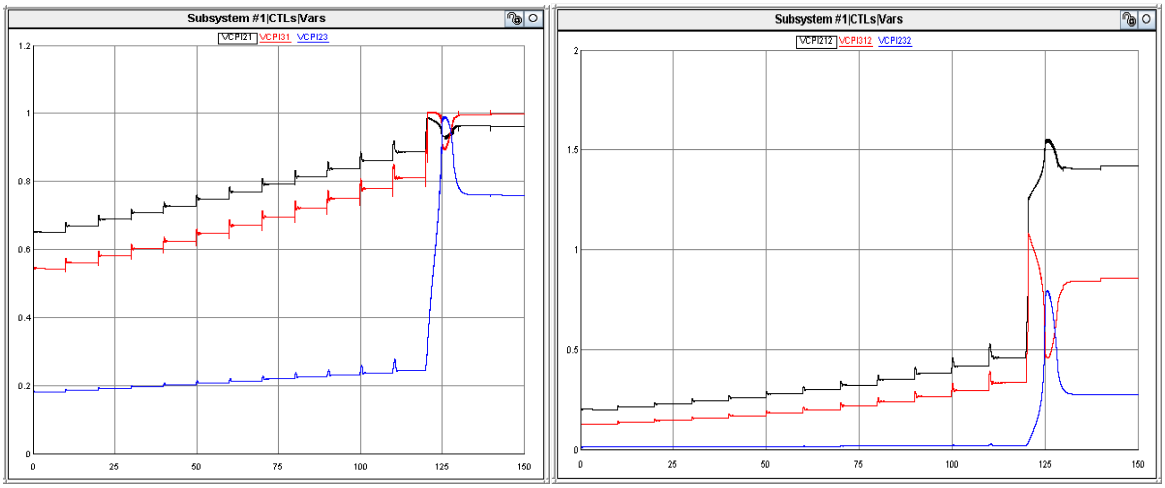

Fig. 7.42 VCPI results (left-power, right-loss)

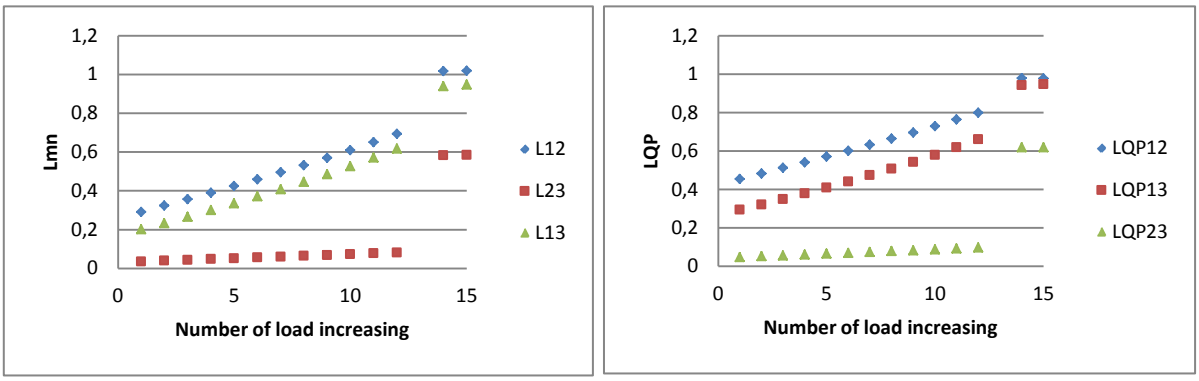

Fig. 7.43 Lmn and LQP steady state results

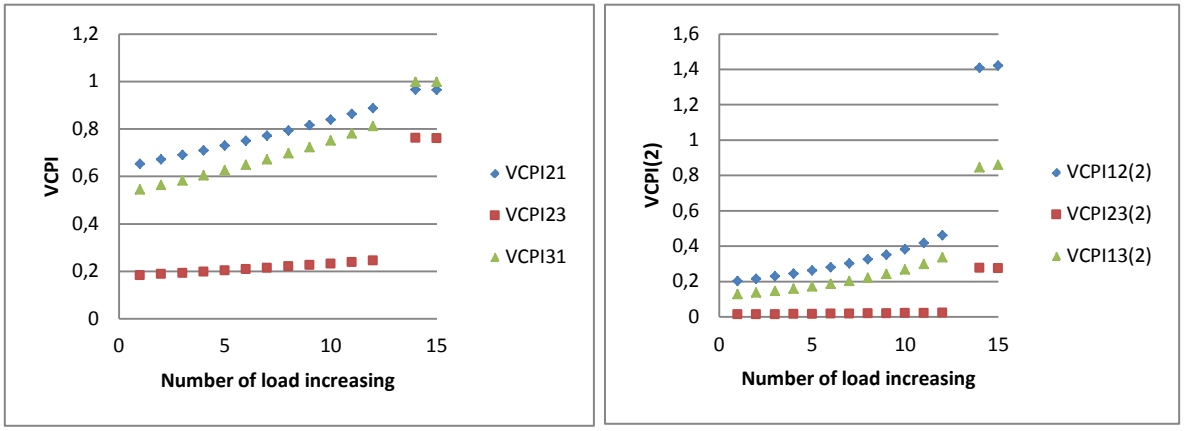

Fig. 7.44 VCPI results (left-power, right-loss)

As done in all of the other cases, a global index is computed by taking the maxim value of the line stability indices at each load step (Fig.7.45), and the quantitative values analysed are also set in a Table (Fig.7.47).

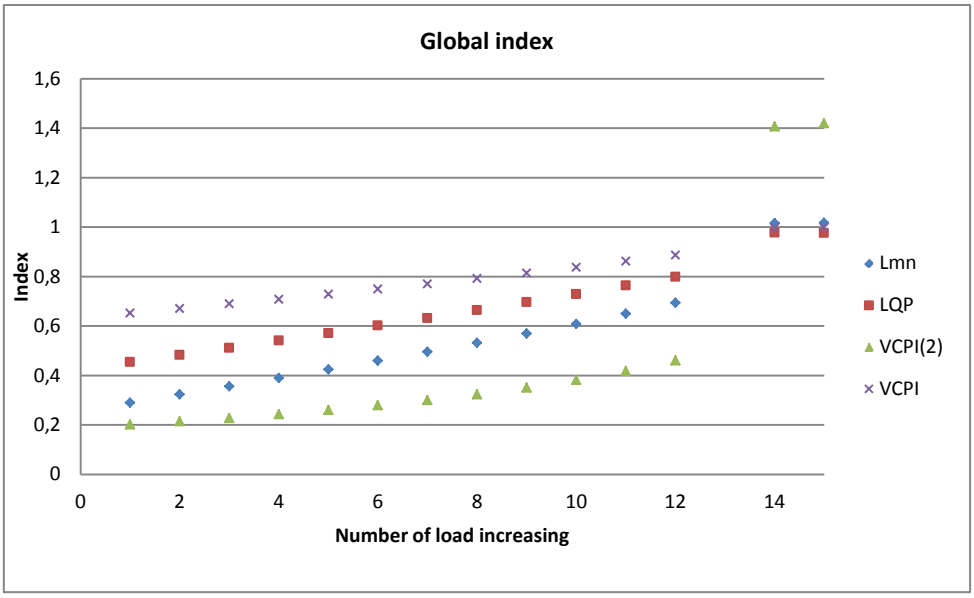

Fig. 7.45 Steady state values for global system indices

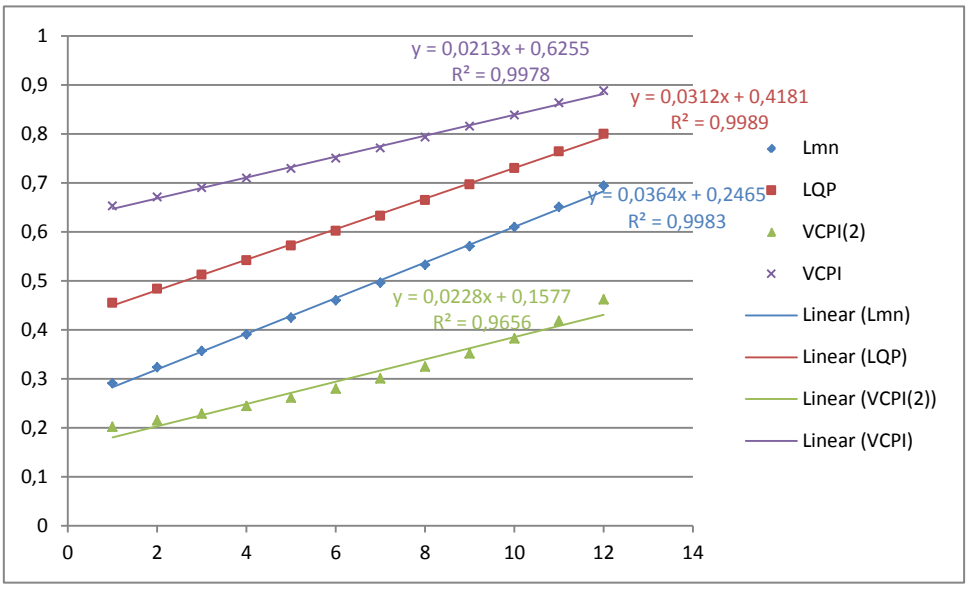

Fig. 7.46 Steady state values for global system indices in stable region and linear line tendency calculation

Index	Last value before voltage collapse	First value after voltage collapse	Increase of value at the voltage collapse point	Linearity in the stable region
VCPI(p)	0,887821	0,997218	0,109397	0,9978
VCPI(2)(l)	0,461411	1,40829	0,946879	0,9656
LQP	0,799553	0,978309	0,178756	0,9989
Lmn	0,693662	1,01701	0,323348	0,9983

Fig.7.47 Quantitative values for Case 4

7.1.5. Case comparison

This chapter aims to compare the indices values in two cases: Case 2, where P and Q are increased by 2,5% at each load step and Case 4, where only Q is increased by 5% every load step. In order to compare these cases, two x axis have been chose. First the line indices are compared based on the apparent power (pu) and secondly, based on the apparent power margin (pu). At the end, the values for the Jacobian matrix index on both cases are also commented. The purpose of this comparison is to know if given an index value, it can be assessed the proximity to voltage collapse without knowing the nature of the load.

By looking at Fig.7.48-Fig.7.51, it can be seen that the system can reach 1,23 pu in apparent power generation in Case 2, while it can only reach 1,105 pu in Case 4. This is natural as the system for the same apparent power consumption, is weaker if it has more reactive power. The apparent power increase for the Case 2 is 0,025 and 0,011 for Case 4.

The procedure to quantify the independence on the nature of the load near the voltage collapse point will be the following: First, considering the last value before collapse in Case 2, the nearest index value to that from Case 4 will be considered and the maximum apparent load increase before collapse from that point will be computed and compared to the one from Case 2. For example, in Fig. the last value before collapse in case 2 is 0,71, the nearest index value in case 4 is 0,69. From this point, the system has four increases before collapse, which is an increase of 0,044, while in case 2 the increase is 0,025. This method is done in all of the indices and the results can be found in Fig.7.52.

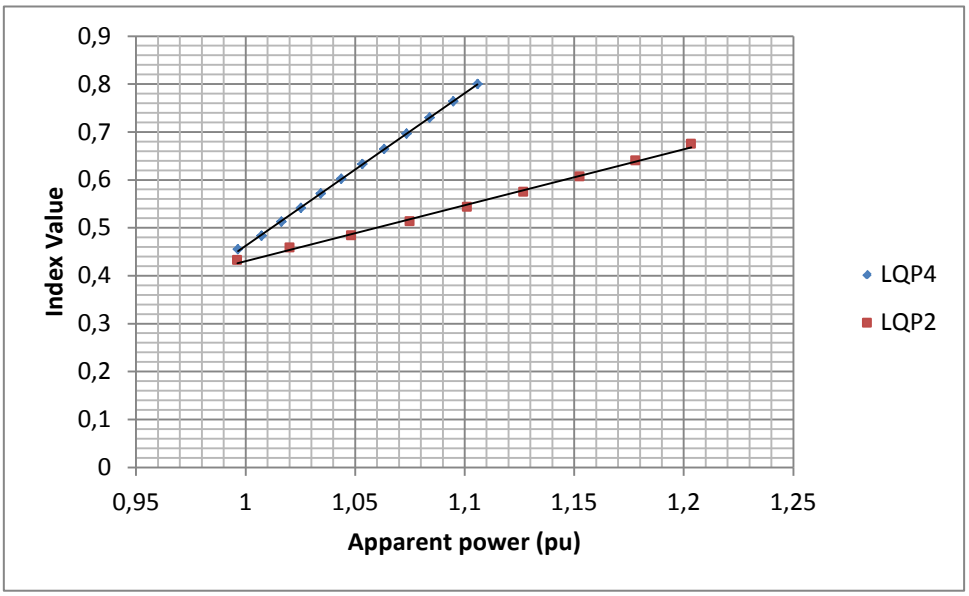

Fig.7.48 LQP versus apparent power (pu) in cases 2 and 4.

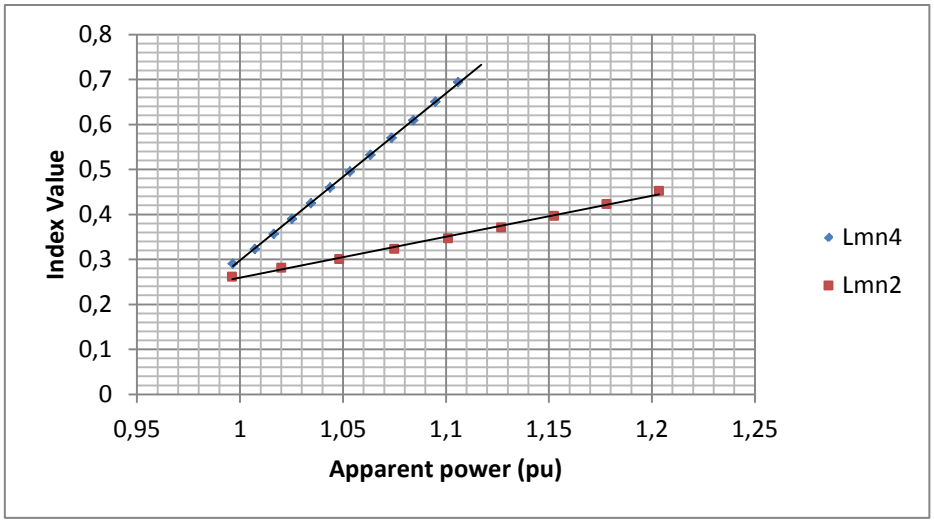

Fig.7.49 Lmn versus apparent power (pu) in cases 2 and 4.

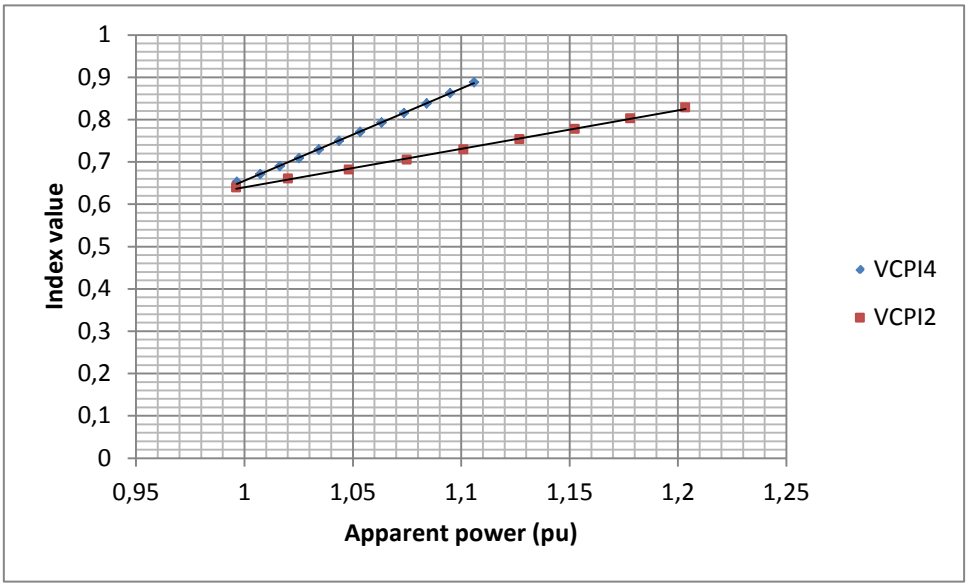

Fig.7.50 VCPI versus apparent power (pu) in cases 2 and 4.

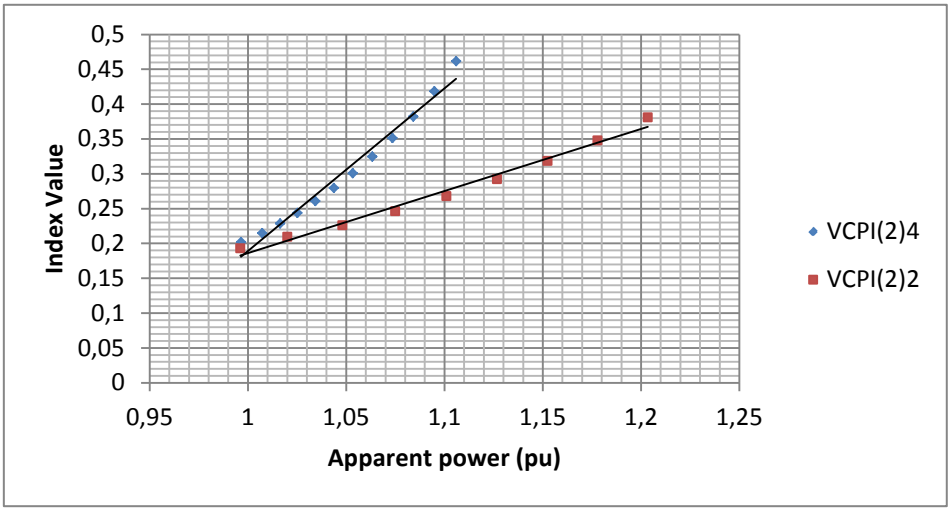

Fig.7.51 VCPI(2) versus apparent power (pu) in cases 2 and 4.

Index	Last value before collapse in case 2	Nearest similar value in case 4	Increase of apparent power before collapse in case 4 (pu)	Increase of apparent power before collapse in case 2 (pu)
VCPI(p)	0,85	0,86	0,022	0,025
VCPI(2)(l)	0,42	0,42	0,022	0,025
LQP	0,71	0,69	0,044	0,025
Lmn	0,48	0,49	0,066	0,025

Fig.7.52 Dependence on the index value to the nature of the load

From the results in Fig.7.52 it can be seen that VCPI indices have similar increase of apparent power before collapse for a same index value, while LQP and Lmn differ more, 0,044 and 0,066, respectively, compared to 0,025.

A more qualitative way of looking at this aspect is by plotting the indices and their apparent power margin, computed as the difference between their currents apparent power (pu) and the apparent power flow just before the voltage collapse point, as done in Fig.7.53-Fig.7.54 In Fig.7.53 can be seen that when getting close to the voltage collapse point, the two cases have really close values. That is, the index is not dependant on the load nature near the voltage collapse and that a value above 0,8 means that the system has less than 0,04 of apparent power margin regardless if it is just the reactive power increasing or if it is both, the active and reactive that are doing so.

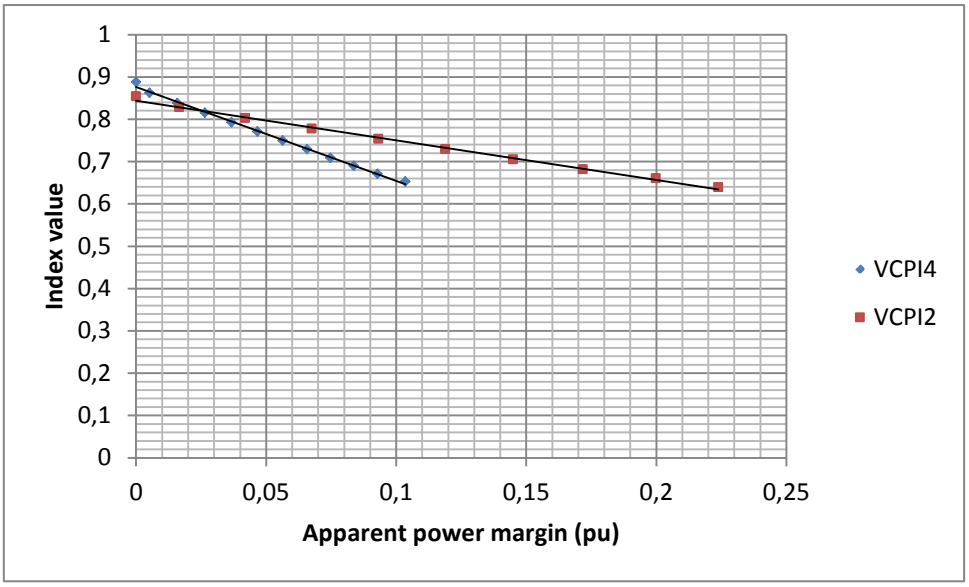

Fig.7.53 VCPI indices values in cases 2 and 4 versus the apparent power margin

On the other hand, it is shown in Fig.7.54 and Fig.7.55, that Lmn and LQP indices are dependent on the nature of the load near the voltage collapse point. For example, in Fig.7.55, a value of 0,5 for the Lmn index, can mean either that is about to collapse if it comes from an increase of reactive and active power, or it can mean it still has 0,05 apparent power margin, if the increase is just produced by an increase in the reactive power. In conclusion, the Lmn and LQP values themself do not provide information on how far the system is to voltage collapse if the nature of the increasing load is unknown.

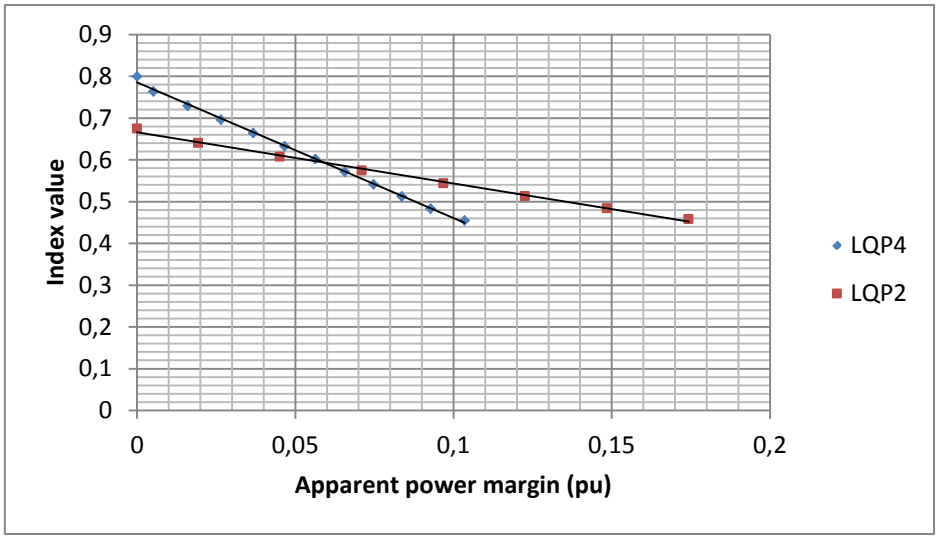

Fig.7.54 LQP indices values in cases 2 and 4 versus the apparent power margin

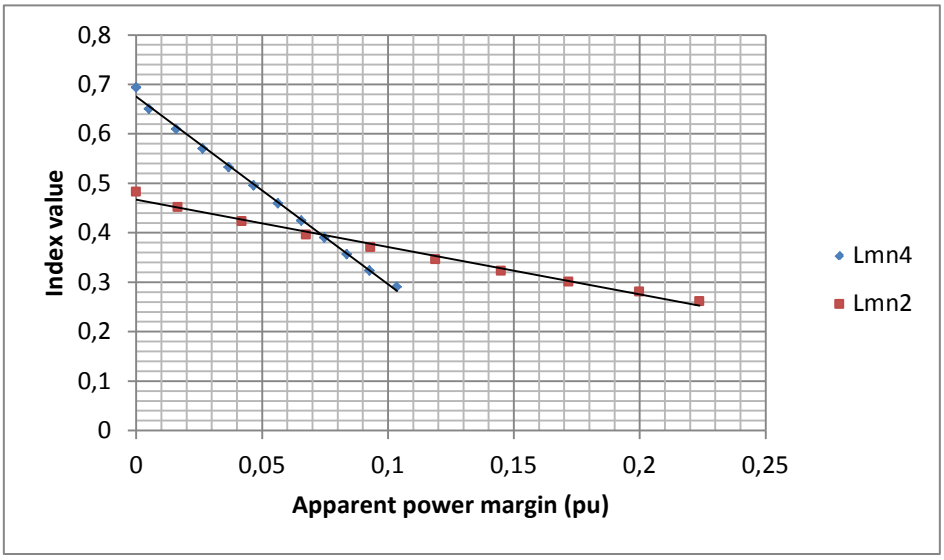

Fig.7.55 Lmn indices values in cases 2 and 4 versus the apparent power margin

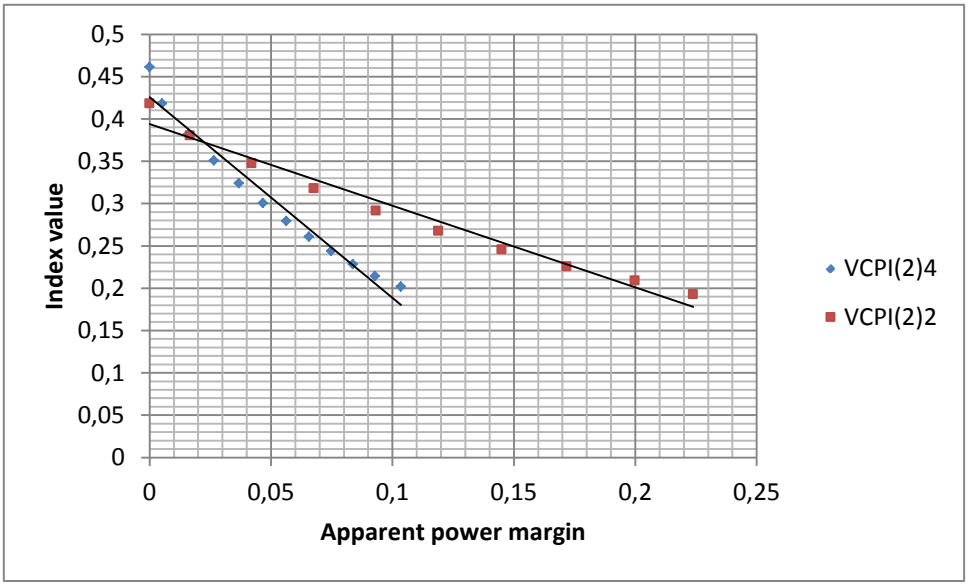

Fig.7.55 VCPI(2) indices values in cases 2 and 4 versus the apparent power margin

From these graphics, it can also be viewed, the point where both lines cross, that is, the point where the apparent power margin is the same regardless the case. This allows to define general intervals of margin, for example, LQP values higher than 0,6 means there is less than 0,06 apparent power margin before voltage collapse, lower than 0,6 the margin is more than 0,06. This can be done for all of the indices, as shown in Fig. 7.56.

Index	Index value	Apparent power margin interval (pu)
VCPI(p)	>0,8	<0,04
	<0,8	>0,04
LQP	>0,6	<0,06
	<0,6	>0,06
Lmn	>0,4	<0,08
	<0,4	>0,08
VCPI(2)(l)	>0,38	<0,015
	<0,38	>0,015

Fig.7.56 Apparent power margin interval (pu) for each index value

From this results, it could be used all the voltage stability indices in a complementary manner; since their results have different apparent power margin intervals. This way, smaller intervals could be defined based on the combination of indices, the following way (Fig.7.57):

Index values	Apparent power margin interval (pu)
Lmn<0,4	>0,08
Lmn>0,4 & LQP<0,6	[0,6, 0,8]
LQP>0,6 & VCPI<0,8	[0,6, 0,4]
VCPI>0,8 & VCPI(2)<0,38	[0,4, 0,015]
VCPI(2)>0,38	<0,015

Fig.7.57 Apparent power margin interval (pu) for each index value

To validate these results, more cases should be tested, since in this thesis only two cases have been compared. The further studies should include the analysis of uncertainty of load increases by using some random method or Monte Carlo simulations, similar of what has been done in [49]. This way, intervals of confidence for each of the apparent power margin intervals could be computed and the probability of the real system being in that interval could be assessed.

In addition, to see what the difference is between case 2 and case 4, the quantitative values used in the previous chapters are written together in a table (Fig. 7.58). First, the last value before voltage collapse, it can be noticed, that all indices present a higher value in the case where only Q is increased. Second, the first value after voltage collapse is lower for the VCPI(1) and VCPI(2) in Case 4, but higher for Lmn and LQP. Next, the increase of value at the voltage collapse point decreases in all of the indices if the only power increased is the reactive one. Finally, the linearity in the stable region is also negatively affected by Case 4, having lower R^2 values in that case.

Index	Last value before voltage collapse	First value after voltage collapse	Increase of value at the voltage collapse point	Linearity in the stable region
VCPI(p) Case 2	0,853651	1,00108	0,147429	0,9995
VCPI(p) Case 4	0,887821	0,997218	0,109397	0,9978
VCPI(2)(l) Case 2	0,418139	1,50854	1,090401	0,9855
VCPI(2)(l) Case 4	0,461411	1,40829	0,946879	0,9656
LQP Case 2	0,711157	0,956645	0,245488	0,9980
LQP Case 4	0,799553	0,978309	0,178756	0,9989
Lmn Case 2	0,482533	0,988773	0,50624	0,9962
Lmn Case 4	0,693662	1,01701	0,323348	0,9983

Fig.7.58 Quantitative values comparison between case 2 and case 4

Regarding the minimum eigenvalue of the Jacobian matrix, Fig.7.59 shows how they compare on the same apparent power base. It can be seen, that in both cases the value of the minimum eigenvalue provides information on how stable the system is at that point. Values above 1,2 indicate in both cases a stable system, where values below 1 indicate, the system is at three load increases to voltage collapse. Therefore, in this cases the Jacobian index value provides information on the stability of the system with independence on the case.

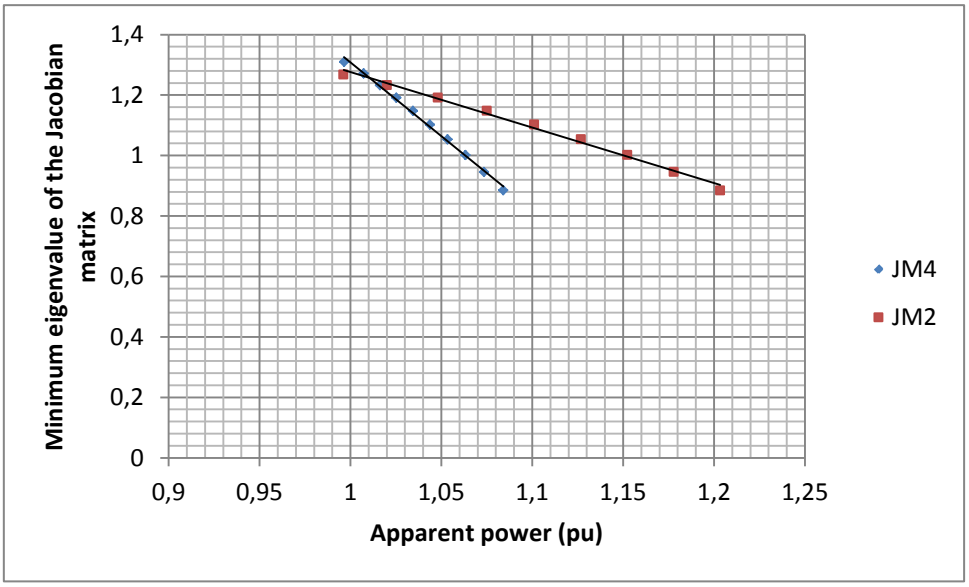

Fig.7.59 Jacobian matrix index values comparison between case 2 and case 4

7.2. 39-bus test network

For the 39-bus test network, two cases have been studied. Starting from a steady state base case, the active and reactive power consumption of the loads at the load buses are increased. At a certain operating point the two generators cannot sustain the voltage with sufficient reactive power anymore due to the increasing loads, and then the voltage collapses. In case 1, the active and reactive power load are increased stepwise by 10 % of the base case every 5 s and by 1% every 0.5 seconds in case 2.

7.2.1. Simulation Case 1

As previously mentioned, the first case in the 39-Bus system increases the load at each load node by a constant rate of 10% of the load base case every 5 seconds. The simulation runs for 50 seconds. The voltage collapse point is observed at the 4th load increase, 20 seconds after the simulation begins. Fig.7.60 and Fig.7.61 illustrate the active and reactive power at the load buses and Fig.7.62 shows the node voltages.

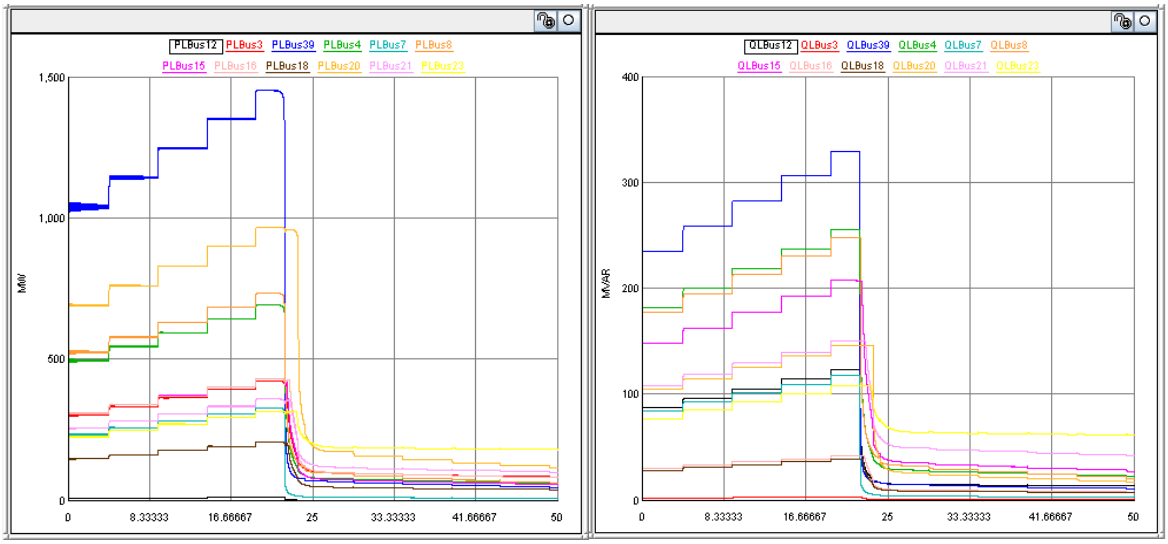

Fig. 7.60 Active and reactive power consumed at the load buses (1) (PloadN: Active power consumed by the load bus N; QloadN: Reactive power consumed by load bus N)

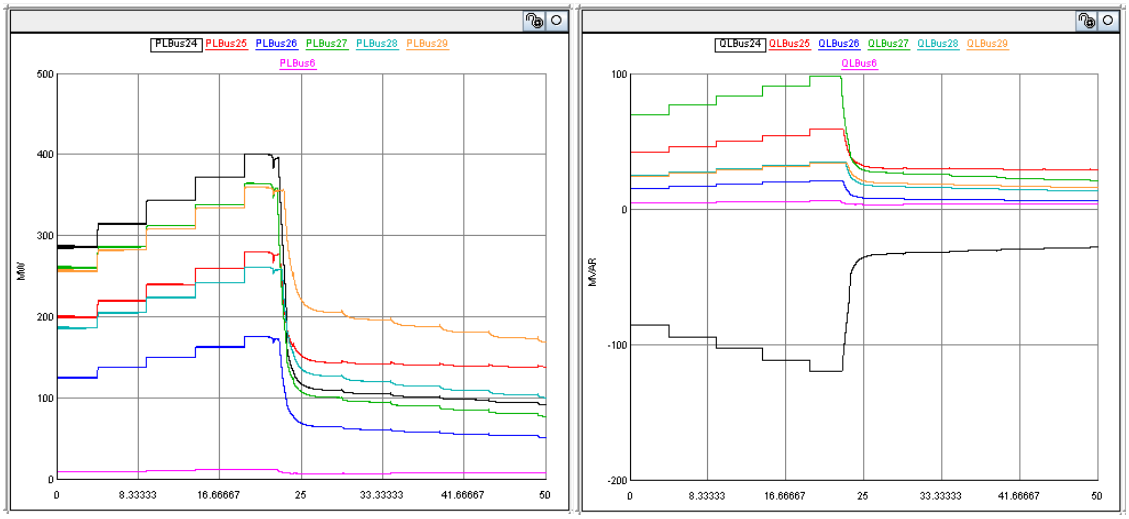

Fig. 7.61 Active and reactive power consumed at the load buses (2) (PloadN: Active power consumed by the load bus N; QloadN: Reactive power consumed by load bus N)

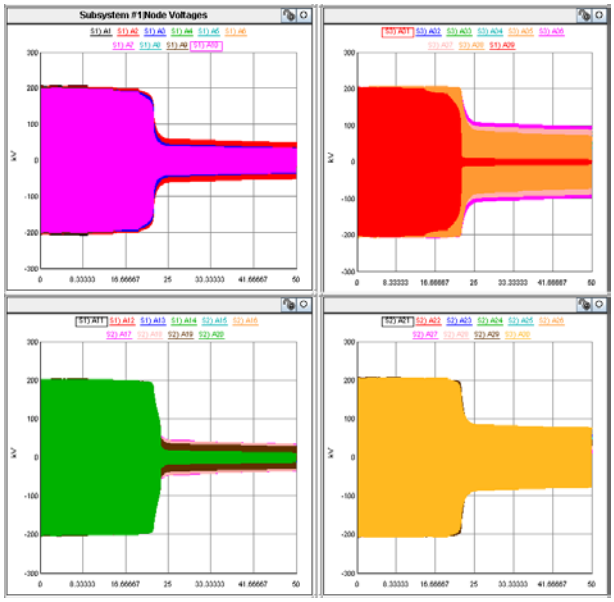

Fig. 7.62 Node voltages (AN: Voltage at node N)

7.2.1.1. Jacobian matrix index

Fig 7.63 shows that the results for the large 39-test network are also similar to the results obtained in the simulations done using the 5-bus test system. The minimum eigenvalues are positive while the system is stable, and the eigenvalues become negative when the system turns unstable, after the fourth load increase. As commented earlier, this index is a global index and therefore, it does not provide any information on the location of the weak bus or line of the system and just gives information on the global system, making it difficult to apply any control strategy to avoid voltage collapse from happening.

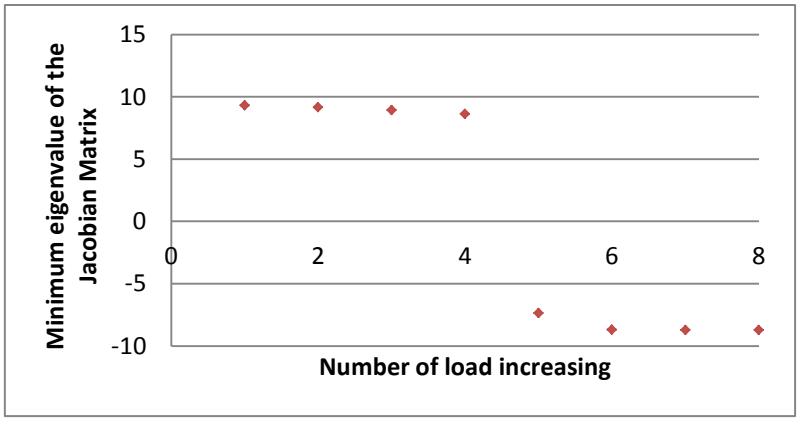

Fig. 7.63 Minimum eigenvalue of the Jacobian Matrix at each load step

7.2.1.2. Line indices

The 39-bus system has 46 lines. For this system, two line stability indices were used: the VCPI and the Lmn. Each line index was calculated using the control blocks components presented in chapter 6.4.2. The following plots were obtained in the Runtime simulation (Fig.7.64-Fig.67). These indices can be useful in such a large network, since they provide information on the weakest lines of the system.

Lmn index

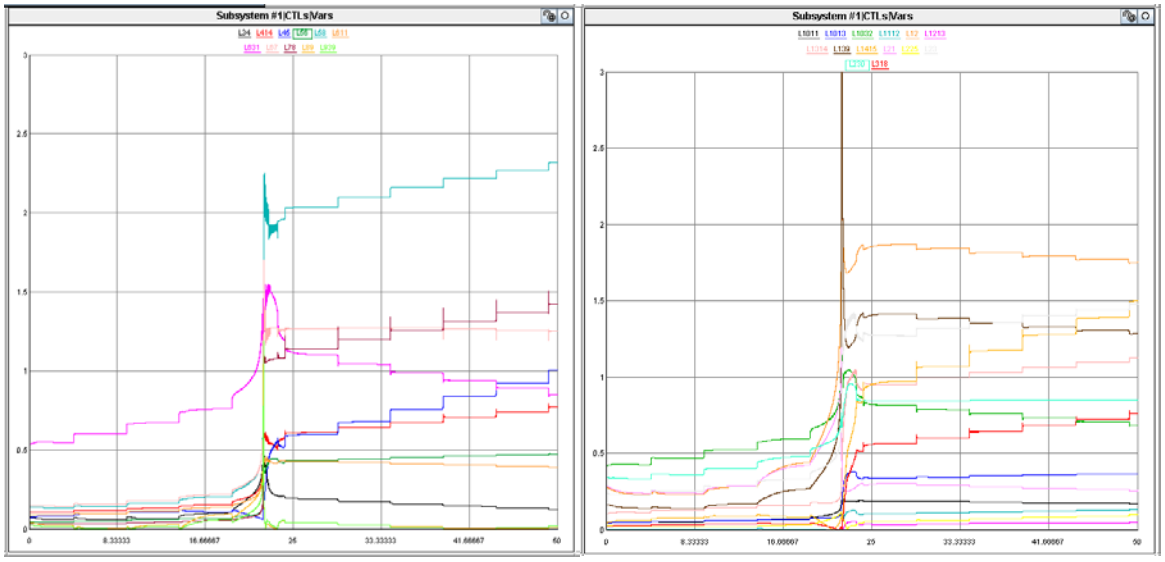

Fig. 7.64 Lmn values at each line of the system (1)

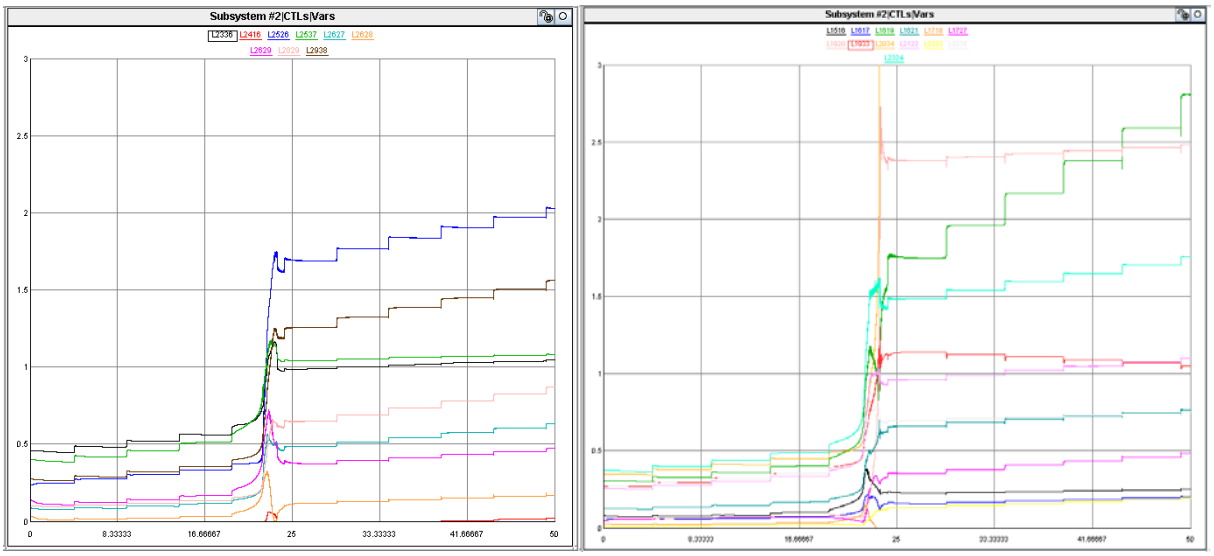

Fig. 7.65 Lmn values at each line of the system (2)

VCPI index

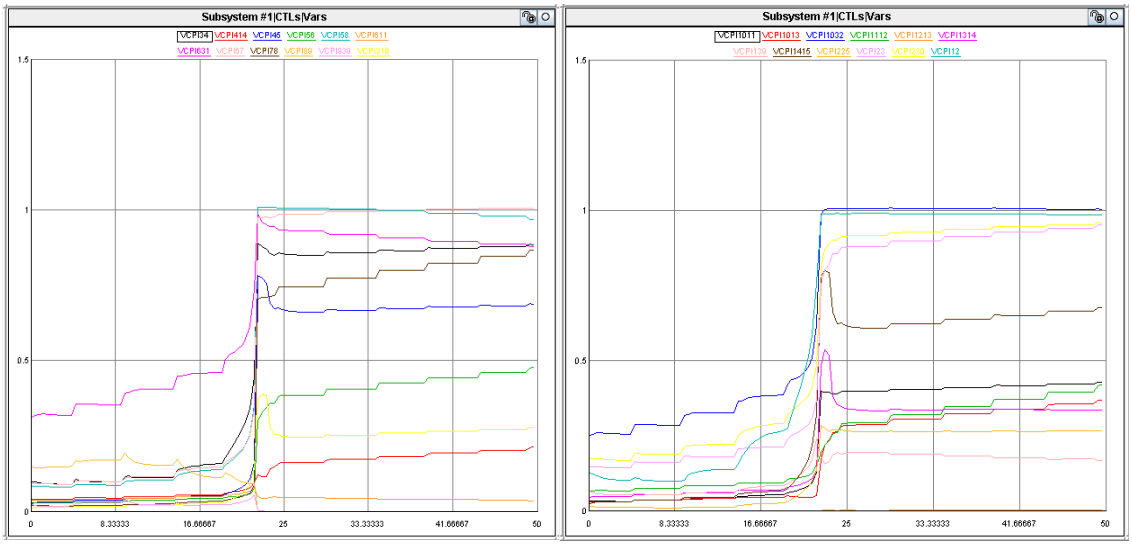

Fig. 7.66 VCPI values at each line of the system (1)

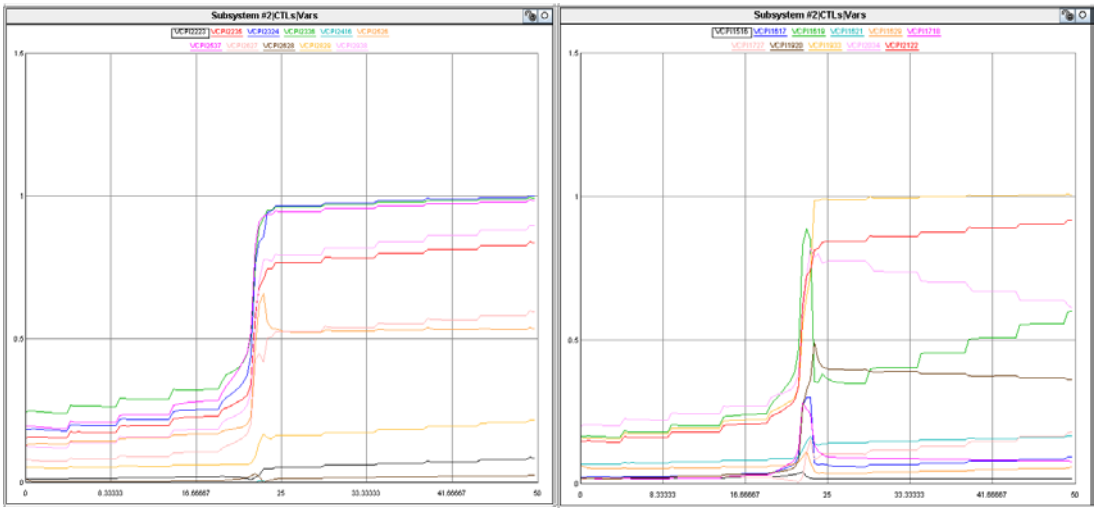

Fig. 7.67 VCPI values at each line of the system (2)

The steady state values of the five weakest lines according to each index are plotted in Fig.7.68. They show a similar form to the VCPI and Lmn indices at the 5-bus system.

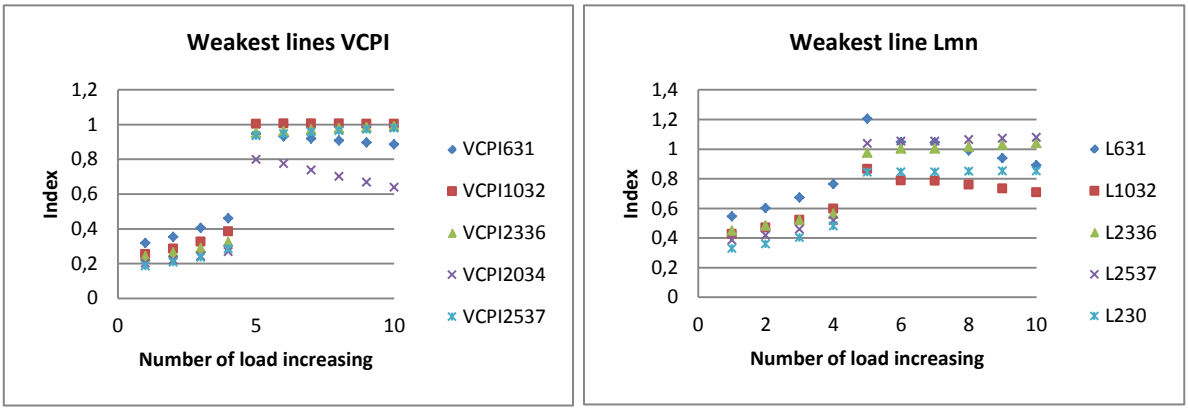

Fig. 7.68 Steady state values for the five weakest lines according to VCPI and Lmn indices

It can also be computed a global index taking the maximum value of all the line indices at each load step, which is shown in Fig.7.69.

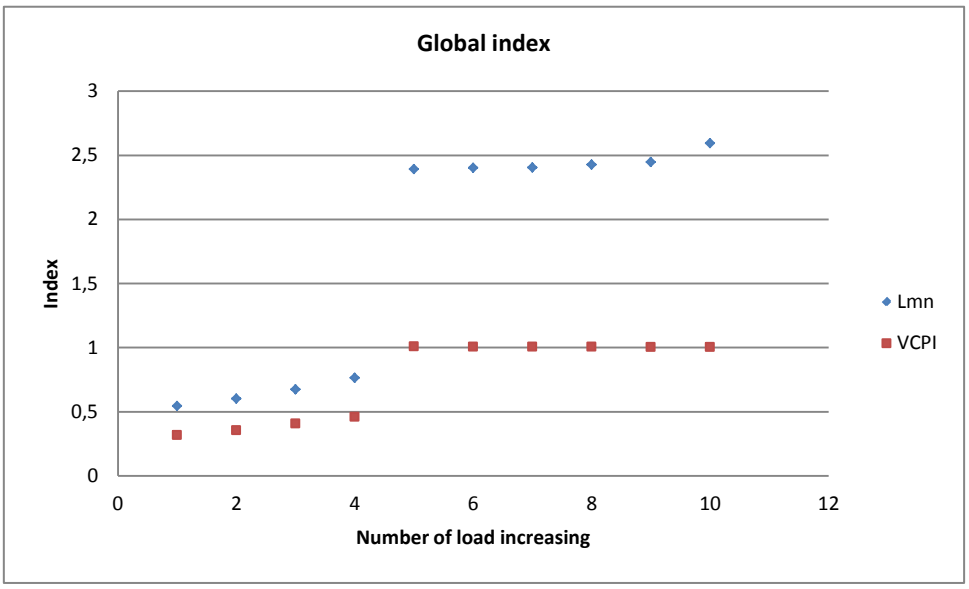

Fig. 7.69 Global index of Lmn and VCPI

As done in the previous 5-bus system, a quantitative comparison has been done in Fig. 7.71 with the following criterion: last value before voltage collapse, first value after voltage collapse, increase of value at the voltage collapse point and linearity in the stable region, showed in Fig.7.70.

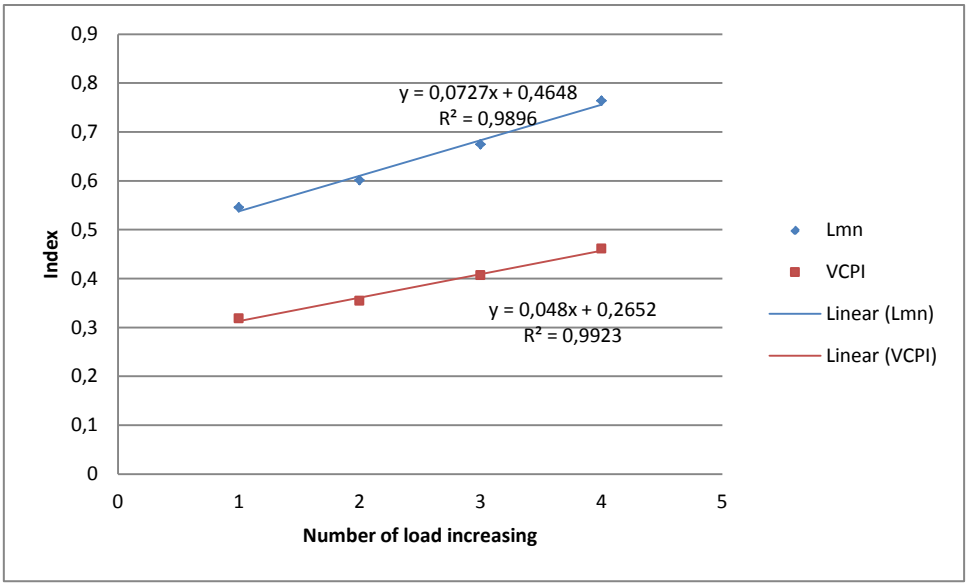

Fig. 7.70 Global index of Lmn and VCPI in stable region

Index	Last value before voltage collapse	First value after voltage collapse	Increase of value at the voltage collapse point	Linearity in the stable region (R^2)
VCPI(p)	0,461012	1,00997	0,548958	0,9896
Lmn	0,763824	2,39181	1,627986	0,9923

Fig. 7.71 Quantitative values comparison VCPI and Lmn

In the 5-bus test system all indices agreed in the ranking of the weakest line of the system, since it was a small network. In the 39-bus system is not exactly the same, so a comment on how they differ should be made. The two following tables (Fig.7.72 and 7.73) present the top ten weakest lines at load increasing 1 and 4, respectively.

Top weakest lines at number of load increasing 1					
VCPI			**Lmn**		
Rank	Line	Value	Rank	Line	Value
1	6-31	0,318381	1	6-31	0,545797
2	10-32	0,254699	2	23-36	0,44818
3	23-36	0,241149	3	10-32	0,426735
4	20-34	0,202423	4	25-37	0,387046
5	25-37	0,18717	5	23-24	0,366693
6	23-24	0,180128	6	20-34	0,348165
7	2-30	0,167367	7	2-30	0,330201
8	16-19	0,161817	8	16-19	0,302908
9	19-33	0,155822	9	19-33	0,26951
10	22-35	0,154898	10	22-35	0,267445

Fig. 7.72 Top ten weakest lines at load increasing 1-VCPI and Lmn

Top weakest lines at number of load increasing 4					
	VCPI			**Lmn**	
Rank	Line	Value	Rank	Line	Value
1	6-31	0,406629	1	6-31	0,763824
2	10-32	0,327218	2	10-32	0,598301
3	23-36	0,289609	3	23-36	0,563995
4	20-34	0,243751	4	25-37	0,518577
5	25-37	0,236027	5	23-24	0,491121
6	2-30	0,22111	6	2-30	0,482443
7	23-24	0,219992	7	20-34	0,447542
8	16-19	0,202212	8	1-2	0,442755
9	22-35	0,196697	9	16-19	0,405155
10	19-33	0,1941	10	19-33	0,358089

Fig. 7.73 Top ten weakest lines at load increasing 4-VCPI and Lmn

It can be noticed that the same lines are set to be the top ten weakest lines of the system using either one of the line stability indices. To see how they differ in terms of their ranking the following table (Fig.7.74), presents the rank difference for these top lines. The maximum rank difference between the indices is 2 at line 20-34, which is considered to be the fourth weakest line for VCPI and the sixth for Lmn rank. This shows that both indices agree on the ranking of line indices for the top ten weakest lines.

VCPI Rank	Line	Lmn Rank	Line	Rank difference
1	6-31	1	6-31	0
2	10-32	3	10-32	1
3	23-36	2	23-36	1
4	20-34	6	20-34	2
5	25-37	4	25-37	1
6	23-24	5	23-24	1
7	2-30	7	2-30	0
8	16-19	8	16-19	0
9	19-33	9	19-33	0
10	22-35	10	22-35	0

Fig. 7.74 Top ten weakest lines rank difference-VCPI and Lmn

Taking into account all of the lines, the rank difference between them is calculated in Fig.7.75. It shows that the maximum difference is 28 at line 8-9, the mean difference is 3,78 and the standard deviation 5,22.

VCPI Rank	Line	Lmn Rank	Line	Rank difference
15	29-38	11	29-38	4
25	28-29	23	28-29	2
24	26-29	21	26-29	3
44	26-28	42	26-28	2
20	26-27	26	26-27	6
5	25-37	4	25-37	1
14	25-26	13	25-26	1
46	24-16	45	24-16	1
3	23-36	2	23-36	1
6	23-24	5	23-24	1
10	22-35	10	22-35	0
42	22-23	43	22-23	1
12	21-22	12	21-22	0
4	20-34	6	20-34	2
9	19-33	9	19-33	0
39	19-20	32	19-20	7
35	17-27	30	17-27	5
40	17-18	38	17-18	2
21	16-21	19	16-21	2
8	16-19	8	16-19	0
34	16-17	31	16-17	3
38	15-16	27	15-16	11
32	14-15	28	14-15	4
26	13-14	20	13-14	6
45	1213	46	12-13	1
22	11-12	44	11-12	22
2	1032	3	10-32	1
31	10-13	33	10-13	2
30	10-11	34	10-11	4
36	9-39	41	9-39	5
1	6-31	1	6-31	0
28	6-11	24	6-11	4
27	4-14	22	4-14	5
41	3-18	37	3-18	4
7	2-30	7	2-30	0
43	2-25	40	225	3
23	1-39	17	1-39	6
11	8-9	39	8-9	28
37	7-8	36	7-8	1
17	6-7	16	6-7	1
19	5-8	18	5-8	1
33	5-6	35	5-6	2
29	4-5	25	4-5	4
18	3-4	29	3-4	11
13	2-3	15	2-3	2
16	1-2	14	1-2	2

Fig. 7.75 Rank difference between VCPI and Lmn

Other graphics that are interesting to comment are Fig. 7.76 and Fig.7.77. In this graphic all of the lines VCPI values are plotted in the first four load increases. It provides interesting information in a very visual way on how the increase in the loads affects each line and which ones are the weakest. It can also be viewed how the rankings change in every situation. For example, line 1-2, at the beginning of the load increase is not a weak line, but the change from load increase 3 to load increase 4 makes it turn into one.

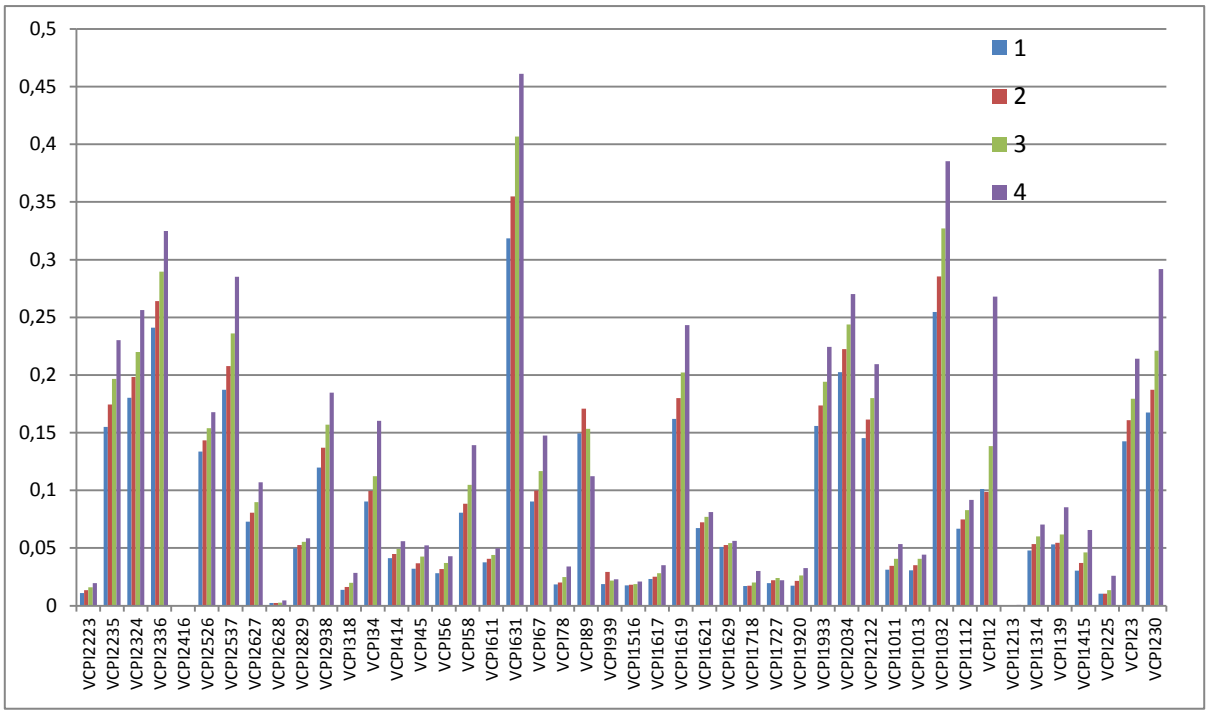

Fig. 7.76 VCPI values for all lines at load increasing 1-4

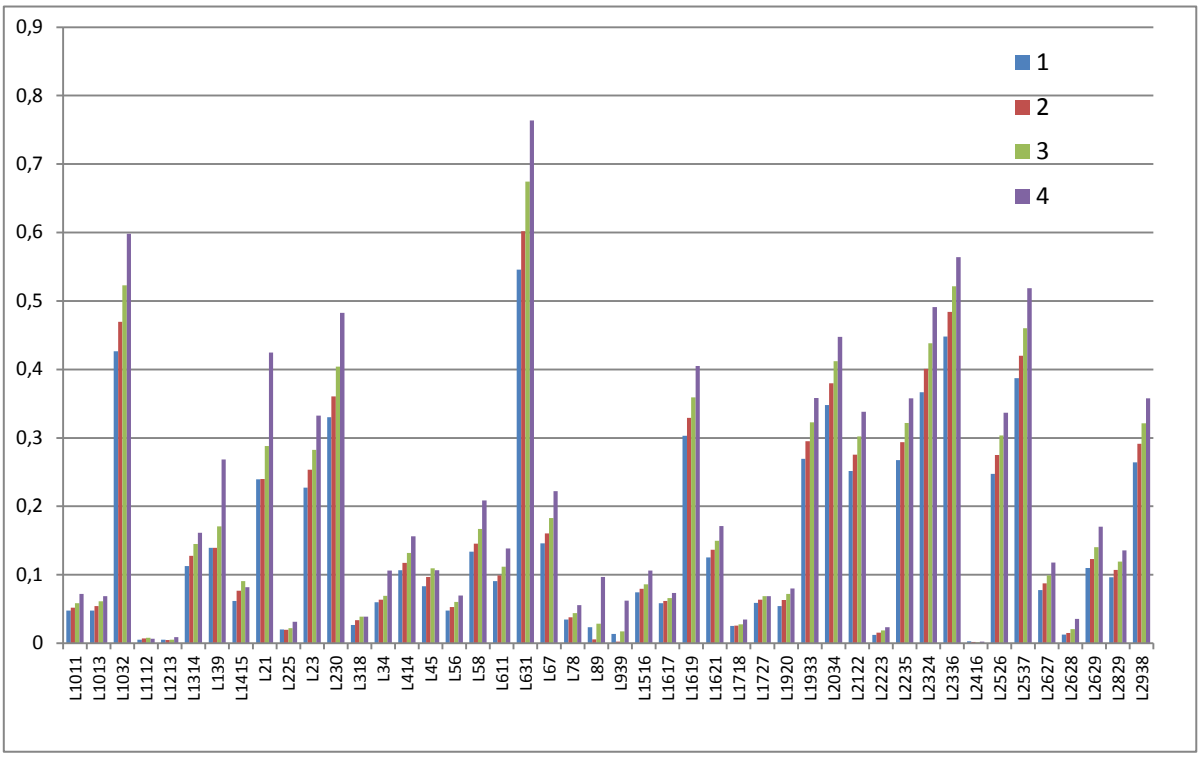

Fig. 7.77 Lmn values for all lines at load increasing 1-4

7.2.2. Simulation case 2

The second case in the 39-Bus system increases the load at each load node by a constant rate of 1% of the load base case every 0,5 seconds. The simulation runs for 50 seconds. The voltage collapse point is observed approximately 20 seconds after the simulation begins. Fig.7.78 and Fig.7.79 illustrate the active and reactive power at the load buses and Fig. 7.80 shows the node voltages.

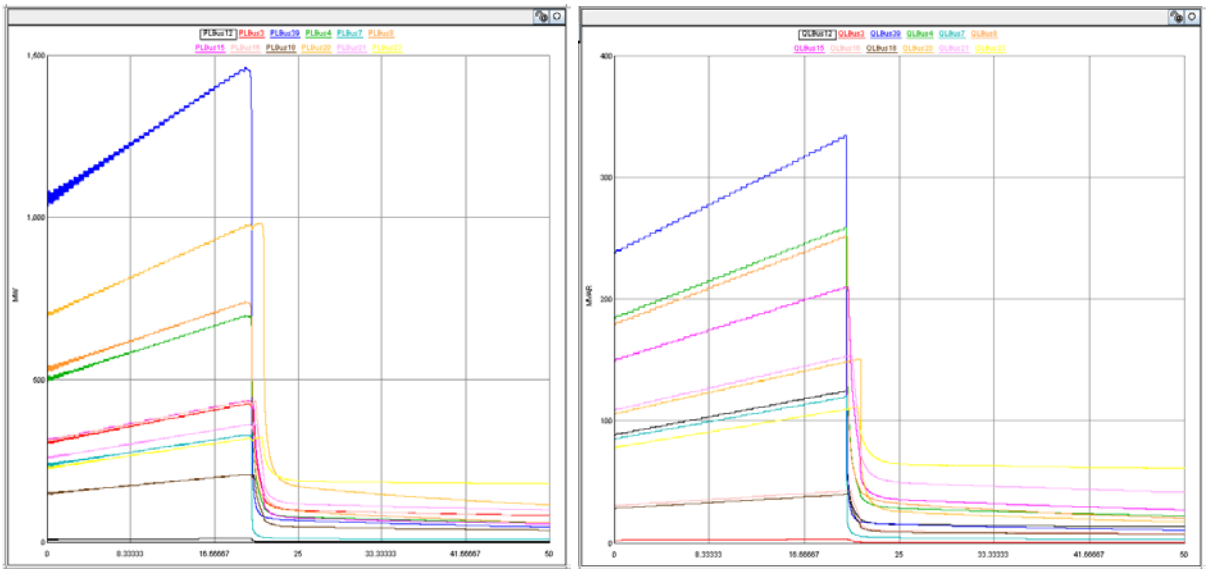

Fig. 7.78 Real and reactive power at the load buses (1)

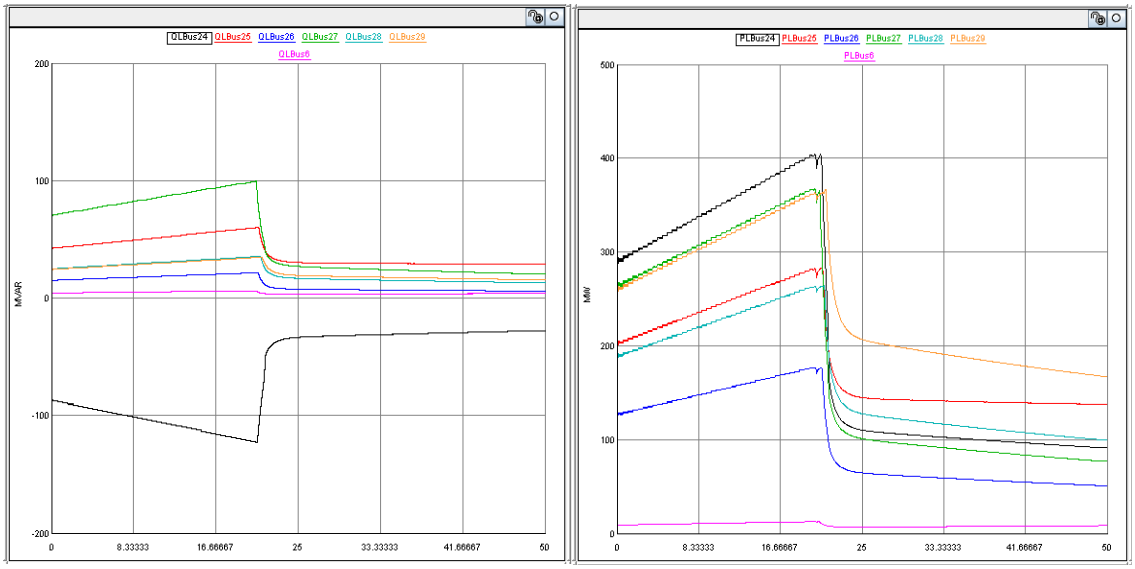

Fig. 7.79 Real and reactive power at the load buses (2)

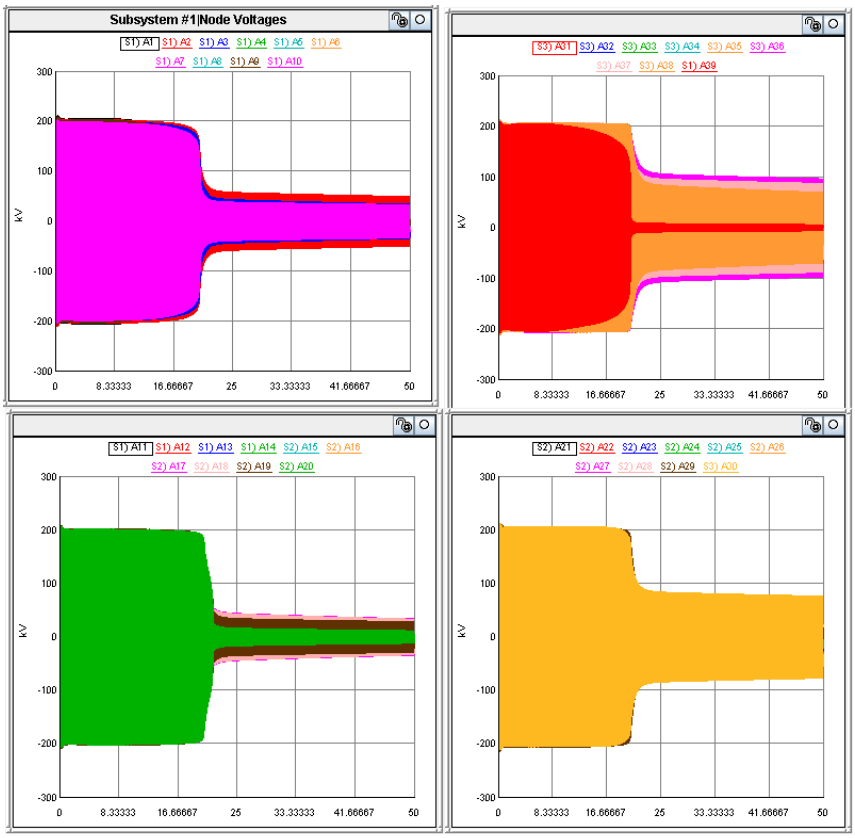

Fig. 7.80 Node voltages (AN: Voltage at Node N)

7.2.2.1. Jacobian matrix index

As done in case 1, the eigenvalues of the Jacobian matrix are computed and the minimum value is plotted at each load step in Fig 7.81. It is clearly seen how there is a high drop around the voltage collapse point that changes from 7 to -16 in just one second. The values in the stable region are plotted separately again in Fig.7.82 to view its shape better. In this case, the index also provides the expected form of positive values on the stable region and negative values on the unstable region.

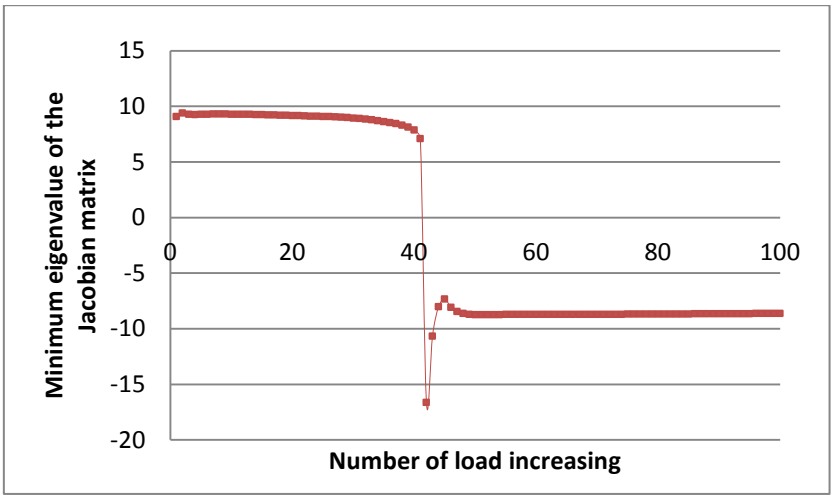

Fig. 7.81 Minimum eigenvalues of the Jacobian matrix

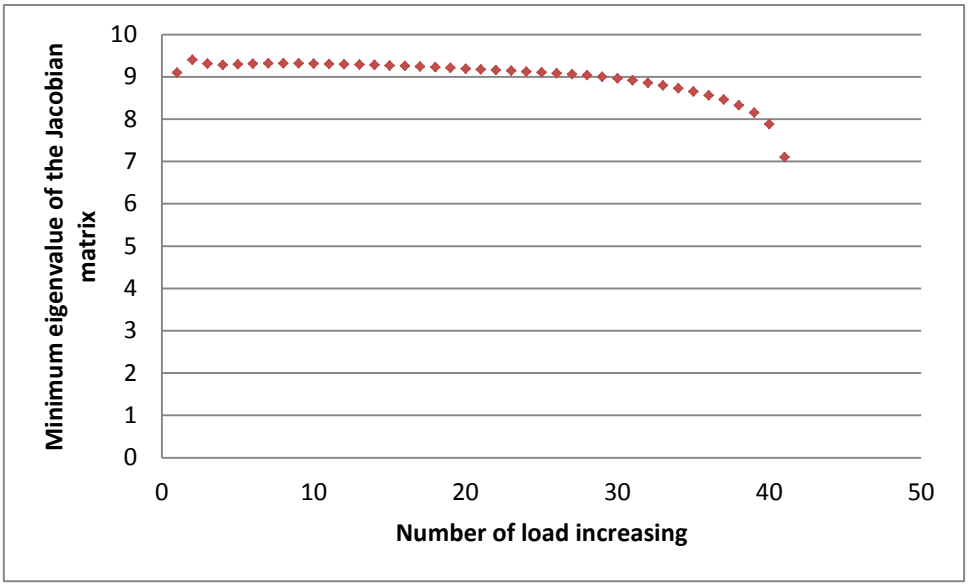

Fig. 7.82 Minimum eigenvalues of the Jacobian matrix at the stable region

7.2.2.2. Line indices

Again, the line indices are plotted in the RunTime. As in the Jacobian matrix index, the form of functions can be clearer observed (Fig.7.83-Fig.7.86), since there are more steps and therefore, more points computed. The steady state values where not computed since the plots in Runtime already offer this information. These figures show clearly the shape of the indices values and the point of collapse is clearly observed 20 seconds from the start of the simulation. The voltage collapse point presents an unstable shape and the index values are higher than previously, with some of them crossing 1 and other just increasing their value.

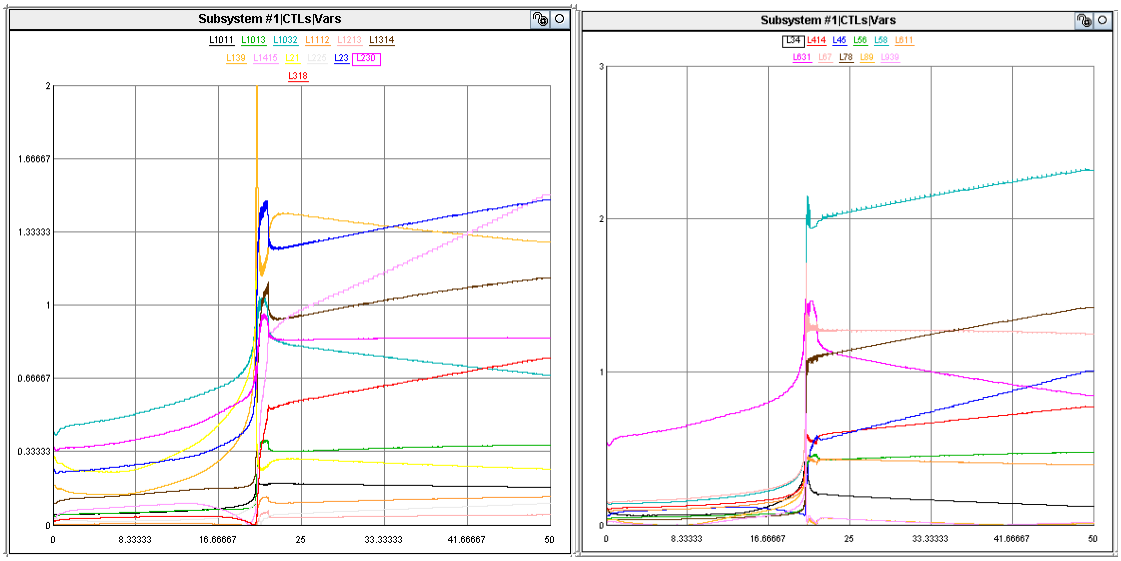

Fig. 7.83 Lmn values at each line of the system (1)

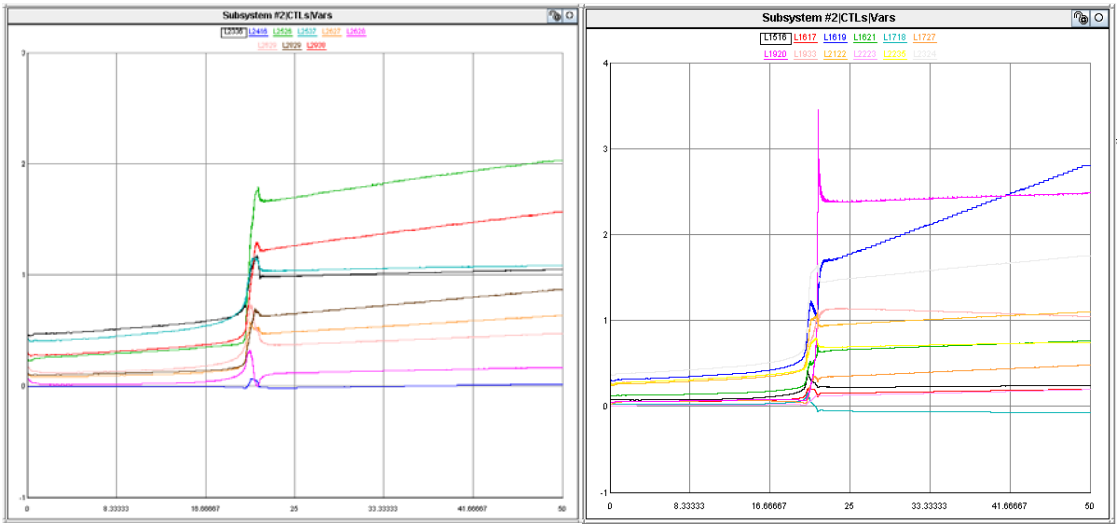

Fig. 7.84 Lmn values at each line of the system (2)

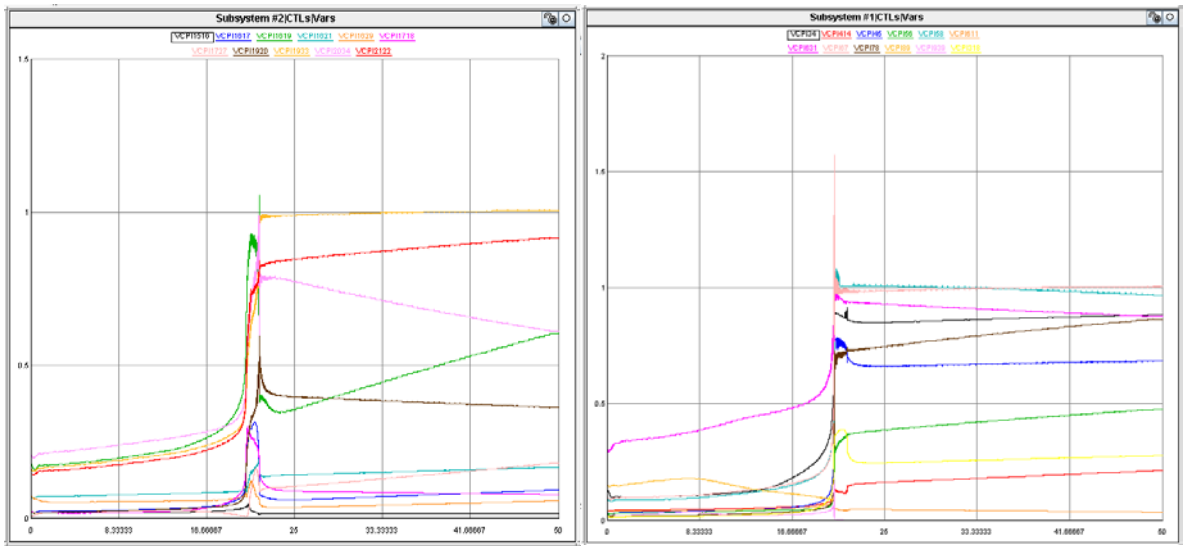

Fig. 7.85 VCPI values at each line of the system (1)

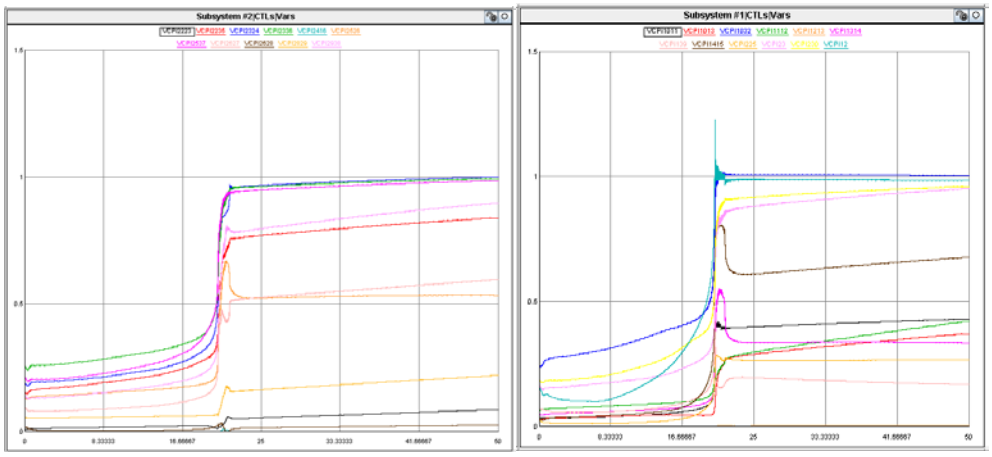

Fig. 7.86 VCPI values at each line of the system (2)

8. Conclusions and Future Work

This thesis compares the performance of different line voltage stability indices including Lmn, FVSI, VCPI, and LQP, as well as the traditional Jacobian index based on the minimum eigenvalue of the Jacobian matrix. The indices were tested in a small 5-bus system and in a larger 39-bus system. The simulation tool used was RTDS® and the indices where computed using the control blocks components in order to monitor the values in Runtime. This method was chosen to have the indices values available for future control algorithm development.

In terms of their general performance, all indices are coherent with their theoretical background. When the system is stable, these line indices present values well below 0 and cross 1 at the voltage collapse point. On the other hand, the minimum eigenvalue index also is consistent with its theoretical background, moving from a positive value, when the system is stable, into a negative value, after the system has collapsed.

Analysing further the results of the Jacobian matrix index, it can be stated that, this index is a global index and therefore, it does not provide any information on the location of the weak bus or line of the system. Therefore, it is not possible to apply a control strategy to avoid voltage collapse from happening. It also presents nonlinearity near the voltage collapse point, making it difficult to know how far the system is to voltage collapse considering the limit to be the theoretical 0, since it crosses this point with short notice.

To better predict the point of collapse with the Jacobian value, the values for each system have to be studied separately, since the last value before collapse, also depends on the system. In the 5-bus system the value is 0,88, where for the 39 bus system is around 8,15. The comparison between Case 2 and Case 4 on the 5-bus system shows that the index value itself provides information on the stability of the system, regardless of the nature of the load, if both active and reactive power are increasing (Case 2) or if it is only the reactive that is doing so (Case 4). In our simulations, minimum eigenvalues above 1,2 indicate in both cases a stable system, where values below 1 indicate, the system is at three load increases to voltage collapse. This statement should be validated with further tests using different load profiles.

Taking into account the results from the line stability indices: Lmn, LQP, FVSI, VCPI (p) and VCPI (l), several conclusions can be drawn. First of all, FVSI, which is an approximation of the Lmn index, cannot be considered a valid approximation, since in the simulations the index has a mean relative error of 16% and 45% in the unstable one.

Secondly, in general terms, all indices provide the same ranking for detecting the weakest lines in the 5-bus system. This information can be used to place shunt FACTS controllers, as done in [48]. For the 39-bus system, VCPI (p) and Lmn have the same top ten weakest lines of the system, with a maximum difference of their ranking in two places. For the overall system, with 46 lines, the mean difference between their ranking is 3,78 and the standard

deviation 5,22. These results show that both indices present a similar classification of the lines regarding their weakness.

Next, from the comparison of the quantitative values used, the indices can be classified in terms of their usefulness of their direct values. This does not mean that by having a bad rating in this category the index is useless, but that their values have to be better adjusted to assess how far the system is to collapse. The quantitative values used to assess this characteristic were: last value before voltage collapse occurs, first value after voltage collapse, increase of value at the voltage collapse point and linearity in the stable region. From this point of view, the best index was VCPI (p), followed by LQP, Lmn and VCPI (2)(l), respectively. It was also noticed, that Lmn and LQP have a better response when the increased is just from reactive power, than when it comes from both, while VCPI (p) and VCPI (l) have present a decrease in their performance.

Another aspect that was analysed, was how the index was independent upon the nature of the power, whether the increase was from both active and reactive, or if it was just due to the increase of reactive. This should be understood as how much does the index tells about the stability of the system by itself, without viewing any other measure or parameter of the system. From this point of view, the best results were obtained by the Jacobian index and VCPI (p), followed by VCPI (l), LQP and finally, Lmn.

This comparison also showed how the complementary use of the indices values could provide information on the apparent power margin interval valid for both cases. This way, smaller intervals could be defined based on the combination of indices, the way it was shown in (Fig.7.57). To validate these results, more cases should be tested, since in this thesis only two cases have been compared. The further studies should include the analysis of uncertainty of load increases by using some random method or Monte Carlo simulations, similar of what has been done in [49]. This way, intervals of confidence for each of the apparent power margin intervals could be computed and the probability of the real system being in that interval could be assessed.

To summarize the performance of the different indices from the results mention above, the following table (Fig.8.1) shows their ranking on three characteristics defined as follows: accuracy (usefulness of their direct values), robustness to uncertainty (independence on the nature of the load increase) and usable for control purposes (detection of weak lines).

Index type	Index	Accuracy	Robustness to uncertainty	Usable for control purposes
Jacobian index	Minimum eigenvalue of the Jacobian matrix	+	+++	+
Line indices	Lmn	+	+	+++
	VCPI (p)	+++	+++	+++
	VCPI(l)	+	++	+++
	LQP	++	+	+++

Fig.8.1. Comparison on VSI regarding their accuracy, robustness to uncertainty and usable for control purposes (+:poor, ++:regular, +++:good)

Interesting future developments based on this thesis will be provided before coming to an end. The first immediate development could be transfer the control blocks of the different line indices into a component using the Cbuilder program in RTDS. This action will make the line indices component easier to work with and less prone to errors. Complementary to this work, it could also be relevant to develop and test control algorithms using the results of the line stability indices.

Secondly, it would also be interesting to build index components using the same program, the CBuilder in RTDS) for the rest of the presented indices, such as all the PMU-based voltage stability analysis. This will enable us to implement and analyse control algorithms based on them. Also, further comparisons on voltage stability indices could be done, for example, line stability indices versus the PMU-based voltage stability. It could also be worth to compare the results obtained using different Thevenin equivalent methods (RLS, Transmission corridors and Approximation) or by choosing one Thevenin equivalent method, and then, comparing the different indices.

Additionally, it is proposed to compare how the different indices in more realistic environments, where the load is not increased stepwise, but introducing uncertainty to it, for example by performing Monte Carlo simulations[49]. This could be done in RTDS, by creating random load increasing number with a particular random distribution in MatLab and then saving the results in a file and use it as the input for the dynamic load component. These results would help in the verification of the independence of the indices values of the nature of the load increase and whether they provide useful information by themselves.

Finally, other encouraged works will be studies on how the indices react to contingencies and faults or compare the effectiveness of placing shunt FACTS controllers at the weakest bus/line, similar to what is being introduced in [48].

Bibliography

[1] P. Pourbeik, P. Kundur, and C.W. Taylor, "The anatomy of a power grid blackout - Root causes and dynamics of recent major blackouts", *Power and Energy Magazine, IEEE,* Sept.-Oct. 2006, pp. 22-29.

[2] P. Kundur, *Power System Stability and Control*. New York: McGraw-Hill, 1994.

[3] T. Van Cutsem and C. Vournas, *Voltage Stability of Electric Power Systems*. Norwell, MA: Kluwer, 1998.

[4] P. Kundur *et al.*, "Definition and classification of power system stability", *IEEE Transactions on Power Systems*, Vol. 19, No. 2, May 2004, pp. 1387-1401.

[5] T. Van Cutsem, "Voltage instability: phenomena, countermeasures, and analysis methods", *Proceeding of the IEEE*, Vol. 88, No. 2, February 2000, pp.208-227.

[6] S. Repo, "On-line voltage stability assessment of power systems - An approach of black-box modelling," Ph.D. dissertation, Tampere University of Technology, 2001.

[7] B. Gao, G.K. Morison and P. Kundur, "Towards the development of a systematic approach for voltage stability assessment of large-scale power systems," *IEEE Transactions on Power Systems*, Vol. 11, No. 3, August 1996, pp. 1314.

[8] C. W. Taylor, *Power System Voltage Stability*. New York: McGraw-Hill, 1994.

[9] F. Karbalaei, H. Soleymani and S. Afsharnia, "A comparison of voltage collapse proximity indicators", *IPEC 2010 Conference Proceedings*, 27-29 Oct. 2010, pp. 429-432.

[10] Y. Gong, N. Schulz and A. Guzman, "Synchrophasor-based real-time voltage stability index", *Proc. Power System Conference and Exposition*, Atlanta, Oct.-Nov. 2006.

[11] C. Reis and F.P. Maciel Barbosa, "A comparison of voltage stability indices", *IEEE MELECON 2006*, 16-19 May 2006, Málaga, Spain, pp.1007-1010.

[12] M.V. Suganyadevi and C.K. Babulal, "Estimating of loadability margin of a power system by comparing voltage stability indices", *International Conference on Control, Automation, Communication and Energy Conservation*, 4-6th June 2009, pp. 1-5.

[13] S. Massuco *et al*, "Evaluation of some indices for voltage stability assessment", *IEEE Bucharest Power Tech Conference*, 28th June-2nd July, Bucharest, Romania, pp.1-8.

[14] C. Canizares *et al*., *Voltage Stability Assessment: Concepts, Practices, and Tools*, IEEE PES Power System Stability Subcommittee, 2002, pp. 4.1-4.69.

[15] P.A. Lof, T.Smed, G.Andersson and D.J. Hill, "Fast calculation of a voltage stability index", *IEEE Transactions on Power Systems*, Vol. 7, No. 1, February 1992, pp.1529-1541.

[16] H.D. Chiang and R.J. Jumeau, "Towards a practical performance index for predicting voltage collapse in electrical power system", *IEEE Transactions on Power Systems*, Vol. 10, No. 2, May 1995, pp. 584-592.

[17] A. Berizzi, P. Finanzzi, D. Dorsi, P. Marannino and S. Corsi, "First and second order methods for voltage collapse assessment and security enhancement", *IEEE Transactions on Power Systems*, Vol. 13, No. 2, May 1998, pp.543-551.

[18] W. Dommel, "Digital computer solution of electromagnetic transients in single- and multiphase networks", *IEEE Transactions on Power Apparatus and Systems*, Vol. PAS-88, No. 4, April 1969, pp.388-399.

[19] A. C. Z. de Souza, C. A. Cañizares and V. H. Quintana, "New techniques to speed up voltage collapse computations using tangent vectors", *IEEE Transactions on Power Systems*, Vol. 12, No. 3, August 1997, pp.1380-1387.

[20] N. D. Hatziargyriou and T. Van Cutsem, "Indices for predicting voltage collapse including dynamic phenomena", technical report TF-38-02-11, *CIGRE*, 1994.

[21] U. Eminoglu and M.H. Hocaoglu, "A voltage stability index for radial distribution networks", *UPEC 2007*, pp.408-413.

[22] P. Kessel and H. Glavitsch, "Estimating the voltage stability of a power system", *IEEE Transactions on Power Delivery*, Vol.PWRD-1, No.3, July 1986, pp. 346-353.

[23] M. H. Haque, "Use of local information to determine distance to voltage collapse", *The 8th International Power Engineering Conference IPEC 2007*, pp. 407-411.

[24] M. Moghavvemi, "New method for indicating voltage stability in power system" *Proceedings of IEEE International Conference on Power Engineering*, Singapore, IPEC, 1997, pp. 223-227.

[25] A. Mohamed, G. B. Jasmon and S. Yusoff, "A static voltage collapse indicator using line stability factors", *Journal of Industrial Technology*, Vol. 7, No. 1, 1989, pp. 73-85.

[26] I. Musirin and T.K.A. Rahman, "Novel Fast Voltage Stability Index (FVSI) for Voltage Stability Analysis in Power Transmission System", *2002 Student Conference on Research and Development Proceedings*, Shah Alam, Malasia, July 2002.

[27] M. Moghavvemi and O. Faruque, "Real-Time Contingency Evaluation and Ranking Technique", *IEEE Proceedings on Generation, Transmission and Distribution*, Vol. 145, No.5, September 1998, pp. 517-524.

[28] IEEE Standard C37.118-2005, "IEEE Standard for synchrophasors for power systems", 2006.

[29] M. Glavic and T. Van Cutsem, "Wide-area detection of voltage instability from synchronized phasor measurements. Part I: Principle," *IEEE Transactions on Power Systems*, Vol. 24, No. 3, August 2009, pp. 1408-1416.

[30] M. Glavic and T. Van Cutsem, "Wide-area detection of voltage instability from synchronized phasor measurements. Part II: Simulation results," *IEEE Transactions on Power Systems*, Vol. 24, No. 3, August 2009, pp. 1417-1425.

[31] M. Glavic and T. Van Cutsem, "Detecting with PMUs the onset of voltage instability caused by a large disturbance," *Proceedings 2008 IEEE Power Engineering Society General Meeting*, Pittsburgh, PA, July 2008.

[32] V. Balamourougan, T. S. Sidhu, and M. S. Sachdev, "Technique for online prediction of voltage collapse," *IEEE Proceedings in Generation, Transmission and Distribution*, Vol. 151, No. 4, July 2004, pp. 453–460.

[33] K. Vu, M. M. Begovic, D. Novosel, and M. M. Saha, "Use of local measurements to estimate voltage stability margin," *IEEE Transactions on Power Systems*, Vol. 14, No. 3, August 1999, pp. 1029–1035.

[34] D. E. Julian, R. P. Schulz, K. T. Vu, W. H. Quaintance, N. B. Bhatt and D. Novosel, "Quantifying proximity to voltage collapse using the voltage instability predictor (VIP*)"*, *Proceedings IEEE PES Summer Meeting*, Seattle, July 2000, pp. 16-20.

[35] L. Warland and A. T. Holen, "Estimation of distance to voltage collapse: Testing and algorithm based on local measurements," in Proceedings 14th Power System Computation Conference (PSCC), Sevilla, Spain, June 2002.

[36] M. Zima, M. Larsson, P. Korba, C. Rehtanz and G. Andersson, "Design aspects for wide-area monitoring and control systems", *Proceedings of the IEEE*, Vol. 93, No. 5, May 2005, pp.980-996.

[37] B. Milosevic and M. Begovic, "Voltage stability protection and control using a wide-area network of phasor measurements," *IEEE Transactions on Power Systems*, Vol. 18, No. 1, February 2003, pp. 121–127.

[38] G. Verbic and F. Gubina, "Fast algorithm for voltage collapse protection based on local phasors", *Power Engineering Society Summer Meeting, 2002 IEEE*, Vol. 3, July 2002, pp. 1650-1655.

[39] G. Verbic and F. Gubina, "A new concept of voltage collapse protection based on local phasors", *IEEE Transactions on Power Delivery*, Vol. 19, No. 20, April 2004, pp. 576-581.

[40] B. Genet and J.C. Maun, "Voltage stability monitoring using wide-area measurement systems" *Power Tech, 2007 IEEE Lausanne*, July 2007.

[41] RTDS, User Manuals, RTDS Technologies.

[42] H. Naishan *et al.*, "The analysis of abundance index of voltage stability based circuit theory", *Guangxi Electric Power*, February 2006, pp.12-14.

[43] J. Tang, J.Liu, F. Ponci *et al.*, "Effects of PMU's uncertainty on voltage stability assessment in power systems".

[44] I. Smon, G. Verbic and F. Gubina, "Local voltage stability index using Tellegen's theorem", *IEEE Transactions on Power Systems*, Vol. 21, No. 3, August 2006, pp. 1267–1275.

[45] W. Li, Y. Wang and T. Chen, "Investigation on the Thevenin equivalent parameters for online estimation of maximum power transfer limits", *IET Generation, Transmission and Distribution*, Vol. 4, Iss. 4, 2010, pp. 1180–1187.

[46] J. Depablos, V. Centeno et al, "Comparative testing of synchronized phasor measurement units", *IEEE Power and Energy Society General Meeting 2004*, June 2004, pp. 948-955.

[47] http://sys.elec.kitami-it.ac.jp/ueda/demo/WebPF/39-New-England.pdf

[48] A.R. Phadke, S.K. Bansal, K. R. Niazi, "A Comparison on Voltage Stability Indices for Placing Shunt FACTS Controllers", *ICETET '08 Proceedings of the 2008 First International Conference on Emerging Trends in Engineering and Technology*, pp. 939-944.

[49] T.Ratniyomchai and T. Kulworawanichpong, "Monte Carlo simulation for voltage stability index evaluation", *WSEAS Transactions on Power Systems*, Vol.3, Iss. 12, December 2008, pp. 735-744.

Appendix

A. 39-bus system parameters

The complete 39-bus system parameters are provided below. They are given in per unit on a 60Hz and 100MVA base.

Generators: Two-axis model of the synchronous machines is shown in the table below.

Unit No	H	Ra	x'd	x'q	xd	xq	T'do	T'qo	xl
1	500,0	0	0,006	0,008	0,02	0,019	7,0	0,7	0,003
2	30,3	0	0,0697	0,170	0,295	0,282	6,56	1,5	0,035
3	35,8	0	0,0531	0,0876	0,2495	0,237	5,7	1,5	0,0304
4	28,6	0	0,0436	0,166	0,262	0,258	5,69	1,5	0,0295
5	26,0	0	0,132	0,166	0,67	0,62	5,4	0,44	0,054
6	34,8	0	0,05	0,0814	0,254	0,241	7,3	0,4	0,0224
7	26,4	0	0,049	0,186	0,295	0,292	5,66	1,5	0,0322
8	24,3	0	0,057	0,0911	0,29	0,280	6,7	0,41	0,028
9	34,5	0	0,057	0,0587	0,2103	0,205	4,79	1,96	0,0298
10	42,0	0	0,031	0,008	0,1	0,069	10,2	0,0	0,0125

Lines/Transformers: The network data for this system is shown in the Table below.

Line Data					Transformer Tap	
From	To	R	X	B	Magnitude	Angle
1	2	0,0035	0,0411	0,6987	0,0000	0,0000
1	39	0,0010	0,0250	0,7500	0,0000	0,0000
2	3	0,0013	0,0151	0,2572	0,0000	0,0000
2	25	0,0070	0,0086	0,1460	0,0000	0,0000
3	4	0,0013	0,0213	0,2214	0,0000	0,0000
3	18	0,0011	0,0133	0,2138	0,0000	0,0000
4	5	0,0008	0,0128	0,1342	0,0000	0,0000
4	14	0,0008	0,0129	0,1382	0,0000	0,0000
5	6	0,0002	0,0026	0,0434	0,0000	0,0000
5	8	0,0008	0,0112	0,1476	0,0000	0,0000
6	7	0,0006	0,0092	0,1130	0,0000	0,0000
6	11	0,0007	0,0082	0,1389	0,0000	0,0000
7	8	0,0004	0,0046	0,0780	0,0000	0,0000
8	9	0,0023	0,0363	0,3804	0,0000	0,0000

9	39	0,0010	0,0250	1,2000	0,0000	0,0000
10	11	0,0004	0,0043	0,0729	0,0000	0,0000
10	13	0,0004	0,0043	0,0729	0,0000	0,0000
13	14	0,0009	0,0101	0,1723	0,0000	0,0000
14	15	0,0018	0,0217	0,3660	0,0000	0,0000
15	16	0,0009	0,0094	0,1710	0,0000	0,0000
16	17	0,0007	0,0089	0,1342	0,0000	0,0000
16	19	0,0016	0,0195	0,3040	0,0000	0,0000
16	21	0,0008	0,0135	0,2548	0,0000	0,0000
16	24	0,0003	0,0059	0,0680	0,0000	0,0000
17	18	0,0007	0,0082	0,1319	0,0000	0,0000
17	27	0,0013	0,0173	0,3216	0,0000	0,0000
21	22	0,0008	0,0140	0,2565	0,0000	0,0000
22	23	0,0006	0,0096	0,1846	0,0000	0,0000
23	24	0,0022	0,0350	0,3610	0,0000	0,0000
25	26	0,0032	0,0323	0,5130	0,0000	0,0000
26	27	0,0014	0,0147	0,2396	0,0000	0,0000
26	28	0,0043	0,0474	0,7802	0,0000	0,0000
26	29	0,0057	0,0625	1,0290	0,0000	0,0000
28	29	0,0014	0,0151	0,2490	0,0000	0,0000
12	11	0,0016	0,0435	0,0000	1,0060	0,0000
12	13	0,0016	0,0435	0,0000	1,0060	0,0000
6	31	0,0000	0,0250	0,0000	1,0700	0,0000
10	32	0,0000	0,0200	0,0000	1,0700	0,0000
19	33	0,0007	0,0142	0,0000	1,0700	0,0000
20	34	0,0009	0,0180	0,0000	1,0090	0,0000
22	35	0,0000	0,0143	0,0000	1,0250	0,0000
23	36	0,0005	0,0272	0,0000	1,0000	0,0000
25	37	0,0006	0,0232	0,0000	1,0250	0,0000
2	30	0,0000	0,0181	0,0000	1,0250	0,0000
29	38	0,0008	0,0156	0,0000	1,0250	0,0000
19	20	0,0007	0,0138	0,0000	1,0600	0,0000

Power and Voltage set points

Bus	**Type**	**Voltage(pu)**	**Load**		**Generator**		
			MW	MVar	MW	MVar	Unit No
1	PQ	-	0,0	0,0	0,0	0,0	
2	PQ	-	0,0	0,0	0,0	0,0	
3	PQ	-	322,0	2,4	0,0	0,0	
4	PQ	-	500,0	184,0	0,0	0,0	
5	PQ	-	0,0	0,0	0,0	0,0	
6	PQ	-	0,0	0,0	0,0	0,0	

7	PQ	-	233,8	84,0	0,0	0,0	
8	PQ	-	522,0	176,0	0,0	0,0	
9	PQ	-	0,0	0,0	0,0	0,0	
10	PQ	-	0,0	0,0	0,0	0,0	
11	PQ	-	0,0	0,0	0,0	0,0	
12	PQ	-	7,5	88,0	0,0	0,0	
13	PQ	-	0,0	0,0	0,0	0,0	
14	PQ	-	0,0	0,0	0,0	0,0	
15	PQ	-	320,0	153,0	0,0	0,0	
16	PQ	-	329,0	32,3	0,0	0,0	
17	PQ	-	0,0	0,0	0,0	0,0	
18	PQ	-	158,0	30,0	0,0	0,0	
19	PQ	-	0,0	0,0	0,0	0,0	
20	PQ	-	628,0	103,0	0,0	0,0	
21	PQ	-	274,0	115,0	0,0	0,0	
22	PQ	-	0,0	0,0	0,0	0,0	
23	PQ	-	247,5	84,6	0,0	0,0	
24	PQ	-	308,6	-92,0	0,0	0,0	
25	PQ	-	224,0	47,2	0,0	0,0	
26	PQ	-	139,0	17,0	0,0	0,0	
27	PQ	-	281,0	75,5	0,0	0,0	
28	PQ	-	206,0	27,9	0,0	0,0	
29	PQ	-	283,5	26,9	0,0	0,0	
30	PV	1,0475	0,0	0,0	250,0	-	Gen10
31	PV	0,9820	9,2	4,6	-	-	Gen2
32	PV	0,9831	0,0	0,0	650,0	-	Gen3
33	PV	0,9972	0,0	0,0	632,0	-	Gen4
34	PV	1,0123	0,0	0,0	508,0	-	Gen5
35	PV	1,0493	0,0	0,0	650,0	-	Gen6
36	PV	1,0635	0,0	0,0	560,0	-	Gen7
37	PV	1,0278	0,0	0,0	540,0	-	Gen8
38	PV	1,0265	0,0	0,0	830,0	-	Gen9
39	PV	1,0300	1104,0	250,0	1000,0	-	Gen1

B. Minimum eigenvalue of the Jacobian Matrix-MatLab code

The main code was provided by T. Junjie from ACS and I just adapted the code to this Thesis needs.

```
clear;
simulation_num=1;
GN(3,3)=0; BN(3,3)=0;
H(6,6)=0;
Node_num =3;
Branch_num=3;
```

```
Branch_first(1)=1; Branch_end(1)=2;   Branch_R(1)=21.16;
Branch_X(1)=0.421*2*pi*50;    Branch_Brab(1)=0;   Branch_k(1)=1;
Branch_first(2)=1; Branch_end(2)=3;   Branch_R(2)=52.9;
Branch_X(2)=0.589*2*pi*50;     Branch_Brab(2)=0;     Branch_k(2)=1;
Branch_first(3)=2; Branch_end(3)=3;   Branch_R(3)=42.32;
Branch_X(3)=0.505*2*pi;    Branch_Brab(3)=0;   Branch_k(3)=1;


for bra_num=1:Branch_num
    Branch_R(bra_num)=Branch_R(bra_num);
    Branch_X(bra_num)=Branch_X(bra_num);
    Branch_Brab(bra_num)=Branch_Brab(bra_num);
end

MeaNum=0;
NOdePQNum=0;
BraPQNum=0;
BraINum=0;
NodeVNum=0 ;
for i=1:Node_num
      MeaNum=MeaNum+1;
    Measure_Firstnode(MeaNum)=i;
    Measure_Endnode(MeaNum)=i;
    Measure_type(MeaNum)=2;
    NOdePQNum=NOdePQNum+1;
    MeaNum=MeaNum+1;
    Measure_Firstnode(MeaNum)=i;
    Measure_Endnode(MeaNum)=i;
    Measure_type(MeaNum)=3;
end

for L= 1:Branch_num
   i=Branch_first(L);
   j=Branch_end(L);
   R=Branch_R(L);
   X=Branch_X(L);
   k=Branch_k(L);
   bm=Branch_Brab(L);
   BN(i,i)= BN(i,i) + bm;
   BN(j,j)= BN(j,j) + bm;
   if k==1
   GN(i,j)=GN(i,j)-R/(R*R + X*X);
   GN(j,i)=GN(i,j);
   BN(i,j)=BN(i,j)+X/(R*R + X*X);
   BN(j,i)=BN(i,j);
   end
   if k~=1
   GN(i,j) = GN(i,j) - R/((R*R + X*X)*k);
   GN(j,i) = GN(i,j);
   BN(i,j) = BN(i,j) + X/((R*R+ X*X)*k);
   BN(j,i) = BN(i,j);
   GN(i,i) = GN(i,i) + R *(1-k)/((R*R + X*X)*k*k);
   BN(i,i) = BN(i,i) - X*(1-k)/((R*R+ X*X)*k*k);
   GN(j,j) = GN(j,j) + R *(k-1)/((R*R + X*X)*k);
   BN(j,j) = BN(j,j) - X*(k-1)/((R*R+ X*X)*k);
   end
end

for i=1:Node_num
  for j=1:Node_num
      if i~=j
```

```
        GN(i,i)=GN(i,i)-GN(i,j);
        BN(i,i)=BN(i,i)-BN(i,j);
      end
  end
end

p=1;
Points= 500;

for p=1:Points

load magnitude9.txt;

load phase9.txt;

mag(:,1:3)=magnitude9(p,2:4);

ang(:,1:3)=phase9(p,2:4);
for sim_num=1:simulation_num

  Node_V=mag(sim_num,:);
  Node_A=ang(sim_num,:);
  reference_angle=Node_A(3);
  for i=1:3

 Node_A(i)=reference_angle-Node_A(i);
  end
end

  for i=1:Node_num
    Vi=Node_V(i);
    Ai=Node_A(i);
    Node_P(i)=0;
    Node_Q(i)=0;
    for j=1:Node_num
      Vj=Node_V(j);
      Aj=Node_A(j);
      Aij=Ai-Aj;
      Node_P(i)=Node_P(i)+ Vi*Vj*(GN(i,j)*cos(Aij)+BN(i,j)*sin(Aij));
      Node_Q(i)=Node_Q(i)+ Vi*Vj*(GN(i,j)*sin(Aij)-BN(i,j)*cos(Aij));
    end;
  end;

for i=1:MeaNum
  iNo=Measure_Firstnode(i);
  jNo=Measure_Endnode(i);

  if Measure_type(i)==2
      Vi=Node_V(iNo);
      Ai=Node_A(iNo);
      Pi=Node_P(iNo);
      Qi=Node_Q(iNo);
      VNo=2*iNo-1;
      ANo=2*iNo;
      H(i,VNo)=(GN(iNo,iNo) * Vi * Vi + Pi)/Vi;
      H(i,ANo)=-BN(iNo, iNo) * Vi * Vi - Qi;
      for j=1:Node_num
       if iNo~=j
        Vj=Node_V(j);
        Aj=Node_A(j);
```

```
        Aij=Ai - Aj;
        VNo= 2 * j -1;
        ANo= 2 * j;
        H(i,VNo)= Vi * (GN(iNo,j) * cos(Aij) + BN(iNo,j) * sin(Aij));
        H(i,ANo)= Vi * Vj * (GN(iNo,j)*sin(Aij) - BN(iNo,j) * cos(Aij));
       end;
      end;

  end

  if Measure_type(i)==3
      Vi=Node_V(iNo);
      Ai=Node_A(iNo);
      Pi=Node_P(iNo);
      Qi=Node_Q(iNo);
      VNo=2*iNo-1;
      ANo=2*iNo;
      H(i, VNo)= (-BN(iNo,iNo) * Vi * Vi + Qi)/Vi;
      H(i, ANo)= -GN(iNo, iNo) * Vi * Vi + Pi;
      for j=1:Node_num
       if iNo~=j
        Vj=Node_V(j);
        Aj=Node_A(j);
        Aij=Ai - Aj;
        VNo= 2 * j -1;
        ANo= 2 * j;
        H(i, VNo)= Vi * (GN(iNo,j) * sin(Aij) - BN(iNo,j) * cos(Aij));
        H(i, ANo)= -Vi * Vj * (GN(iNo,j)*cos(Aij) + BN(iNo,j) * sin(Aij));
       end;
      end;

  end
end

for nms=1:3

  JP_a(nms,nms)=H(2*nms-1,2*nms);
  JP_V(nms,nms)=H(2*nms-1,2*nms-1);
  JQ_a(nms,nms)=H(2*nms,2*nms);
  JQ_V(nms,nms)=H(2*nms,2*nms-1);

end

J_R=JQ_V-JQ_a*inv(JP_a)*JP_V;
Index_H_true(sim_num)=min(eig(J_R));
Index_Det(sim_num)=det(H);
J(p)=Index_H_true(sim_num);
p=p+1;
end
```